Design and Control of an Offshore Wind Farm connected to Main Grid with High Voltage Direct Current Transmission

M.Sc. Thesis

In

Electrical and Electronics Engineering

University of Gaziantep

Supervisor

Assoc. Prof. Dr. Ahmet Mete VURAL

By

Auwalu Ibrahim ISMAIL

January 2018

REPUBLIC OF TURKEY

UNIVERSITY OF GAZİANTEP

GRADUATE SCHOOL OF NATURAL & APPLIED SCIENCES

DEPARTMENT OF ELECTRICAL AND ELECTRONICS ENGINEERING

Name of the Thesis: Design and Control of an Offshore Wind Farm Connected to
Main Grid with High Voltage Direct Current Transmission
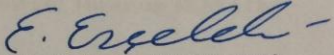
Name of the student: Auwalu Ibrahim ISMAIL

Exam date: 22nd January 2018

Approval of the Graduate School of Natural and Applied Sciences
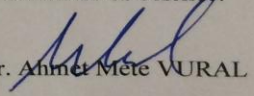
Prof. Dr. A. Necmeddin YAZICI

Director

I certify that this thesis satisfies all the requirements as a thesis for the degree of
Master of Science.

Prof. Dr. Ergun ERÇELEBİ

Head of Department

This is to certify that we have read this thesis and that in our consensus opinion it is
fully adequate, in scope and quality, as a thesis for the degree of Master of Science.
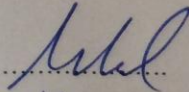
Assoc. Prof. Dr. Ahmet Mete VURAL

Supervisor
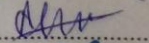
Examining Committee Members   signature

Assoc. Prof. Dr. Ahmet Mete VURAL   ....

Assist. Prof. Dr. Mehmet Ali ÖZÇELİK   ....

Assist. Prof. Dr. Erdal KILIÇ   ....

I hereby declare that all information in this document has been obtained and presented in accordance with academic rules and ethical conduct. I also declare that, as required by these rules and conduct, I have fully cited and referenced all material and results that are not original to this work.

Auwalu Ibrahim ISMAIL

ABSTRACT

DESIGN AND CONTROL OF AN OFFSHORE WIND FARM CONNECTED TO MAIN GRID WITH HIGH VOLTAGE DIRECT CURRENT TRANSMISSION

ISMAIL, Auwalu Ibrahim
M.Sc. in Electrical and Electronics Engineering
Supervisor: Assoc. Prof. Dr. Ahmet Mete VURAL
January 2018
100 pages

One of the fastest growing renewable energy sources in the present day technology is the wind energy that has many benefits such as being clean and sustainable. Offshore wind locations are the best option for wind energy production due to the fact that onshore locations are already occupied or planned as new wind farm locations. Also, higher wind speed up to twenty percent are available on sea than on land locations, as a result, more power can be extracted in offshore locations. Furthermore, the absence of obstacles such as hills and smooth surface of the sea makes offshore wind energy more reliable than onshore. Offshore wind farms inherently need AC grid connection with undersea cables. However, this requires high reactive power compensation equipment that is not practical and difficult for stable operation. For this reason, high voltage direct current (HVDC) transmission is a promising solution because no reactive power is needed. Moreover, the DC power flow between offshore and onshore locations can easily be controlled by means of voltage source converters. In this thesis an offshore wind farm connected to onshore main grid through undersea cables were designed and the power transfer was in the form of HVDC. The overall system including wind farm, offshore and onshore converters, HVDC transmission and main grid side were designed and tested in simulation program. The designed control systems of the HVDC converters were tested by various case studies.

ÖZET

ANA ŞEBEKEYE YÜKSEK GERILIM DOĞRU AKIM İLE BAĞLANAN KIYI ÖTESI RÜZGAR ÇIFTLIĞININ

ISMAIL, Auwalu Ibrahim
Yüksek Lisans, Elektrik ve Elektronik Müh. Bölümü
Tez Yöneticisi: Assoc. Prof. Dr. Ahmet Mete VURAL
Ocak 2018
100 Sayfa

Günümüzün teknolojisinde en hızlı büyüyen yenilenebilir teknolojilerin biri temiz olma ve sürdürülebilir gibi bir çok avantajı olan rüzgar enerjisidir. Kıyıötesi rüzgar yerleşimleri, kıyı bölgeleri çoktan işgal edilmiş veya yeni rüzgar çiftliği konumu olarak daha önceden planlandıkları için rüzgar enerji üretimi için en iyi seçimdir. Ayrıca, deniz üzerinde yüzde yirmilere varan daha fazla rüzgar hızı mevcuttur, sonuç olarak kıyı ötesi konumlardan daha fazla güç alınabilir. Üstelik, tepe gibi engellerin olmayışı ve denizin düzgün yüzeyi kıyıötesi rüzgar enerjisini kıyıda bulunanlara göre daha güvenilir yapar. Kıyıötesi rüzgar çiftlikleri doğal olaraj sualtı kabloları ile AC şebekeye bağlantıya ihtiyaç duyarlar. Fakat, bu pratik olmayan ve kararlı çalışma için zor olan yüksek reaktif güç kompanzasyon ekipmanına ihtiyaç duyar. Bu sebepten dolayı, yüksek gerilim doğru akım (YGDA) iletimi umut vaat eden bir çözümdür çünkü reaktif güce ihtiyaç duyulmaz. Dahası, DC güç akışı, gerilim kaynaklı çeviriciler sayesinde kıyı ötesi ve kıyı arasında kolay bir şekilde denetlenebilir. Bu tezde kıyıya yeraltı kabloları ile bağlanan bir kıyıötesi rüzgar çiftliği tasarlanmıştır ve güç transferi YGDA formunda olmuştur. Rüzgar çiftliği, kıyıötesi ve kıyıda bulunan çeviriciler, YGDA iletimi ve ana şebekeyi kapsayan tüm sistem benzetim programında tasarlanmış ve test edilmiştir. YGDA çeviricilerinin tasarlanan denetim sistemleri farklı vaka analizleri ile test edilmiştir.

Anahtar kelimeler: Kıyı ötesi rüzgar çiftlikleri, rüzgar türbin jeneratörleri, Çift Beslemeli İndüksiyon Jeneratörleri (ÇBİJ) , Yüksek Gerilim Doğru Akım (YGDA), sualtı kablosu ,aktif güç kontrol, reaktif güç kontrol, DC voltaj kontrol, AC ana şebeke.

To my father, Alhaji Ibrahim Ismail

ACKNOWLEDGEMENT

TABLE OF CONTENT

Page

LIST OF FIGURES

LIST OF TABLES

LIST OF ABBREVIATIONS

HVDC	High Voltage Direct Current
HVAC	High Voltage Alternating Current
AC	Alternating Current
DC	Direct Current
VSC	Voltage Source Converter
CSC	Current Source Converter
LCC	Line Commutated Converter
MMC	Modular Multilevel Converter
GTO	Gate Turnoff Thyristor
FACTS	Flexible Alternating Current Transmission System
PCC	Point of Common Coupling
STATCOM	Static Compensation
UPFC	Unified Power Flow Controller
ASG	Adjustable Speed Generators
PMSG	Permanent Magnet Synchronous Generator
DFIG	Doubly Fed Induction Generator
SCIG	Squirrel Cage Induction Generator
IGBT	Insulated Gate Bipolar Transistor
PWM	Pulse Width Modulation
SVPWM	Space Vector Pulse Width Modulation
PLL	Phase Lock Loop
MPPT	Maximum Power Point Tracking
DPC	Direct Power Control
RSC	Rotor Side Converter
GSC	Grid Side Converter
WFVSC	Wind Farm Voltage Source Converter
GSVSC	Grid Side Voltage Source Converter

CHAPTER 1

INTRODUCTION

Renewable energy as a natural abundance source for mankind offers infinite opportunities as well as challenges to power system architecture. Among the benefit derived from the renewable energy sources are free energy available that can be exploited in its natural form, thereby providing quite economical sources of energy.

Conventional energy sources like coal, nuclear or natural gas can contaminate environment whereas fuel cell, wind, geothermal and solar energy that are renewable sources are fresh and richly available in nature. Wind energy system has been described as the best among others for use in the present world because of its greater potentiality especially in European countries. In 2008 alone, about 27-GW of wind power was installed worldwide, which brought to around 120.8 GW of the total installed capacity [1].

Wind industries experienced a strong growth few years ago, which has led to an improved significance in offshore application [2]. This development set to be a footstep on planning of the European power system. Offshore wind farms have been on growing trend compared to their counterpart located onshore due to unavailability of onshore sites and wind is more powerful and persistent in offshore sites. A 1100 MW of power has been developed for 25 projects in five European countries in the year 2007 and which are big projects and completely marketed [2][3].

Wind farm exploitation requires an installation of a number of wind turbines located distant from the shoreline in excess of hundred of kilometers. The installation mostly employs Double Fed Induction Generators (DFIGs), which involves decouple control of

back-back converters so as to permit adjustable speed operation of the turbine and a cost effectiveness [2].

HVDC transmission known as 'High Voltage Direct Current' transmission has been a reasonable solution economically and technologically for connection between offshore located wind farms with their intended loads over a long distance taking into account the continuous increase in demand on the required capacity of an offshore located wind farms. Generally there is a long distance between most offshore-located wind farms and the point of common coupling (PCC) at onshore. HVDC transmission is more suitable solution for connecting the two converter stations due to weakness of the connection as a result of long distance transmission.

HVDC transmission using voltage source converter (VSC) was first launched in Sweden in 1997 rated at 3 MW as a trail, it covers a distance of 10km, during that year the project went into operation to demonstrate the feasibility of the technology to operate in a network. The Gotland HVDC light, a 50 MW that covers a distance of 70km, transport wind power from southern Gotland to the center of the island. It has been in operation since November 1999. Directlink is a 180 MVA HVDC light project that connects the regional electricity markets of new South Wales and Queensland.
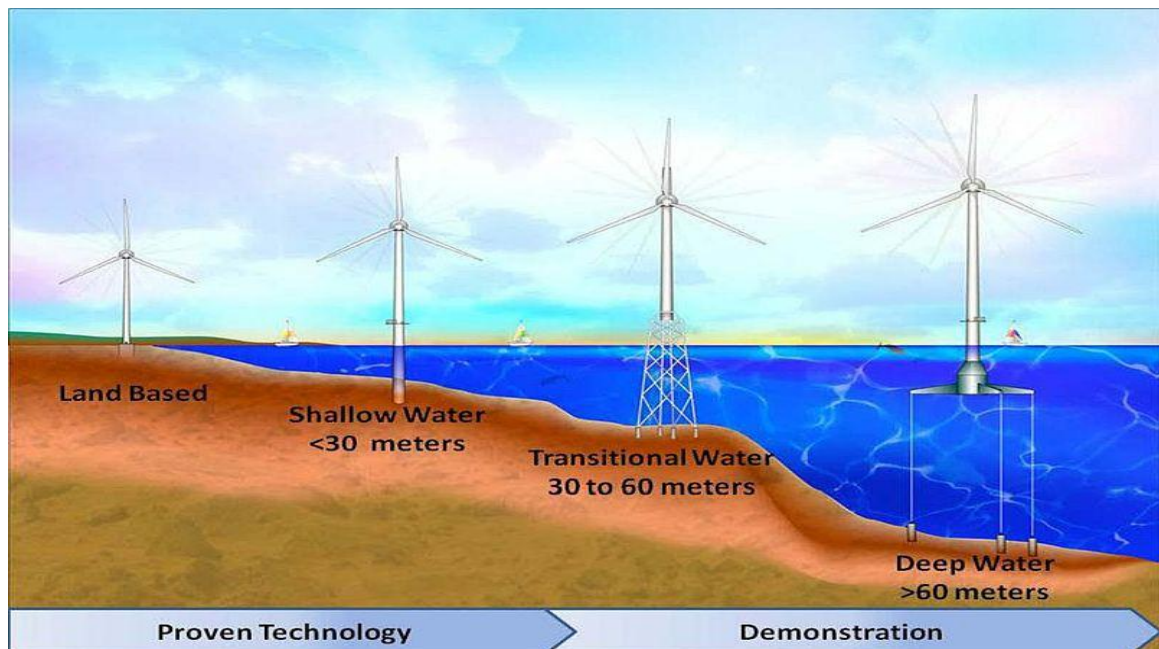
Figure 1.1 Development of anticipated wind turbine evolution to deeper water [4].

Offshore wind farm was first installed in Denmark by the year 1991 as a major offshore wind farm for the whole Europe and it serves as the pioneer for offshore wind farm technology first of its kind. It was recorded that in 2013 offshore wind power brings to total capacity of 11 GW following the addition of 1.5 GW that year.

	UK	Germany	PR China	Denmark	Netherlands	Belgium	Sweden	Japan	S Korea	Finland	US	Ireland	Spain	Norway	Portugal	Total
Total 2015	5,100	3,295	1,035	1,271	427	712	202	53	5	32	0.02	25	5	2	2	12,167
New 2016	56	813	592	0	691	0	0	7	30	0	30	0	0	0	-2	2,219
Total 2016	5,156	4,108	1,627	1,271	1,118	712	202	60	35	32	30	25	5	2	0	14,384

Source: GWEC
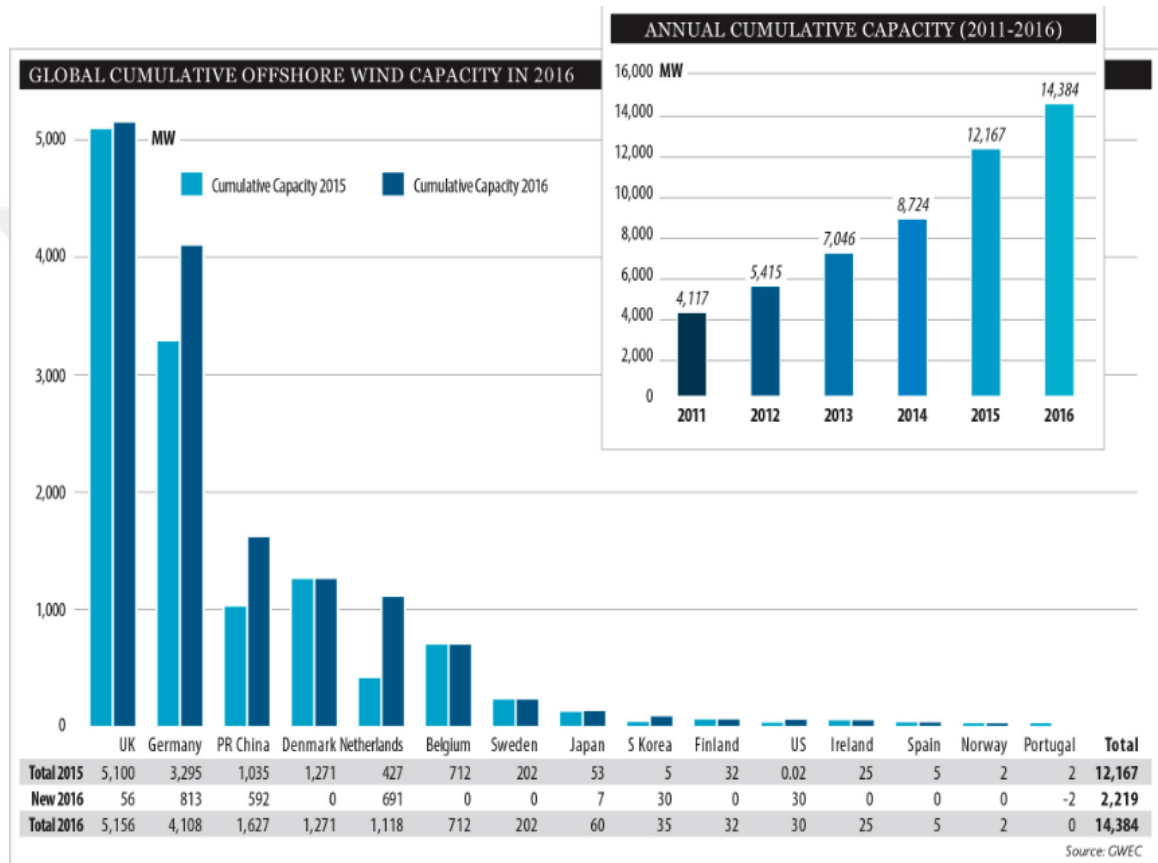
Figure 1.2 World collective offshore capacity (in MW) [5]

The VSC-HVDC is a newer technology that employs connection of multilevel converter when compared with the Line Commutated Converter based HVDC link. It is expected that wind farms with high power rating can provide high and significant energy in the near future. Constant wind speed and its availability for offshore areas offer a greater chance for large-scale integration of renewable energy generation. Low direct vision and environmental impact are also another reason in support of large-scale offshore wind generation when compared to onshore generation. High towers and big diameter of rotors in onshore wind farms also minimized their public compliance for large-scale integration.

New transmission investment is needed to make best use of offshore wind energy. Though this novel technology are long term and expensive but must be carefully organized. The construction of transmission system especially in offshore requires high investment. It's also vital for a grid planner to address with potential alternatives rather than affordable solution having other advantages rather than just lower charges. Usually a radial connection is employed for linking offshore wind farm that are of short distance to the main electricity grid. An integrated approach is employed when connection of wind farms which aims at optimizing the offshore transmission system investment [6].

1.1 Electrical Power Generation

There are several means of generating electrical power, but the most common are:

1.1.1 Hydroelectric Energy

The conversion of hydroelectric power depend on two components, the turbines are placed into dam to produce a torque that is converted into mechanical energy. Secondly, small DC are used to the generator for further conversion into electrical energy. A transmission is added if rotational speed is different for the requirement of turbine and generator or if both components are in different axis.

1.1.2 Solar Energy

The radiation released by the sun at a speed of approximately 500km/s (solar wind) is covering the entire frequency from short wave to long wave radiation. This radiation is converted into electrical power by releasing the electrons in the semiconductor layers (PV cell) so it produces electrical voltage. The PV cell produces small power and voltage, PV can be connected in series or parallel to get desirable voltage.

1.1.3 Wind Energy

Wind turbines operate by converting kinetic energy in the air into electrical energy. The movement of air on appreciable scale is caused by temperature differential. The wind speed depends on temperature, climate change, height above the ground and terrain.

1.1.4 Geothermal Energy

Geothermal heat under groundwater is influenced by solar radiation. This radiation flow through the pipes at high pressure, then the turbine converts the steam into electrical energy through generator. The temperature profile within the earth's crust is

characterized by a heat flux to the surface of the earth; the magnitude of this heat is proportional to the temperature gradient in the earth's crust.

1.1.5 Biomass Energy

Biomass comprises trees, plant, and animal wastes. The idea is how to convert the wastes into energy form such as biogas, biofuel and heat. Hence the waste is converted into energy, and then the biomass supply must follow through special conversion stages as pretreatment (substrate), gas condition, gas utilization (heat) and electricity is produced.

1.2 Formulation of the problem

In current years, one of the fastest growing renewable-energy resources is the wind energy that has many benefits such as being clean and sustainable [7]. Offshore locations are very suitable for energy production by wind. This is true because of the following reasons:

1. In most of the countries, the best onshore locations for wind energy production are already occupied or will be already planned as new wind farm locations,

2. Higher wind speeds (up to 20% greater) are available above the sea when compared to land location, as a result more power (up to 70%) can be extracted from wind,

3. The absence of obstacles such as hills and the smooth surface of the sea make wind energy more reliable when compared to land location.

An offshore wind farm inherently needs AC grid connection with undersea cables. However AC transmission of electrical power with these cables requires high amount of reactive power which is not practical, expensive and difficult to control for stable operation [3]. Due to these limitations, HVDC transmission option is very ideal for undersea power transfer between the offshore wind farm and the onshore power substation. There are many projects of this type exists such as BorWin and DolWin projects in Europa. HVDC power transmission inherently requires no reactive power and it is reliable. Moreover DC power flow can be easily controlled by means of voltage source converters (VSC) located both offshore and onshore, between the two ends of the undersea cable. Another advantage of HVDC power transmission option is that it can be connected to weak radial systems. In order to fully benefit an offshore wind farm with

HVDC, the control system of the VSCs should be designed so as to satisfy reliable operation with high sustainability and efficiency of energy.

1.3 Objective of the Study

In this thesis, an offshore wind farm connected to the onshore AC grid with undersea cable will be designed. The power transfer through the cable will be in the form of HVDC. The objective of the thesis is summarized below:

1. Implementation of wind farm model employing doubly fed induction generator (DFIG).
2. Design of converter(s) for offshore and onshore sites and connected through HVDC transmission.
3. Control system of the converters will be design for the optimistic transfer of high quality power to onshore AC substation from the onshore wind farm.
4. The overall system including wind farm, converter(s), HVDC transmission and the AC grid side will be design and tested in a simulation environment.

CHAPTER 2

UNDERSTANDING OFFSHORE WIND FARM WITH VSC-HVDC

2.1 Introduction

DC transmission system for conveying power to the grid from an offshore wind farm with advantage of reducing reactive power and harmonics etc., have been an attractive solution following a rise in size of offshore connected wind farm and the distance amid offshore sites and a land location. In this chapter, an attempt is made to present a far-reaching review on the entire model consisting of offshore wind farms comprising turbine generators, HVDC transmission employing VSCs and undersea cables, onshore and offshore converter components, and finally the AC main grid substation.

2.2 Wind turbine overview

Generally there are two types of wind turbine generators:

- Constant speed wind turbine generators and
- Fixed speed wind turbine generators.

The performance and construction of fixed-speed wind turbines depend solely on mechanical sub-circuit features e.g. pitch-control time constant, maximum switching rate of main circuit breaker. Today's high power wind turbines are generally capable of variable speed operation.

Considering an offshore HVDC system, the use of squirrel-cage induction generator (SCIG) is very simple where the grid-side generator frequency is regulated for attaining maximum power from the turbines. Frequency of each turbine can be the same but wind speed should be different because of the difference in operating condition. Maximum

Power Point Tracking control of the turbine-generators is not possible independently. In other word, overall efficiency decreases because of limitation in varying the frequency [8].

2.3 Adjustable speed generators

Also called variable speed generators, Adjustable speed generators are generators that are capable of variable speed operation. They have benefits of

1. Reducing mechanical stress
2. Cost effectiveness
3. Simple pitch control
4. Dynamically compensate for power pulsation and torque cause by back pressure of the tower
5. Improving power quality
6. Reducing acoustic noise
7. Improving system efficiency

2.4 Types of Adjustable Speed Generators (ASG)

Basically there are various types of adjustable speed generators (ASG) [8], but the most common are:

2.4.1 Direct-in-line ASG System

In this scheme, a synchronous generator generates variable frequency AC power. This power is transformed using power converters connected in series with an ASG into fixed-frequency AC power. ASG system has disadvantages of cost for power converters that are rated in per unit; difficulty in design of filters and they are expensive; dependence on system effectiveness.

As wind power industries rapidly increasing, three types of wind turbine generators are widely used for offshore application. These generators are differentiated based on their operational speed range as fixed, limited variable and variable speed.

2.4.2 Squirrel cage induction generators (SCIG)

Frequency regulation of local generator grid side makes squirrel cage induction generator the simplest selection for offshore generator in order to deliver quality power to the grid. This advantage of SCIG makes it simpler to use when choosing generators for offshore wind farm application. It should be noted that effective cost and losses in generators are much higher for structures with separate converter arrangements than those with common single converter arrangement. Also wind speed variation for wind turbines can affect its operating condition irrespective of the common frequency of the generators. MPPT cannot be possible when the turbine generators are connected separately.
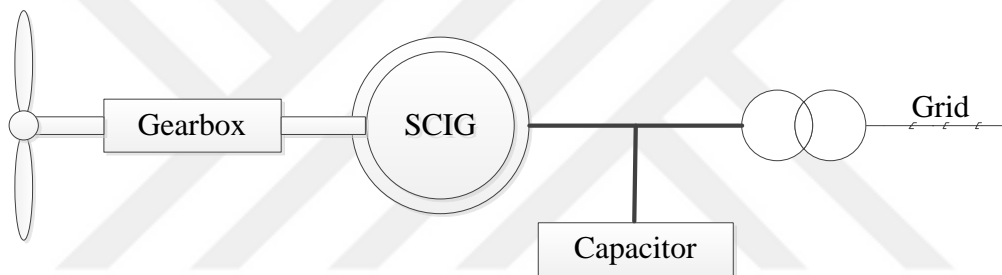
Figure 2.1 Squirrel cage induction generator

2.4.3 Permanent magnet synchronous generator (PMSG)

In this type of generator arrangement, an AC/DC/AC converter connected back-to-back are used to convert the generator output power to a nominal frequency of local grid, which later conveyed to offshore rectifier station. Permanent magnet synchronous generators do not have gearboxes and have multiple poles, which makes them efficient and reliable, however they are expensive.
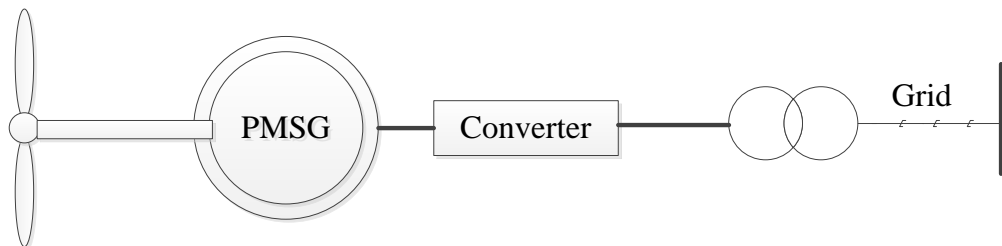
Figure 2.2 Configuration of PMSG

2.4.4 Doubly-fed induction generator (DFIG)

This type of generator is the most common turbine-generators system used in offshore wind farm. They are capable of variable speed operation and have lower cost and losses compared to other variable speed turbine generators. One disadvantage of DFIG over PMSG is its limited speed variation range. But it can be avoided by regulating the generator-side local grid frequency there by increasing the range of allowed speed variation of DFIGs.
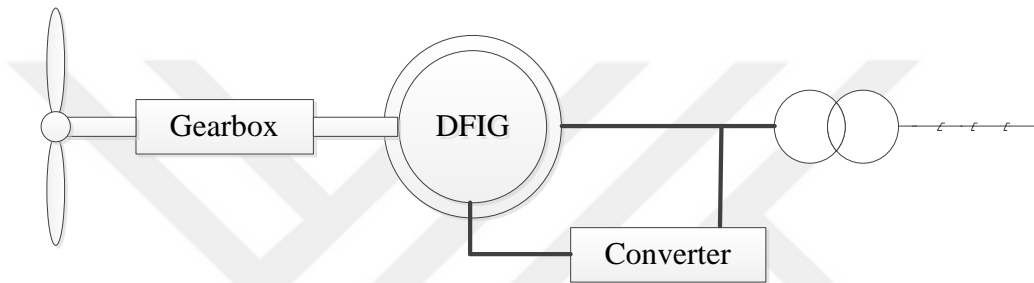
Figure 2.3 Doubly fed induction generator

In this thesis, a DFIG is considered, where the rotor winding of a DFIG is fed through back-to-back variable frequency VSC. An offshore wind farm connected to main grid with HVDC transmission is schematically shown in Figure 2.4.
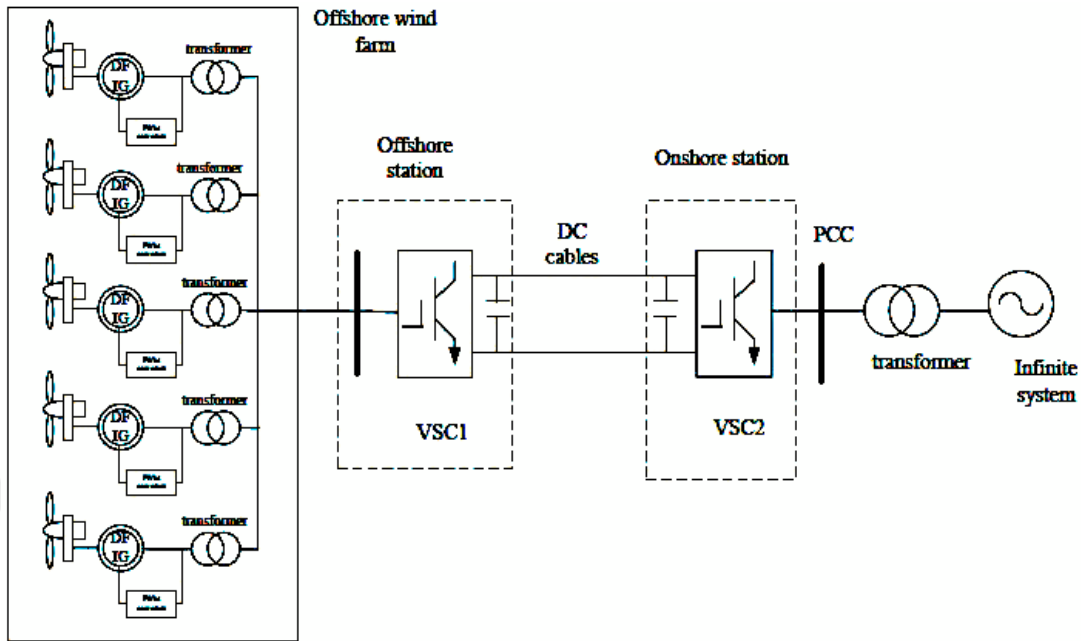
Figure 2.4 The designed offshore wind farm model connected to main grid with HVDC transmission [10].

2.5 Understanding HVDC System

For short distance transmission of power, high voltage alternating current is a suitable solution because it's cheaper since it needs no converters and DC filters. But when transmission exceeds 70 km, HVDC becomes more economical because it reduces the use of bulk transmission AC cables and does not require reactive power compensation equipment like STATCOM in order to deliver the real power flows toward the land over such long distance.

HVDC based VSC technology is a promising solution for transmitting bulk power from offshore sites to onshore AC main grid. It uses power electronic converters that employ insulated gate bipolar transistor (IGBT) switches aims at decoupling control of active and reactive power. It allows connection of two or more AC systems that are operating at different frequency. It also permits connection to weak AC system networks.

It is obvious that two alternative methods of connections are possible to connect wind farm through high voltage to main grid:

HVAC that can transmit power in the range of few hundred MW and transmission distance not more than 75 km. When transmission distance is over 50-75 km, HVDC transmission can be more efficient and economic solution.

2.6 HVDC System Arrangements

Converter bridges or cables are arranged in a various configuration to achieve better performance. The arrangement should either be mono-polar or bipolar depending on the type of transmission

2.6.1 Mono-polar HVDC System Arrangement

In this type of HVDC system arrangement, a single pole line connects two converters. DC voltage should either be positive or negative. It has only single transmission conductors while the ground is used as current return. The example of this type of arrangement is the Konti-Skan project in 1965. Metallic conductor is used as a current return.
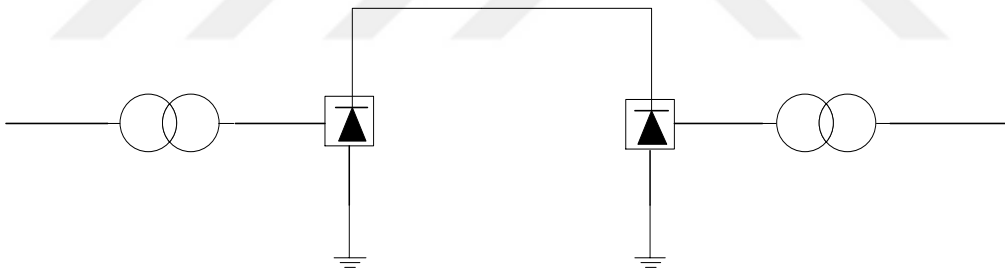
Figure 2.5 Monopolar HVDC system arrangements

2.6.2 Bipolar HVDC System Arrangement

Two insulated conductors are used as positive and negative poles in this arrangement. These poles operate independently when their neutral are grounded which result in increase in power transfer capability.

Advantages

1. Flow of current in each pole is the same
2. Absence of ground current
3. Continuous flow of power even when one pole fails to work
4. Reliable

Overhead line transmission mostly used this type of arrangement
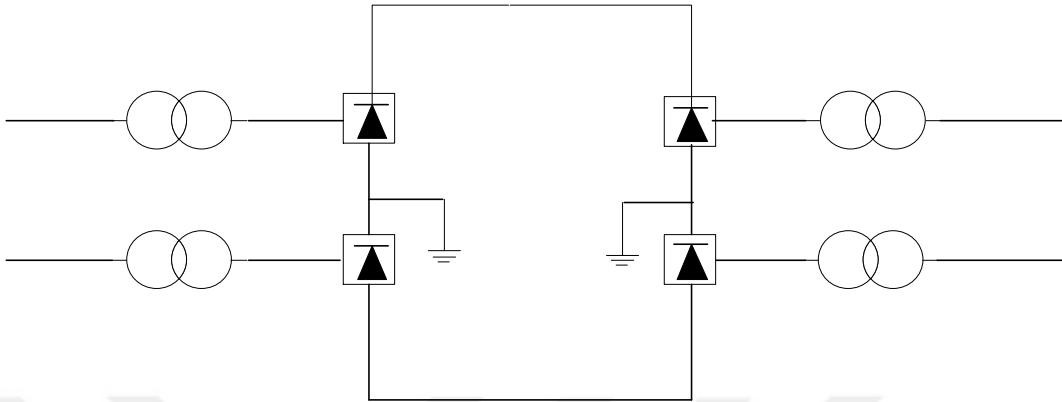
Figure 2.6 Bipolar HVDC system arrangement

2.7 HVDC System Configuration

Configuration of HVDC system depends on the function and location of converter substation. The common configurations are:

2.7.1 Back-to-Back HVDC System Configuration

Two converter stations are constructed at the same location without visible transmission between the converter bridges. Connection arrangement may be mono-polar or bipolar. They have advantage of interconnection of two systems with different operating frequency. However they have low DC voltage. Example of this configuration was found in japan and America.

Figure 2.7 Back-to-back configuration of HVDC system

2.7.2 Point-to-Point HVDC System Configuration

This is the most common configuration for HVDC system. It is used to transfer power through HVDC transmission from one location to another. The transmission can connect

two non-synchronous systems. Example of this project is connection between Sweden and Denmark.
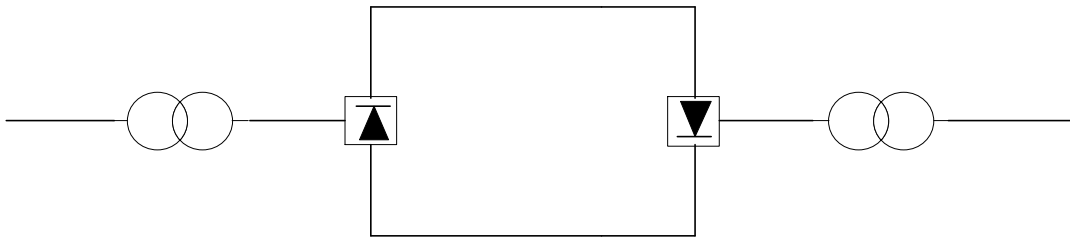
Figure 2.8 Point-to-point HVDC system configurations

2.7.3 Multi-terminal HVDC (MTDC) System Configuration

This allows interconnection of three or more converter substations. When connection is of the same voltage level, the system is called parallel multi-terminal DC. It is referred to as series multi-terminal DC if one or more converter bridges are added serially in one or both poles. Combine connection of series and parallel multi-terminal is called hybrid multiterminal system.
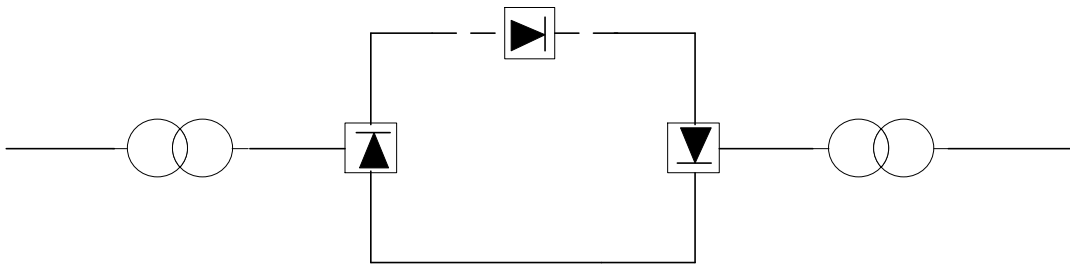
Figure 2.9 Series multiterminal HVDC system configuration

MTDC system configuration is economically inappropriate because of cost in substation that is difficult to tackle. Example of multiterminal HVDC configuration is Sardinia-Corsica-Italy (SACOI).
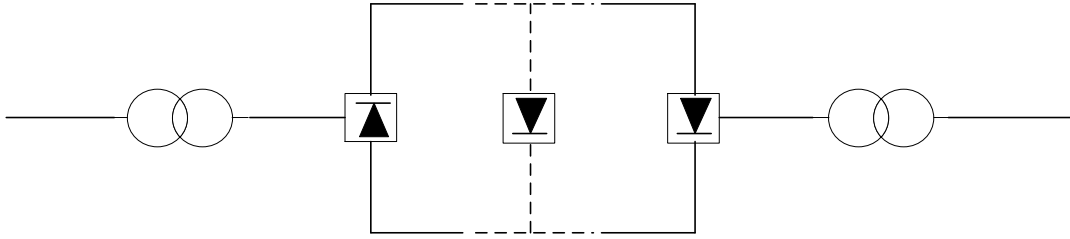
Figure 2.10 Parallel multiterminal HVDC system configuration

2.8 Converters for HVDC System

VSC-based-HVDC transmission represents an important improvement over the classical HVDC. Control of reactive power exchange is achieved by VSC-HVDC, it provides low harmonics and allows the connection of passive AC grids. Some of the advantages of using VSC-HVDC over classical HVDC make it the best choice for offshore power transmission over long distance. These are:

1. Fast and independent active and reactive power control
2. Black start capabilities
3. Capacity of variable frequency operation
4. Allowance of multiterminal network structures
5. Constant improvement of control quality instabilities

VSC-HVDC transmission can decouple two AC systems operating at different frequencies, a phenomenon that prevents dynamic disturbance going through the DC link from one end to the other.

Converters are generally categorized as line commutated and self-commutated converters based on their circuit topology and the number of voltage level at output.

The first category is a line-commutated converter that requires an AC current in order to operate in a network. This current is shifted in phases when AC voltage forces it to commutate. A self-commutated converter, which is the second category of converters, can work in the system without connecting to an AC system.

Self-commutated converters are further classified as voltage source converters (VSC) and current source converters (CSC). For the operation of CSC, a smoothing DC current

is provided by the reactors, while in VSC, a smoothing DC voltage is provided by the capacitors in order to operate in a system.
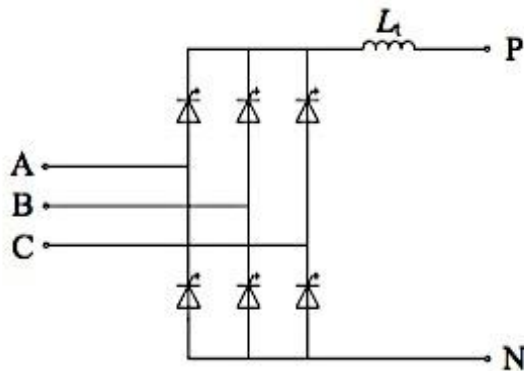
Figure 2.11 6-Pulse valve line commutated converter [9]

2.9 Converter Topology

VSC based HVDC transmission represents an important improvement over the classical HVDC. Control of reactive power exchange are achieve with VSC-HVDC, it provides low harmonics and allows the connection of passive AC grids. Self-commutated converters are broadly divided as 2-level and 3-level VSCs.

2.9.1 Two level VSC Topology

This is the simplest form of VSC configuration, which generates two-voltage level. It consists of 6-pulse bridge equipped with IGBTs and anti-parallel connected 6-pulse bridge diodes. It uses pulse width modulation for its output waveform.
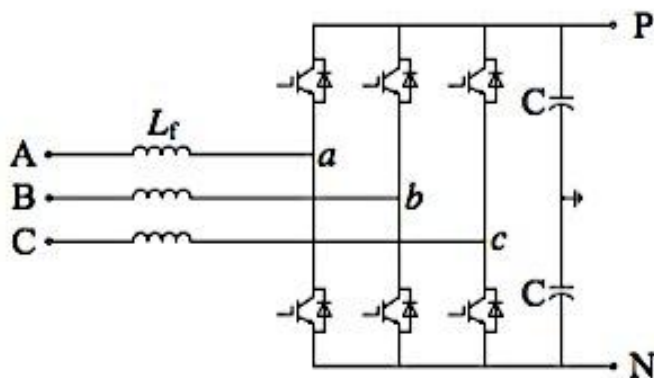
Figure 2.12 Two-level VSC [9]

2.9.2 Three level VSC Topology

Three-level VSC topology comprises 4-valve in one phase leg as shown in Figure 2.13. The switching rule is that any two valves that are directly connected in series can be switched-on at a time.
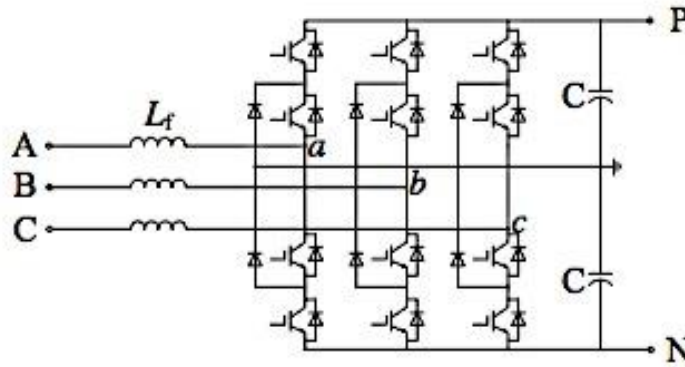
Figure 2.13 Three-level VSC [9]

2.9.3 Modular Multi level Converter (MMC)

Modular Multilevel converter is suitable for high or medium-voltage power conversion because of its simpler construction and flexibility in converter design. It is based on cascaded connection of multiple bi-directional chopper-cells per leg, thus requiring voltage-balancing control of the multiple floating DC capacitors. Multilevel converters that achieve power conversion without transformers are:

Diode-clamp multilevel converters (DCMC) and flying capacitors multilevel converters (FCMC). A three-phase MMC configuration comprises of two stacks of multiple bi-directional cascaded chopper-cells and two non-coupled buffer inductors.

MMCs are classified according to their topologies as:

- Double-star-configured MMCs
- Star-configured MMCs
- Delta-configured MMCs and
- Dual MMCs

Double-star-configured MMCs are further divided as: chopper-cell type and bridge-cell type MMCs.
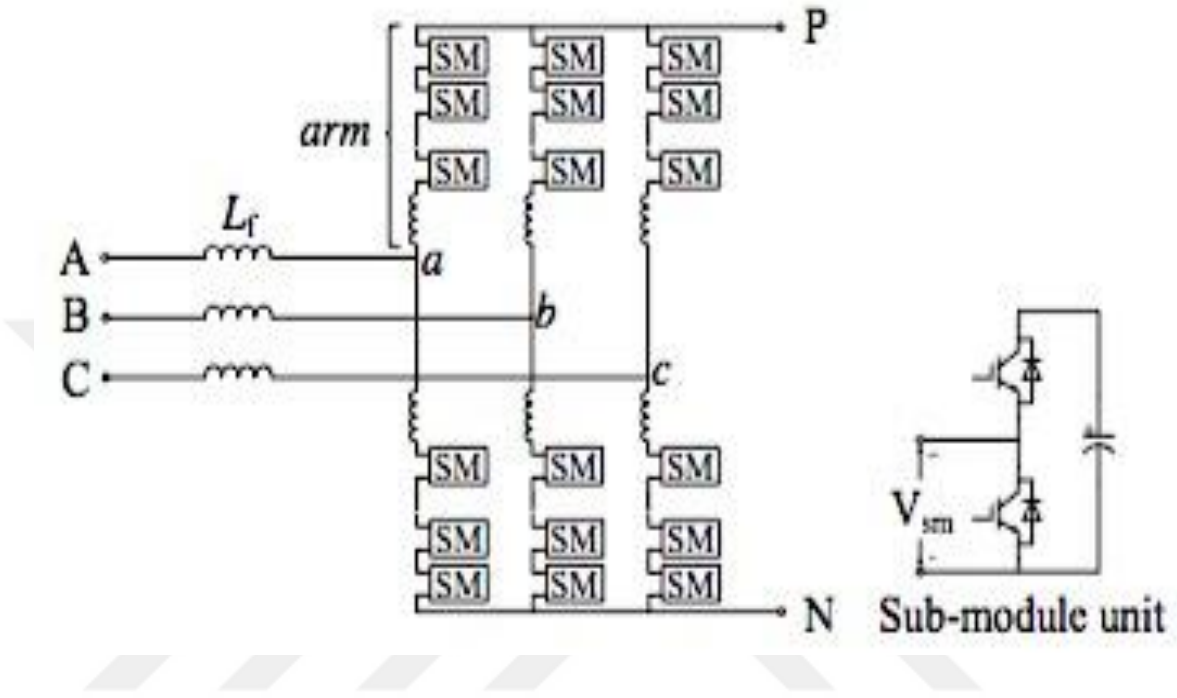
Figure 2.14 Modular Multilevel Converter (MMC) [9]
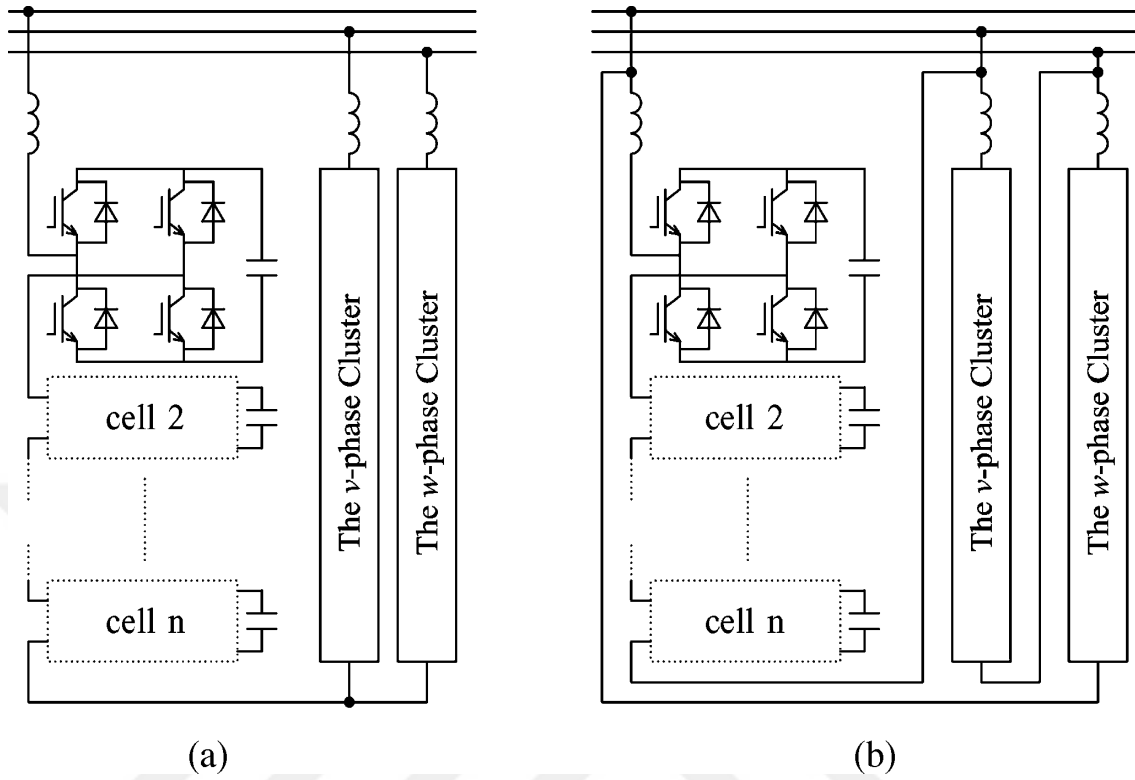
Figure 2.15 Circuit configuration of MMCs

(a) Star-configured MMC (b) Delta-configured MMC
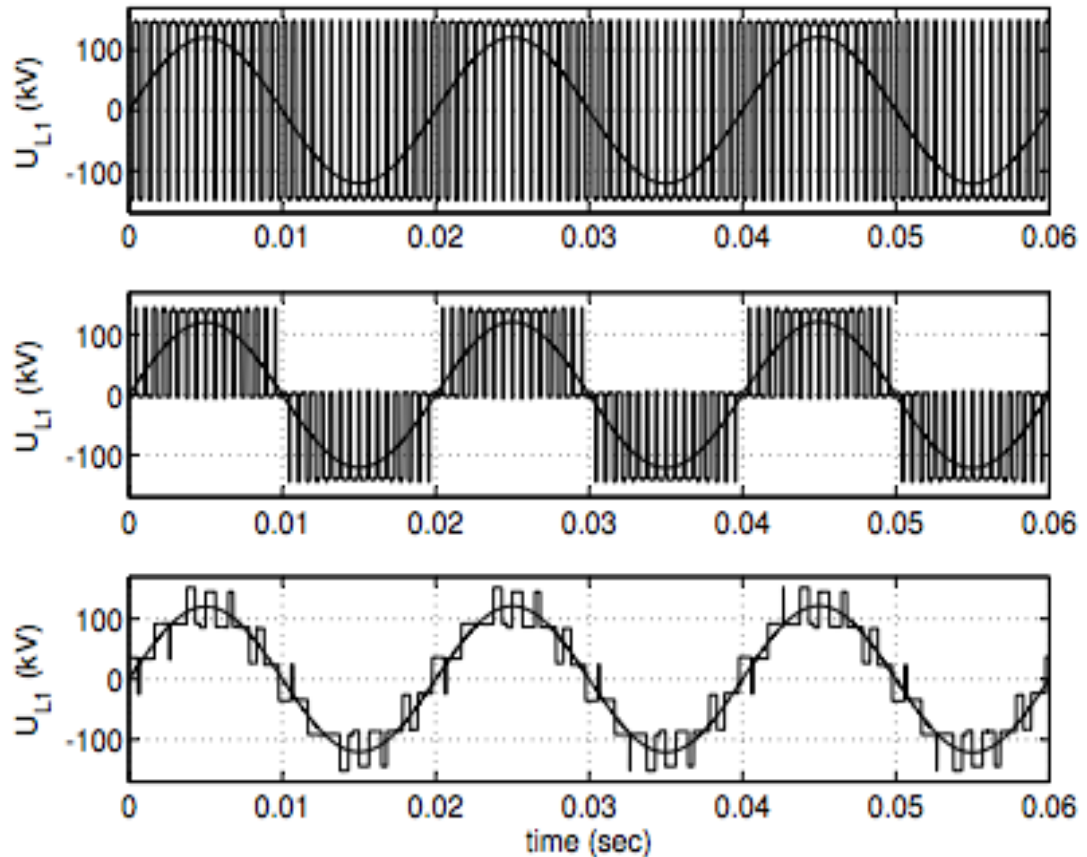
Figure 2.16 PWM for different converter topologies; Upper plot: 2-level converter. Middle plot: 3-level converter. Lower Plot: MMC with five modules

2.10 Other Converter Components

There are some other components that are connected together to make VSC. These are:

Transformers: They are designed based on the function they performed in a system. Transformers can connect two single converters that are of different DC potentials. Converter AC terminals and AC systems are separated with reactors to give reactance to the system. Different transformer configuration is design as

1. Single-phase two-windings
2. Single-phase three-windings and
3. Three-phase two-windings

In this entire configuration, a transformer leakage reactance is selected to limit short-circuit current going through valves. The valve side winding which is a primary winding is connected in delta or star with neutral ungrounded. The secondary winding that comes from the AC side of the system is connected in parallel with neutral grounded.

AC Harmonic Filters: It is a reactive power and AC current limiting circuit against harmonics

High Frequency Filter: A circuit use to filter out high-frequency interference propagating into AC side of the system from converter bus bar

DC Filter: AC harmonic current limiting circuit running into the DC line.

DC Smoothing Reactor: This circuit is used for smoothing DC waveform, minimize losses and enhance system performance.

DC Switchgear: This a device for disconnecting the DC circuit in case of reconfiguration or maintenance.

DC Transducers : This is use to measure the DC quantities of current and voltage**.**

2.11 Power semiconductor classification

FACTs and HVDC that are power electronic application-based-semiconductor devices, which are grouped, based on their switching controls as fully controlled, half-controlled and uncontrolled devices. Power diodes are example of controlled devices, thyristors as half-controlled due to their switching-on control behavior. Fully controlled semiconductor devices are also referred to as power electronic switches.

Table 2.1 Fully controlled semiconductors

Title	Class	Meaning
GCT	Thyristor	Gate Commutated Turnoff
GTO	Thyristor	Gate Turn Off
IEGT	Transistor	Insulated Enhanced Gate Transistor
IGCT	Thyristor	Insulated Gate Commutated Thyristor
IGBT	Transistor	Insulated Gate Bipolar Transistor

HVDC voltage level is too high when compared to voltage level of single semiconductor devices.

2.12 Pulse Width Modulation (PWM)

Pure sinusoidal PWM is the simplest method used for VSC converters.

2.12.1 Space Vector Pulse Width Modulation (SVPWM)

In this form of modulation, reducing switching losses can minimize a number of switches. SVPWM transformation techniques is also applicable to line voltage (line switching states) of voltage source converter as shown in Table 2.2 which indicate the generated eight space vectors switching state from one to six are non zero line voltage while seven and eight are insignificant line-voltage vectors.

The important reason of using the Space Vector techniques is to estimate the line-modulating signal space Vc with 8-space vector. For the generated voltage to be on sample period T_s, vector Vc, should be equal to the average vector

Real and imaginary solution for a line-load voltage that features amplitude restricted to $0 \leq \hat{V}_c \leq 1$ gives,

$$T_i = T_s . \hat{V}_c . \sin(\frac{\pi}{3} - \theta) \tag{2.1}$$

$$T_{i+1} = T_s . \hat{V}_c . \sin\frac{\pi}{3} \tag{2.2}$$

$$T_z = T_s - \hat{V}_i - T_{i+1} \tag{2.3}$$

The above preceding expression equations shows that the determined primary line-voltage is unity as $0 \leq \theta \leq \frac{\pi}{3}$.

The relationship between the switching variable vector $[a, b, c]t$ and the line voltage vector $[Vab, Vbc, Vca]t$ is given by,

$$\begin{bmatrix} V_{ab} \\ V_{bc} \\ V_{ca} \end{bmatrix} = V_{dc} \begin{bmatrix} 1 & -1 & 0 \\ 0 & 1 & -1 \\ -1 & 0 & 1 \end{bmatrix} \begin{bmatrix} a \\ b \\ c \end{bmatrix} \tag{2.4}$$

Also the switching variable $[a, b, c]t$ and the phase voltage vector $[Va, Vb, Vc]t$ can be expressed below,

$$\begin{bmatrix} V_{ab} \\ V_{bc} \\ V_{ca} \end{bmatrix} = V_{dc}/3 \begin{bmatrix} 2 & -1 & -1 \\ -1 & 2 & -1 \\ -1 & -1 & 2 \end{bmatrix} \begin{bmatrix} a \\ b \\ c \end{bmatrix} \tag{2.5}$$
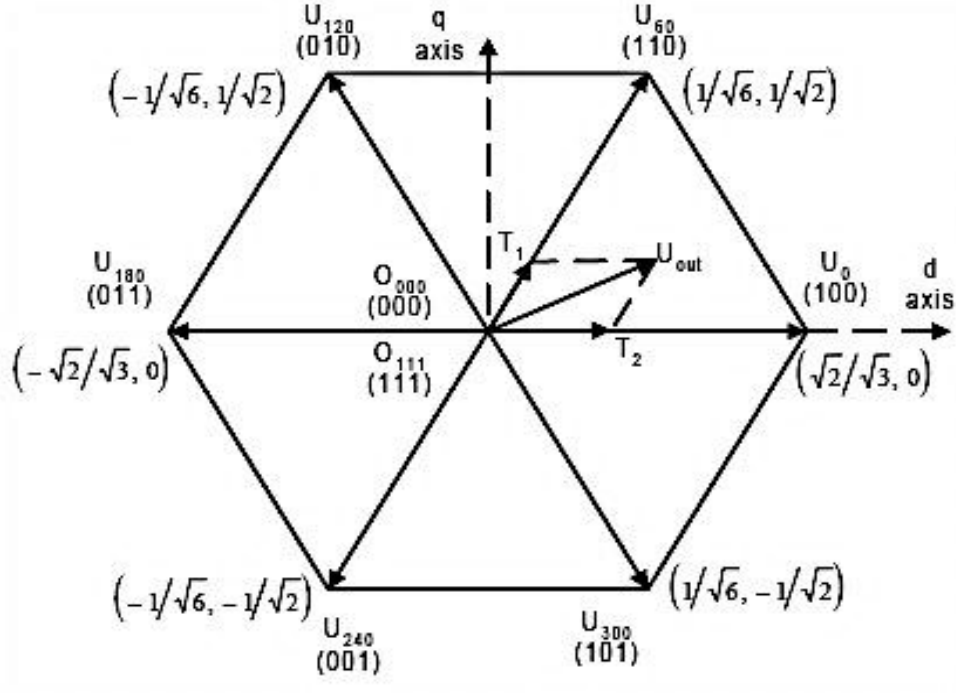
Figure 2.17 SVPWM switching map

U_{out} in Figure 2.17 shows desired phase voltage in d-q reference frame. Analyzing the duty ratio of U_{out}, identify U_{out} sector, then duty cycle can be found using voltage-time balance on one switch period (T_W).

$$T_{sw}U_{out}e^{j\theta} = T_{sw}(d_0 0 + d_1 U_0 + d_2 U_{60})$$

$$= T_{sw}\frac{U_{DC}}{2}(d_1 + d_2 e^{j\pi/3}) , d_0 + d_1 + d_2 = 1 \qquad (2.6)$$

where d_0 is the duty circle of 0, and d_1 is the duty circle of U_0 and d_2 is the duty cycles of U_{60} voltage vectors.

d-q components are denoted by:

$$U_{out}\cos\theta = d_1 V_0 + \frac{1}{2}d_2$$

$$U_{out}\sin\theta = \frac{\sqrt{3}}{2}d_2 \qquad (2.7)$$

Hence

24

$$d_2 = \frac{2}{\sqrt{3}} U_{out} \sin \theta$$

$$d_1 = \frac{1}{\sqrt{3}} U_{out}(\sqrt{3} \cos \theta \sin \theta) \qquad (2.8)$$

$$d_0 = 1 - d_1 - d_2$$

$T_0/4$	$T_1/2$	$T_2/2$	$T_0/2$	$T_2/2$	$T_1/2$	$T_0/4$

a

b

c

O_{000}	U_0	U_{60}	O_{111}	U_{60}	U_0	O_{000}
(000)	(100)	(110)	(111)	(110)	(100)	(000)
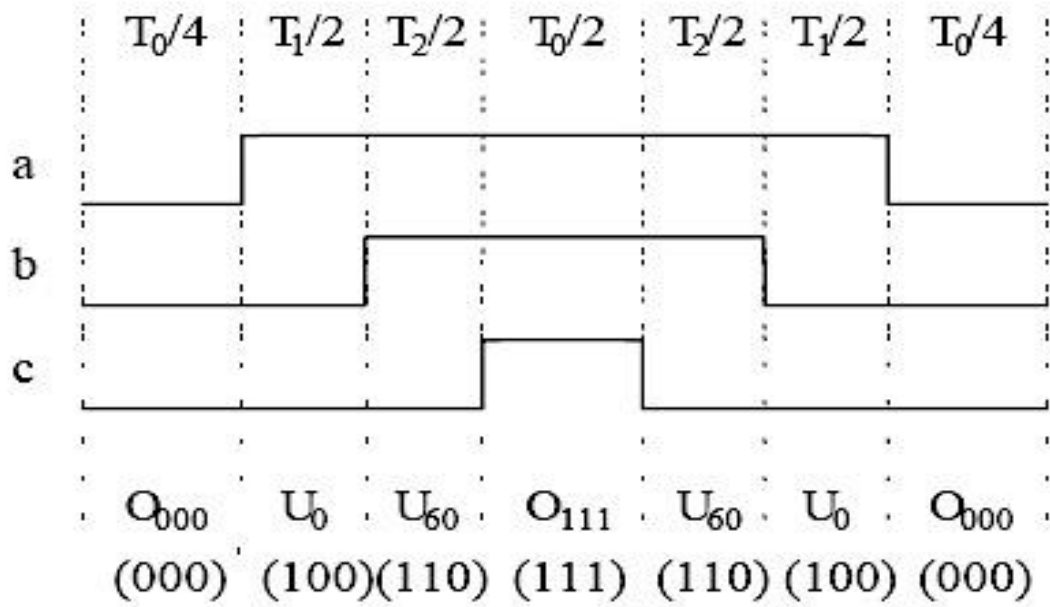
Figure 2.18 Switching pattern for U_{out} in $U_0 - U60$

Table 2.2 IGBT Switching Table

Output voltage vector	Status of switches		
	T_{A+}	T_{B+}	T_{C+}
U_0	1	0	0
U_{60}	1	1	0
U_{120}	0	1	0
U_{180}	0	1	1
U_{240}	0	0	1
U_{300}	1	0	1

2.12.2 Optimized PWM

This method of modulation is used to minimize the switching value to an instantaneous one by maximizing the value of flow of current. It has advantage of minimizing power loss. The disadvantage is difficulty in design and problem of proper operation of the converters because of change in frequency.
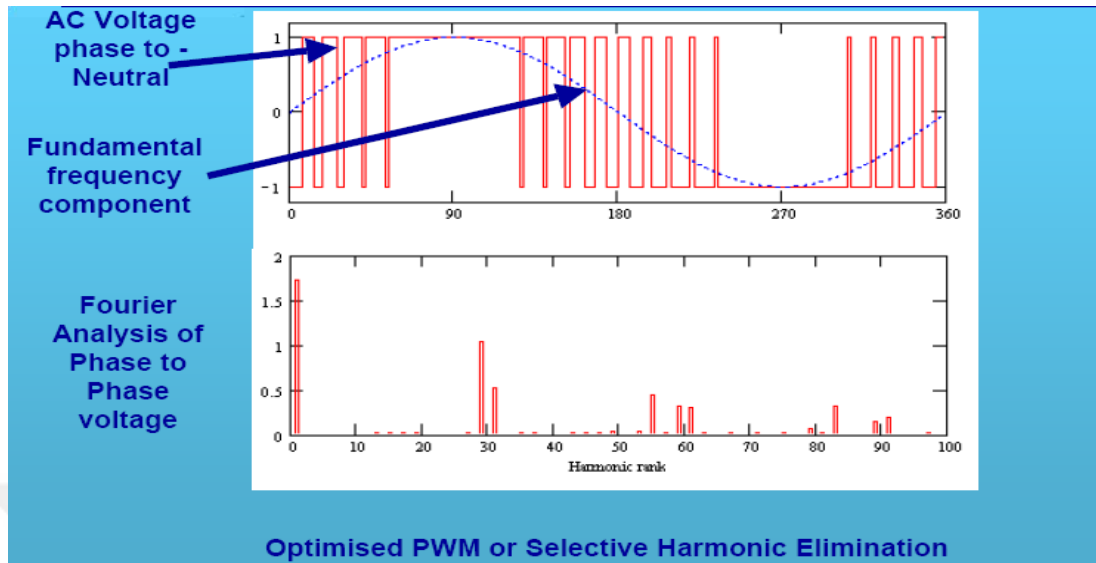
Figure 2.19 Harmonic spectrum of optimized PWM

2.12.3 Sinusoidal PWM

Sinusoidal PWM compares the sinusoidal input reference with that of instantaneous triangular waveform by generating pulse width modulated signal. The phase difference moving from 0^0-120^0-240^0 of the half cycle (180^0), for achieving out-of-phase load voltage that is an ideal waveform of SPWM. For the feature of PWM techniques the normal carrier frequency of PWM techniques, the normal carrier frequency m_f could be odd multiplier of three. The phase V_{aN}, V_{bN}, V_{cN} is identical but 120^0 out of phase without even harmonics. The harmonic frequency of 3 is identical in amplitude and phase to all phases.
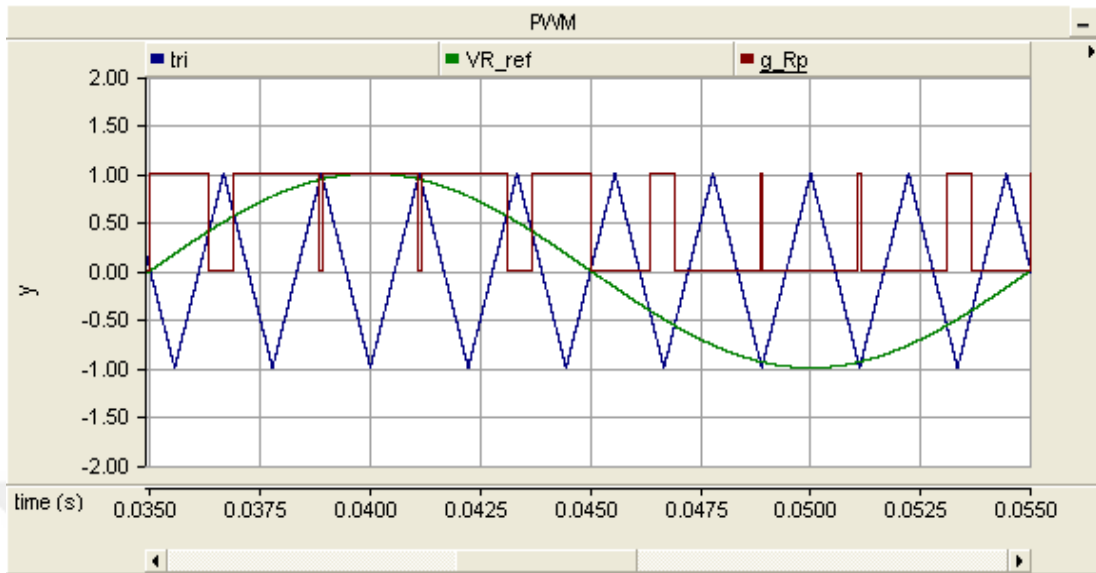
Figure 2.20 Pure SPWM

2.13 Two level and Three level Converters

Two level VSCs are the converters that have only two instantaneous AC voltage level. When converter has more than two instantaneous voltage levels, they are called multilevel converters [7].
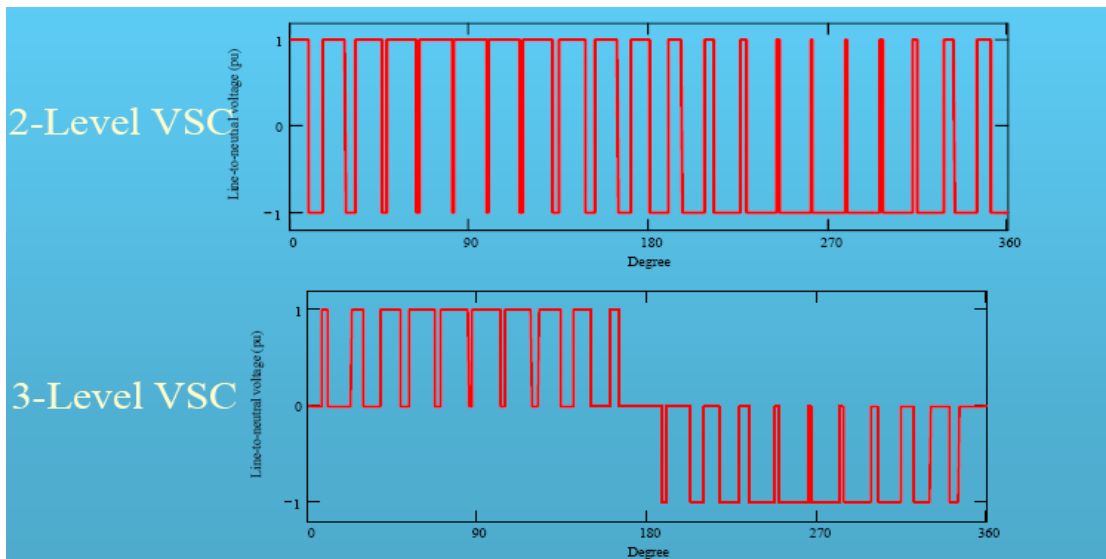
Figure 2.21 Two level and Three level switching patterns for VSC

28

2.14 Multilevel converters

The topologies for multilevel converter are:

a. Flying capacitor clamp

b. Diode clamp

c. Cascaded multiterminal converter

Figure 2.22 shows the above mentioned topologies of MMC.
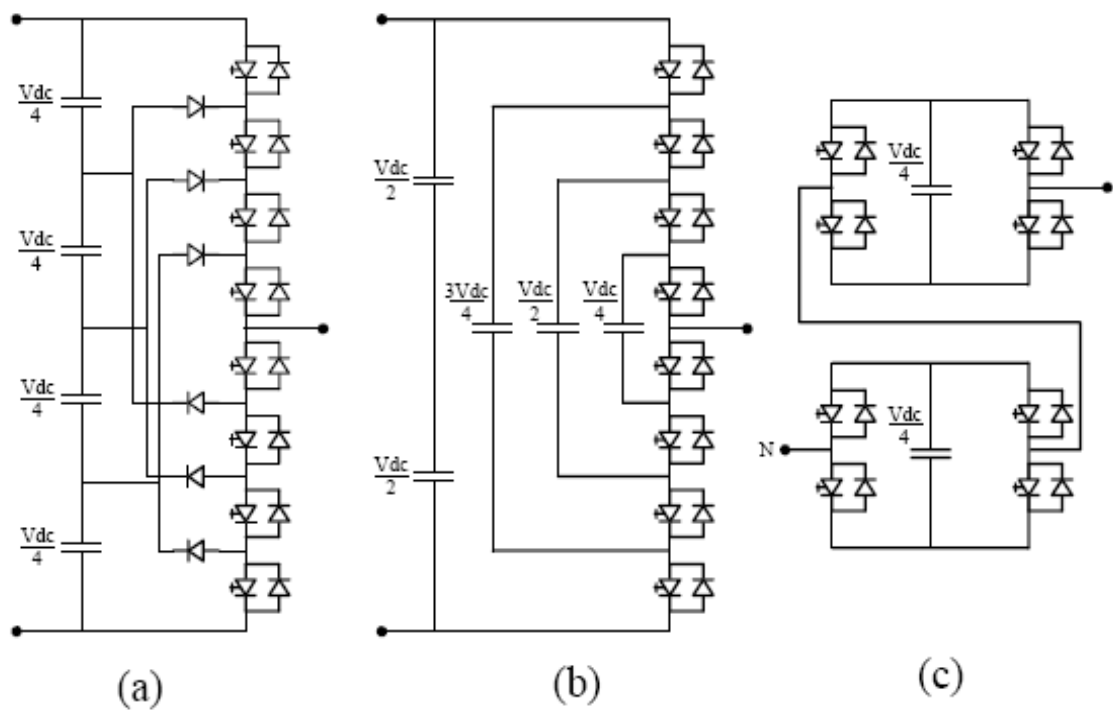
Figure 2.22 MMC topologies for (a) Diode clamp (b) Flying capacitor clamp and (c) Cascaded multiterminal converter

CHAPTER 3

DESIGN AND CONTROL OF OFFSHORE WIND FARM CONNECTED TO VSC-HVDC

3.1 Introduction

This chapter entails modeling, design and control of offshore wind farm comprising wind turbine, turbine generators (DFIG is considered in this thesis), drive train, grid side converter, rotor side converter, crowbars and other components that makeup the entire offshore wind farm. Also offshore and onshore side converters are designed for optimistic transfer of high quality power to the grid via HVDC undersea transmission cables.

3.2 Modeling of wind turbine

The mechanical power of aerodynamic model that can be obtained after wind blows is stated thus

$$P_w = \frac{1}{2} \rho \pi R^2 v^3 C_p(\theta, \lambda) \tag{3.1}$$

P_w is the wind obtainable power in (W), ρ as density of air in (kg/m^3), v is the wind speed in (m/s), R is the radius of the blade in (m), and C_p is the power coefficient which is a function of the pitch angle of rotor blades θ (deg) and of the tip speed ratio λ.
where $\lambda = \omega_w R / v$, ω_w is the wind turbine speed.
The power coefficient is computed thus

$$C_p = 0.73 \left(\frac{151}{\lambda_i} - 0.58\theta - 0.002\theta^{2.14} - 13.2 \right) . e^{-18.4/\lambda_i} \tag{3.2}$$

with

$$\frac{1}{\lambda_i} = \frac{1}{\lambda - 0.02\theta} - \frac{0.003}{\theta^3 + 1} \qquad (3.3)$$

The above three equations can be used to derive power curves for different wind speed [11][12]. The control of wind turbine is to allow ideal power factor to capture the optimum power in case of low to moderate speeds. But in higher wind speeds, pitch angle controller turns to be functional to avoid the rotor speed for being very extreme. A turbine speed at any given wind velocity obtains optimal output power.
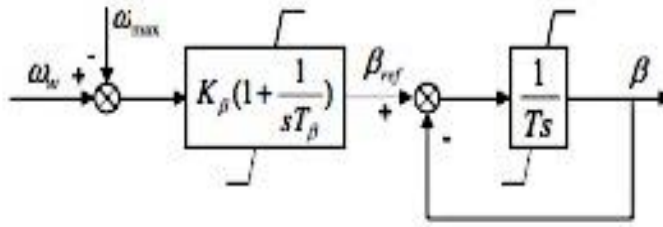
Figure 3.1 Pitch angle controller block diagram

3.2.1 Drive train Model

Two-mass drive train model is suitable for a relative analysis of wind turbine system for distinctive models of drive train [13][14]. It is described by the expression as:

$$J_w \frac{d\omega_w}{dt} = T_w - K\theta_{wg} - D(\omega_w - \omega_g) \qquad (3.4)$$

$$J_g \frac{d\omega_g}{dt} = K\theta_{wg} + D(\omega_w - \omega_g) - T_g \qquad (3.5)$$

where

T_w is wind turbine aerodynamic torque (N m)

T_g is the loading torque of the generator

J_w represent wind turbine inertia constant

J_g is generator inertia constant

θ_{wg} is the angle between generator and turbine rotor (deg)

ω_w is wind turbine speed (m/s)

ω_g is generator rotor speed (rad/ s)

D is the mutual damping between two masses (N ms/ rad)

K is the elastic characteristics of the shaft (N m/rad) [11][13]

3.3 Mathematical Modeling of DFIG

A DFIG employs a wound rotor induction generator, where the rotor winding is fed via back-to-back variable frequency VSCs. Voltage limit and an over-current 'crowbar' circuit is employed to protect the machine and converters. Decouple control of power system electrical frequency and rotor mechanical frequency is achieved through converter system providing variable speed operation of wind turbines.
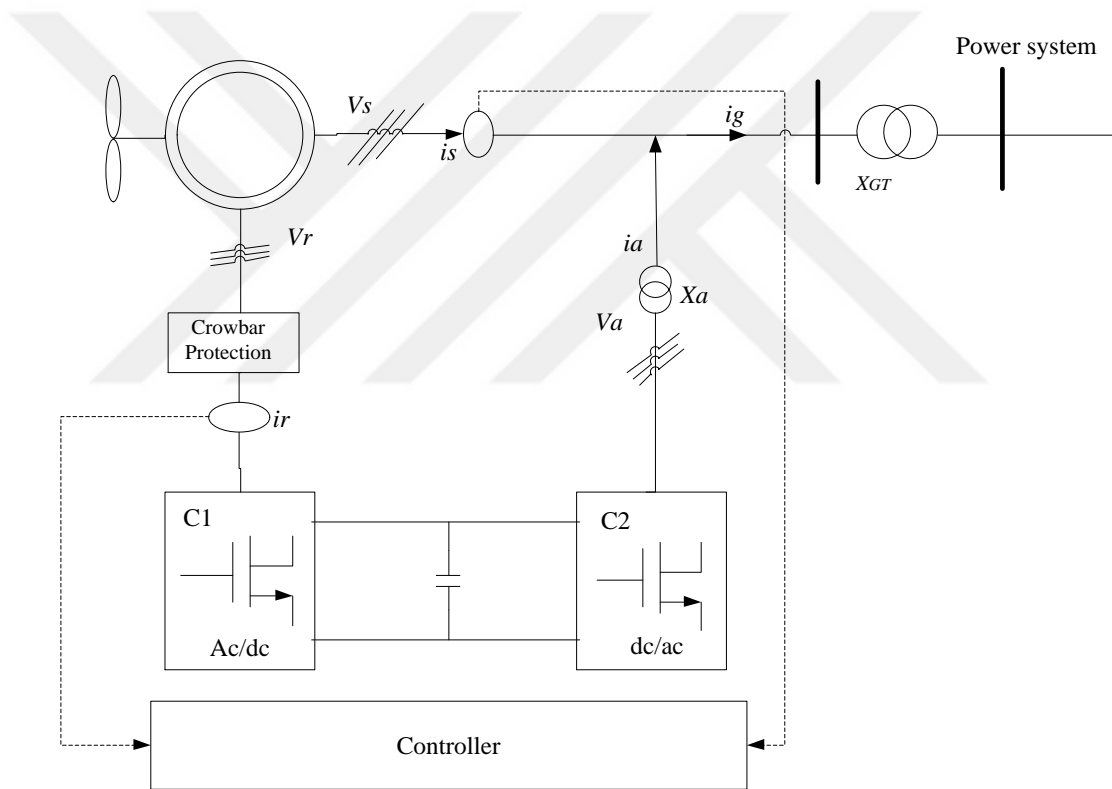
Figure 3.2 DFIG wind turbine basic configuration [15]

3.3.1 Machine modeling

The general reduce order form for DFIG machine model is implemented under the stated assumptions

- Stator current flowing toward the machine was assumed positive
- The quadrature axis assumed at 90 degree ahead of direct axis rotation direction.
- Synchronous reference frame using d-axis and q-axis representation were used to

derived the equation

- Real part of the generator bus bar voltage is equals to the stator voltage component for model initialization.

- The stator transient current has a DC component but is hereby neglected to permit for a simple basic frequency component representation

- Highest order harmonic mechanisms in the rotor-injected voltages remain ignored.

In the aim to set up DFIG modeling, model of wound rotor and squirrel cage induction machines were designed using the same technology but with non zero difference in rotor voltage. Rotor winding is star connection and its phases connected to sliding contact permitting entry to rotor current and voltages. This strategy allows operation as motor or generator independent of the rotation speed.

The general electrical model of DFIG in 3-phase reference is in the form:

$$\begin{bmatrix}[V_s]\\ [V_r]\end{bmatrix} = \begin{bmatrix}[R_s] & [I_s]\\ [R_r] & [I_r]\end{bmatrix} + \frac{d}{dt}\begin{bmatrix}[\phi_s]\\ [\phi_r]\end{bmatrix} \tag{3.6}$$

its flux equation

$$\begin{cases}[\phi_s] = L_s.\,[I_s] + M.\,[I_r]\\ [\phi_r] = M.\,[I_s] + L_r.\,[I_r]\end{cases} \tag{3.7}$$

where

$$L_s = I_s - M_s, L_r = L_r - M_r; M = \frac{3}{2}M_{sr}$$

which gives (3.8) when Concordia and park transformation in (3.6) is applied

$$\begin{cases} V_{sd} = R_s I_{sd} + \dfrac{d\phi_{sd}}{dt} - \dot{\theta}_s \phi_{sq} \\[2mm] V_{sq} = R_s I_{sq} + \dfrac{d\phi_{sq}}{dt} - \dot{\theta}_s \phi_{sd} \\[2mm] V_{rd} = R_r I_{rd} + \dfrac{d\phi_{rd}}{dt} - \dot{\theta}_r \phi_{rq} \\[2mm] V_{rq} = R_r I_{rq} + \dfrac{d\phi_{rq}}{dt} - \dot{\theta}_r \phi_{rd} \end{cases} \tag{3.8}$$

$$\begin{cases} \phi_{sd} = L_s I_{sd} + M I_{rq} \\ \phi_{sq} = L_s I_{sq} + M I_{rq} \\ \phi_{rd} = L_s I_{rd} + M I_{sd} \\ \phi_{rq} = L_s I_{rq} + M I_{sq} \end{cases} \tag{3.9}$$

The mechanical expression is

$$J \frac{d\Omega}{dt} = T_{em} - T_r \tag{3.10}$$

where T_{em} and T_r are electromagnetic torque and load torque respectively

$$T_{em} = p \frac{M}{L_s} (I_{rq} \phi_{sd} - I_{rd} \phi_{sq}) \tag{3.11}$$

we can deduce

$$\phi_{sd} = \phi_s \quad and \quad \phi_{sq} = 0 \tag{3.12}$$

$$T_{em} = p \frac{M}{L_s} I_{rd} \phi_{sd} \tag{3.13}$$

Consequently with regards to above equation, the flux equation becomes

$$\begin{cases} \phi_{sd} = L_s I_{sd} + M I_{rq} \\ 0 = L_s I_{sq} + M I_{rq} \end{cases} \tag{3.14}$$

Supposing that a system grid is steady with a single voltage Vs, leading to a constant

stator flux Q. with respect to equation (3.13), the quadrature rotor current is directly proportional to the electromagnetic torque [16][17].

Neglecting stator-winding resistance, stator voltage equations of the machine are computed thus:

$$\begin{cases} V_{sd} = \frac{d\phi_{sd}}{dt} \\ V_{sq} = \omega_s \phi_s \end{cases} \tag{3.15}$$

where ω_s is pulsation of the stator

$$\begin{cases} V_{sd} = 0 \\ V_{sq} = \omega_s \phi_s \end{cases} \tag{3.16}$$

From 3.14, a difference between stator current and rotor current is observed

$$\begin{cases} I_{sd} = \frac{-M}{L_s} I_{rd} + \frac{\phi_s}{L_s} \\ I_{sq} = \frac{-M}{L_s} I_{rq} \end{cases} \tag{3.17}$$

The active and reactive powers of the stator (P, Q) could be define as:

$$\begin{cases} P = V_{sd} I_{sd} + V_{sq} I_{sq} \\ Q = V_{sq} I_{sd} + V_{sd} I_{sq} \end{cases} \tag{3.18}$$

By assuming constant flux and recall equation 3.16, we get

$$\begin{cases} P = V_s I_{sq} \\ Q = V_s I_{sd} \end{cases} \tag{3.19}$$

Substituting equation 3.19 by its current expression, we get

$$\begin{cases} P = -V_s \frac{M}{L_s} I_{rq} + \frac{\phi_s}{L_s} \\ Q = V_s \frac{M}{L_s} I_{rd} + V_s \frac{\phi_s}{L_s} \end{cases} \tag{3.20}$$

From equation 3.15 and 3.16 we get stator flux as

$$\phi_s = \frac{V_s}{\omega_s} \tag{3.21}$$

Rewriting equation 3.20

$$\begin{cases} P = -V_s \frac{M}{L_s} I_{rq} \\ Q = -V_s \frac{M}{L_s} I_{rd} + \frac{V_s^2}{L_s \omega_s} \end{cases} \tag{3.22}$$

Magnetic inductance (*M)* is kept constant

From 3.22, at a constant close $\frac{V_s^2}{L_s \omega_s}$, active power of the stator is directly proportional to rotor current quadrature I_{rq}

Establishing a relationship between the rotor current and voltage can control machines errors.

Replacing stator current (3.9) by (3.17) we obtained rotor flux equation:

$$\begin{cases} \phi_{sd} = (L_r - M^2)I_{rd} + \frac{MV_s}{L_s \omega_s} \\ \phi_{rd} = \left[L_r - \frac{M^2}{L_s}\right] I_{rd} \end{cases} \tag{3.23}$$

From rotor flux equation in (3.23) and stator current expression in (3.9), we can obtain

$$\begin{cases} V_{rd} = R_r I_{rd} + (L_r - M^2)\frac{dI_{rd}}{dt} - S\omega_s(L_r - M^2)I_{rq} \\ V_{rq} = R_r I_{rq} + \left(L_r - \frac{M^2}{L_s}\right)\frac{dI_{rq}}{dt} - S\omega_s(L_r - M^2)I_{rq} + S\frac{MV_s}{L_s} \end{cases} \tag{3.24}$$
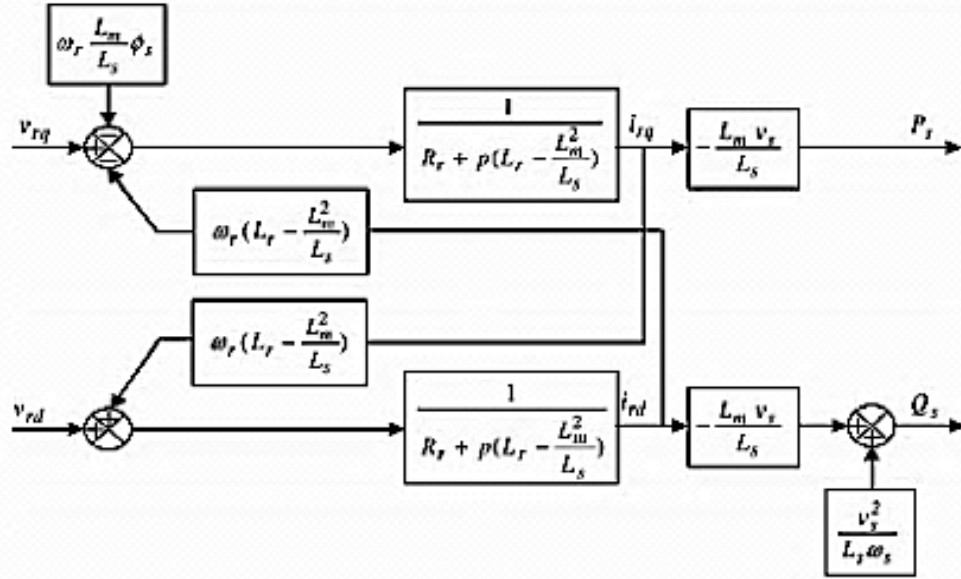
Figure 3.3 DFIG inner structures [17]

3.3.2 Modeling of DFIG converters

The DFIG converter typical block diagram, which is connected back-to-back, is shown in Figure 3.2, it consists of two VSCs. The first converter called rotor side converter generates a three-phase voltage with variable amplitude and frequency in order to control the generator torque and the power exchange between the stator and the grid. The grid side converter, which is the second converter, is employed to exchange the injected or active power obtained by the rotor side converter with the VSC at the grid side. Capacitors are placed among the converters for maintaining DC link voltage [11][18].

3.3.3 Grid side converter

This converter is a three-phase one consisting of double-pole VSC employing six IGBT switches. Grid side converter allows bi-directional power flow. It is a force-commutated converter with PWM. The current drawn by the converter from the grid is kept constant. Capacitors are placed between the converters for maintaining DC link voltage. Capacitors are evaluated by using the relation

$$C = P_{out} \frac{\sqrt{2} + \sqrt{3} V_{L-L\,rms}/V_{DC}}{2\sqrt{2} f_s V_{L-L\,rms} \Delta V_{DC}} \qquad (3.25)$$

where ΔV_{DC}, f_s, $V_{L-L\,rms}$ and V_{DC} are the ripple in the DC link voltage, sampling frequency, line-to-line rms voltage and link voltage respectively.

A current control strategy is employed as grid side converter control. It comprises of two control loops, the inner current loop and the outer current loop. The inner current loop ensures grid reactive power and the outer current loop keeps the DC voltage to a continuous value. PI processes the error signal. PI controller output is compared to the actual current element of the VSC. Also, grid reactive power and reactive current element of the inverter are compared and their error values are computed using this controller. Reference values of *d-q* and *abc* frames are converted using voltage input reference. Then the modulation index is computed at the PI controller output. The converter AC terminals and the machine stator are linked via transformer. SVPWM receives its reference signal from PI controller to produce pulses to the grid side converter controls [18].

We can deduce the voltage passing through reactor as

$$\begin{bmatrix} v_a \\ v_b \\ v_c \end{bmatrix} = R \begin{bmatrix} i_a \\ i_b \\ i_c \end{bmatrix} + L\frac{d}{dt}\begin{bmatrix} i_a \\ i_b \\ i_c \end{bmatrix} + \begin{bmatrix} v_{a1} \\ v_{b1} \\ v_{c1} \end{bmatrix} \tag{3.26}$$

in $d-q$ transformation is given below taking $[T]$ as the transformation matrix

$$\begin{bmatrix} v_d \\ v_q \\ v_0 \end{bmatrix} = [T]\begin{bmatrix} v_a \\ v_b \\ v_c \end{bmatrix} \tag{3.27}$$

now

$$[T] = \begin{bmatrix} \cos\rho & -\sin\rho & \frac{1}{2} \\ \cos\left(\rho - \frac{2\pi}{3}\right) & -\sin\left(\rho - \frac{2\pi}{3}\right) & \frac{1}{2} \\ \cos\left(\rho - \frac{2\pi}{3}\right) & -\sin\left(\rho - \frac{2\pi}{3}\right) & \frac{1}{2} \end{bmatrix} \tag{3.28}$$

also

$$v_d = Ri_d + \frac{L di_d}{dt} - \omega_e L i_q + v d_1 \qquad (3.29)$$

and

$$v_q = Ri_q + \frac{L di_q}{dt} - \omega_e L i_d + v q_1 \qquad (3.30)$$

where ω_e is the grid frequency and ρ is transformation angle for PLL.

Computing the control equations when reference voltages are associated with constant reference rotating frames yield:

$$v_{d1}^* = -v_d' + (\omega_e L i_q + v_d) \qquad (3.31)$$

and

$$v_{q1}^* = -v_q' - (\omega_e L i_d) \qquad (3.32)$$

The terms with asterisk and bars are the figured references and Proportional Integrator (PI) regulator outputs respectively. Bracket terms are the cross coupling between reference frame axes.
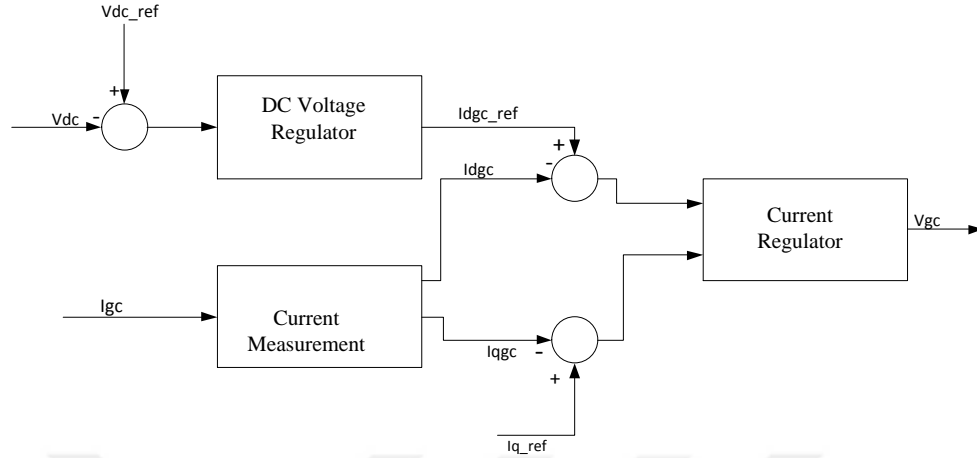
Figure 3.4 Grid side converter control structure [10]

3.3.4 Rotor side converter (RSC)

The control of power in the stator is achieved by the rotor side converter (RSC). Reference signal is generated to control stator power, which depends on the power reference. [18][19]. Vector control technique is used for RSC control. Field-oriented control (FOC) is used for rotor side converter control, which later modified to direct power control (DPC). The DPC is based on direct control of active and reactive power of DFIG stator that is determined by the following current and voltage equation:

.

$$P_s = \frac{3}{2} R_e \{\overrightarrow{V_s} . \overrightarrow{I_s}\} \tag{3.33}$$

$$Q_s = \frac{3}{2} I_m \{\overrightarrow{V_s} . \overrightarrow{I_s}\} \tag{3.34}$$

The above equations respectively represent active and reactive power. I_s and V_s are stator component of current and voltage. Using $d - q$ transformation of voltage and current, stator active and reactive power were calculated thus:

$$P_s = \frac{3}{2} (V_{ds} . i_{ds} + V_{qs} . i_{qs}) \tag{3.35}$$

and

$$Q_s = \frac{3}{2}(V_{qs} \cdot i_{ds} + V_{ds} \cdot i_{qs}) \tag{3.36}$$

Active and reactive power of the stator from equation (3.33) and (3.34) are compared by their reference values and the error is processed with PI controller to generate a dq component of grid voltage reference. This grid voltage reference is then transformed into abc reference frame, which gives a three-phase voltage reference given to space vector modulation system of the rotor side.

The $d - q$ variables conversion is done using DFIG slip speed as

$$S = \frac{\omega_s - \omega_r}{\omega_s} \tag{3.37}$$

the rotor voltage

$$V_{dr} = S.V_{ds} \tag{3.38}$$

and stator voltage

$$V_{ds} = S.V_{qs} \tag{3.39}$$

By integrating the expression for the rate of change of flux, the stator flux orientation Φ_s is given by

$$\begin{bmatrix} V_{sa} \\ V_{sb} \\ V_{sc} \end{bmatrix} = \frac{d}{dt}\begin{bmatrix} \lambda_{sa} \\ \lambda_{sb} \\ \lambda_{sc} \end{bmatrix} + \begin{bmatrix} i_{sa} \\ i_{sb} \\ i_{sc} \end{bmatrix}\begin{bmatrix} R_{sa} \\ R_{sb} \\ R_{sc} \end{bmatrix} \tag{3.40}$$

The instantaneous orientation of stator flux

$$\Phi_s = \tan^{-1}\frac{\lambda_{\beta s}}{\lambda_{\alpha s}} = \tan^{-1}\frac{\int(V_{\alpha s} - R_s i_{\alpha s})}{\int(V_{\beta s} - R_s i_{\beta s})} \tag{3.41}$$

$$\omega_s = \frac{d\theta_s}{dt} \tag{3.42}$$

$$\lambda = \sqrt{\lambda_{\alpha s}{}^2 + \lambda_{\beta s}{}^2} \tag{3.43}$$

where

$\lambda_{\beta s}, \lambda_{\alpha s}$ are the $\alpha - \beta$ transform of stator flux

$V_{\alpha s}, V_{\beta s}$ are the $\alpha - \beta$ transform of the stator voltage

$i_{\beta s}, i_{\alpha s}$ are the $\alpha - \beta$ transform of the stator current [19]
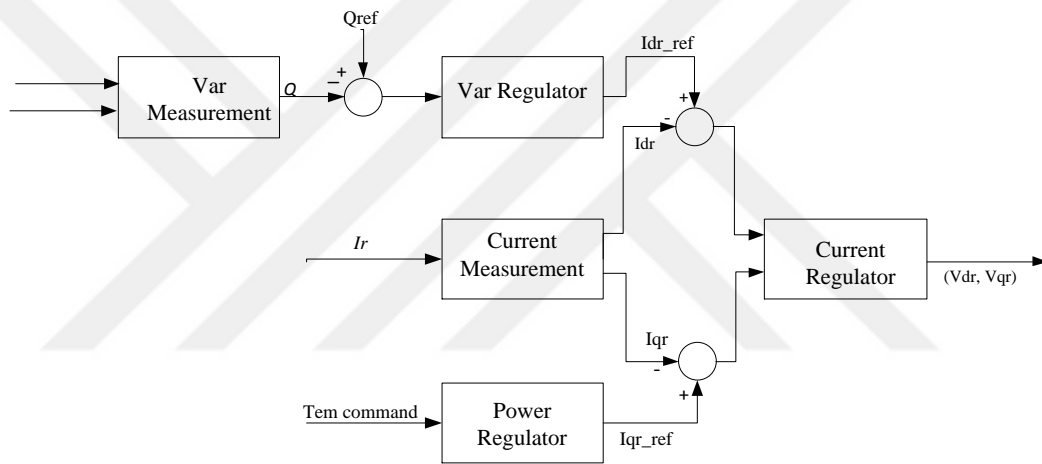
Figure 3.5 Rotor side converter control structure [10]

3.4 DFIG-grid connection

For better accuracy and performance, DFIG generator is connected to the grids by coordinating reference variables of DFIG and the grid ΔV_s and ΔI_s. This strategy applies only when wind farms are connected directly to an infinite AC system where the generated power is automatically absorbed by the source. The grid reference variable is the infinite bus voltage angle. It is possible through the use of dq to DQ reference frame linearized transformation.. There is no extra frequency or active power control loops are required. Whether the power is active or reactive, there is no effect on VSC control system based offshore wind farm.

Traditionally, control of DFIG wind turbine system comprises two strategies.

1.   Stator flux-oriented vector control.

2.   Stator voltage-oriented vector control.

This strategy decouples the rotor current into active and reactive power components. The control of these components is achieved by the use of current controller. For the grid side converter, the aim is to control DC link voltage [20].

3.5 DFIG-WFVSC coordination

One of the basic objectives of wind farm side converter is to collect power from wind farm. Due to the fact that power electronic converter controls output power from DFIG's, its frequency variation has small impact on power generation. As a result, variation in frequency and change in active power have no strong response to local wind farm network. For simplicity of system control design, wind farm VSC is designed in such a way that it represents an infinite voltage source having constant frequency, phase angle and voltage amplitude [21]. The schematic diagram of the proposed control strategy for WFVSC is shown in Figure 3.6.
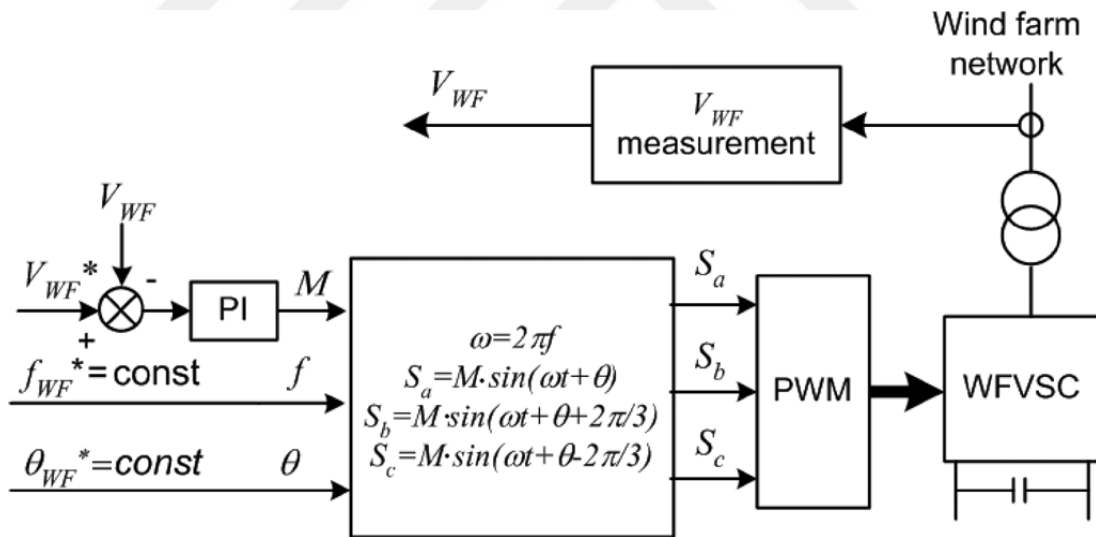
Figure 3.6 Wind farm side VSC control block diagram [21]

3.6 Grid side VSC (GSVSC)

The operation of GSVSC based HVDC is similar to VSC transmission connecting two conventional AC systems. It serves as DC voltage controller that maintains a constant DC link between two converter networks. The equivalent AC and DC circuit of GSVSC are illustrated in Figure 3.7. AC side system in synchronous d-q reference frame rotating

at a speed of ω_s when the d-axis is fixed to the sources voltage V_s is:

$$\frac{d}{dt}\begin{bmatrix} i_{sd} \\ i_{sq} \end{bmatrix} = [A]\begin{bmatrix} i_{sd} \\ i_{sq} \end{bmatrix} + \frac{1}{L}\begin{bmatrix} -V_{sd} + V_{cd} \\ -V_{sq} + V_{cq} \end{bmatrix} \tag{3.44}$$

where

$$[A] = \begin{bmatrix} -\frac{R}{L} & \omega_s \\ -\omega_s & -\frac{R}{L} \end{bmatrix} \tag{3.45}$$

By using power balancing, DC side equation is computed thus:

$$P_{ac} = \frac{3}{2}\left(V_{cd}\cdot i_{sd} + V_{cq}\cdot i_{sq}\right) \tag{3.46}$$

where $P_{dc} = I_{dc}\cdot V_{dc}$

$$I_{dc}\cdot V_{dc} = \frac{3}{2}\left(V_{cd}\cdot i_{sd} + V_{cq}\cdot i_{sq}\right) + c\frac{dV dc}{dt}\cdot V_{dc} \tag{3.47}$$

using PWM technique, amplitude voltage

$$V_c = M\cdot\frac{V_{dc}}{2} \tag{3.48}$$

where M is the modulation index.

The two complex systems of AC and DC can be combined thus

$$\frac{d}{dt}\begin{bmatrix} i_{sd} \\ i_{sq} \end{bmatrix} = [A]\begin{bmatrix} i_{sd} \\ i_{sq} \end{bmatrix} - \frac{1}{L}\begin{bmatrix} V_{sd} \\ V_{sq} \end{bmatrix} + \frac{V_{dc}}{2L}\begin{bmatrix} M_d \\ M_q \end{bmatrix} \tag{3.49}$$

$$\frac{dV_{dc}}{dt} = \frac{1}{C}\cdot I_{dc} - \frac{3}{4C}\left(M_d\cdot i_{sd} + M_q\cdot i_{sq}\right) \tag{3.50}$$

$$d\text{-axis modulation index } M_d = 2.\frac{V_{cd}}{V_{dc}}$$

$$q\text{-axis modulation index } M_q = 2.\frac{V_{cq}}{V_{dc}}$$

In the above expression state variables and inputs are non-linear. GSVSC operation requires i_{sd} and i_{sq} to follow varying reference points, while DC voltage V_{dc} is maintained at a predetermined value. An inner current loop and outer voltage control loop provides the desired control for current and DC voltage. The loops interaction is restricted by its dynamic separation [21].

(a)   (b)
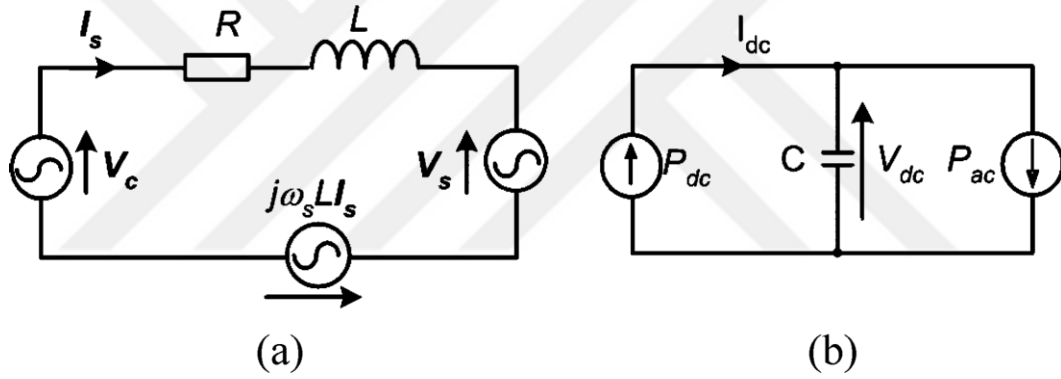
Figure 3.7 Grid side VSC equivalent circuit [21]

The current control loop auxiliary input is defined as

$$\begin{bmatrix} V_d \\ V_q \end{bmatrix} = \begin{bmatrix} di_{sd}/dt \\ di_{sq}/dt \end{bmatrix} \tag{3.51}$$

The controller is implemented as

$$u_d = \frac{di_{sd}}{dt} = K_p 1(i_{sd}^* - i_{sd}) + K_i 1 \int (i_{sd}^* - i_{sd})dt \tag{3.52}$$

$$u_q = \frac{di_{sq}}{dt} = K_p 1(i_{sq}^* - i_{sq}) + K_i 1 \int (i_{sq}^* - i_{sq}) dt \tag{3.53}$$

i_{sd} and i_{sq} are independently controlled by u_d and u_q respectively

$K_p 1$ and $K_i 1$ are the current controller gains

Controller variables modulation index references M_d and M_q are expressed thus

$$M_d = \frac{2L}{V_{dc}} \left(u_d + \frac{R}{L} i_{sd} - \omega_s . i_{sq} + \frac{1}{L} V_{sd} \right) \tag{3.54}$$

$$M_q = \frac{2L}{V_{dc}} \left(u_q + \frac{R}{L} i_{sq} - \omega_s . i_{sd} + \frac{1}{L} V_{sq} \right) \tag{3.55}$$

The design for the DC voltage controller is implemented thus

$$i_e = \frac{dV_{dc}}{dt} = K_p 2(V_{dc}^* - V_{dc}) + K_i 2 \int (V_{dc}^* - V_{dc}) dt \tag{3.56}$$

$K_p 2$ is the proportional gain of DC voltage controller

$K_i 2$ is the integral gain of DC voltage controller

The current reference i_{sd}^* d-axis component is computed thus

$$i_{sd}^* = \frac{4C}{3M_d} \left(-i_e + \frac{1}{C} I_{dc} - \frac{3}{4C} M_q . i_{sq} \right) \tag{3.57}$$

i_{sq}^* is either reactive power control or AC voltage control reference, and the reactive power output from grid side converter is assumed by quadrature axis (q- axis) current [21].
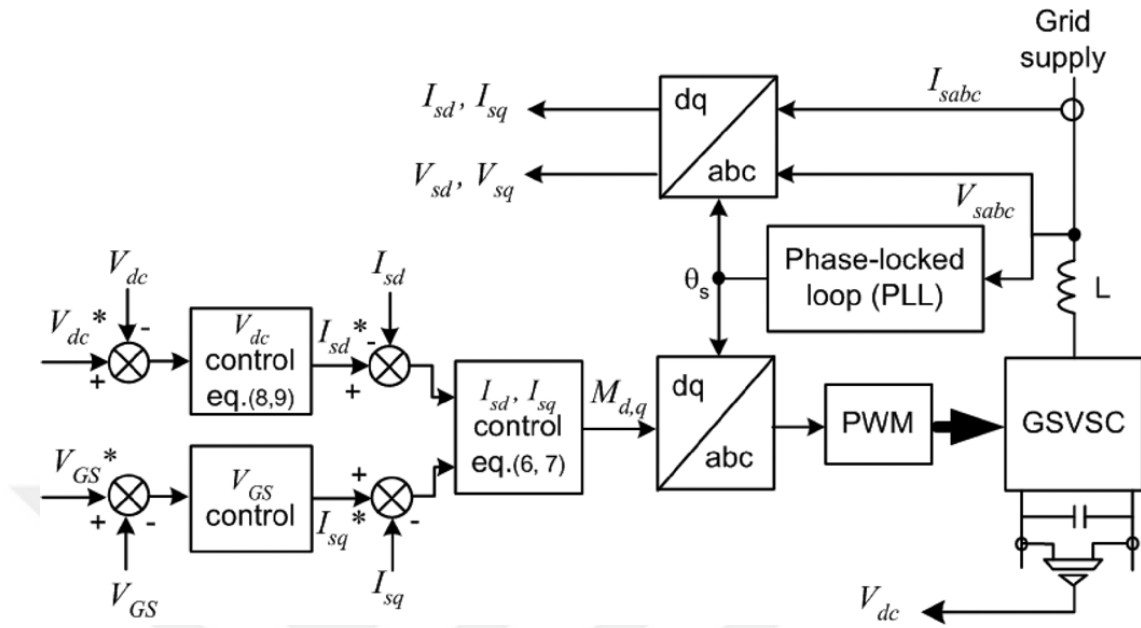
Figure 3.8 Grid side VSC control block diagram [21]

CHAPTER 4

DESIGN AND CONTROL SYSTEM OF VSC-HVDC

4.1 Introduction

This chapter considers more on designing VSC-HVDC. VSCs have unlimited collections of usages extending from slight electrical energy system to HVDC transmission system. Thyristor-based converter also called LCC has firing angle (α) as its degree of freedom. Normally VSCs have two-degree of freedom, i.e. the phase displacement (φ) and the amplitude modulation index (m_a). The number of specified variable is referred to as degree of freedom. [22].

4.2 VSC-HVDC design

A three level VSC with space vector PWM is considered in this work. The VSC configuration is an arrangement of single IGBTs and diodes components connected in parallel. The configuration is illustrated in Figure 4.1.
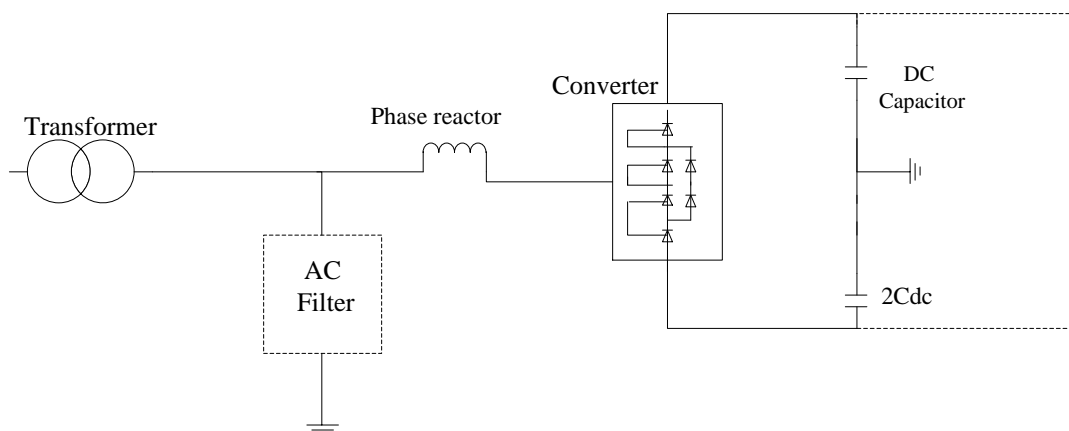
Figure 4.1 VSC-HVDC configuration [22]

4.2.1. AC Filters

The filters used in this model are high pass filters that are shunt connected with PWM frequency order arrangement. They are reactive power and AC current limiting circuit against harmonics.
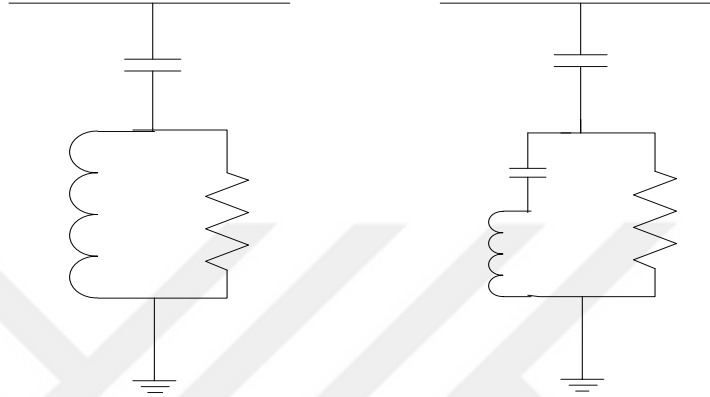
Figure 4.2 Filters (High Pass Filters) [22]

4.2.2. L filter (Current smoothing inductance)

Series inductance is used for smoothening of phase current. It is configured as:

$$L = Max(\frac{V_h}{h\omega_o I_h}) \quad\quad\quad (4.1)$$

where

I_h is the harmonic current

V_h is harmonic voltage

h is the number of harmonics.

4.2.3. Transformer

They are designed based on the function they performed in a system. Transformers can connect two single converters that are of different DC potentials. They are connected between converters and AC systems and are used to step up or step down the voltage to a suitable value for the converters.

4.2.4. Phase reactors

Active and reactive power control circuit by limiting the current through them and minimizing harmonic frequency in a VSC based HVDC transmission.

4.2.5. DC capacitors

Current harmonics occurs at the DC side of VSC because of the use of PWM. These harmonic current create ripple. Therefore, the use of shunt-connected capacitors gives a smoother DC voltage by filtering out this ripple. A time constant is the ratio between capacitor storage energy at rated DC voltage and the rated apparent power [22]. Mathematically:

$$\tau = \frac{C{U_{DC}}^2}{2S_n} \qquad (4.2)$$

where

C is the DC capacitance in μF

U_{DC} is the DC voltage in KV

S_n is the rated power in MVA

The above formula can be used to determine the value of the DC capacitor

4.2.6 DC Cables

When modeling a DC cable, shunt capacitance and resistance are ignored. Only series resistance is model as lumped resistive element. Series inductance is also ignored.

4.3 VSC- HVDC controller design

4.3.1 Phase Lock Loop

The Phase Lock Loop circuit is provided to ensure that the local oscillator (voltage controlled oscillator) is in same phase and frequency with a reference sinusoidal input. This is achieved by detecting the frequency and phase at a reference point. Since the VSC-HVDC is connected to an active AC system, the converter should be synchronized accordingly [25].
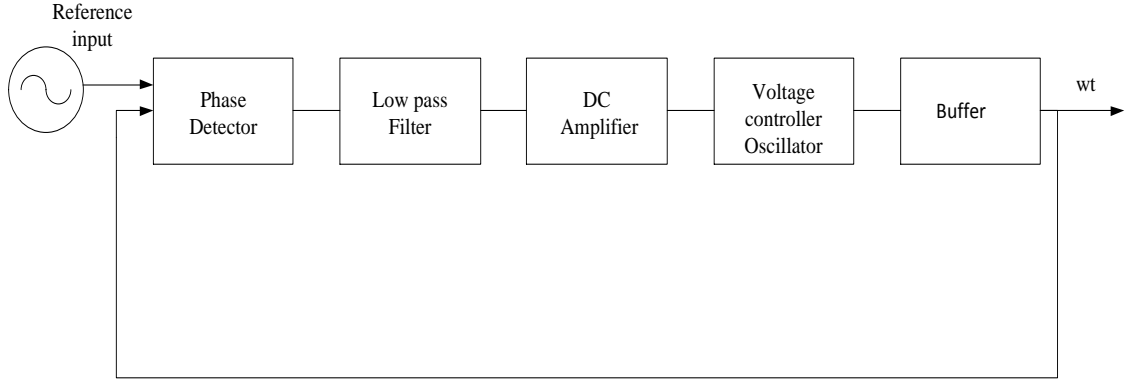
Figure 4.3 PLL block diagram [25]

In Figure 4.7 PLL circuit is implemented in DQZ form
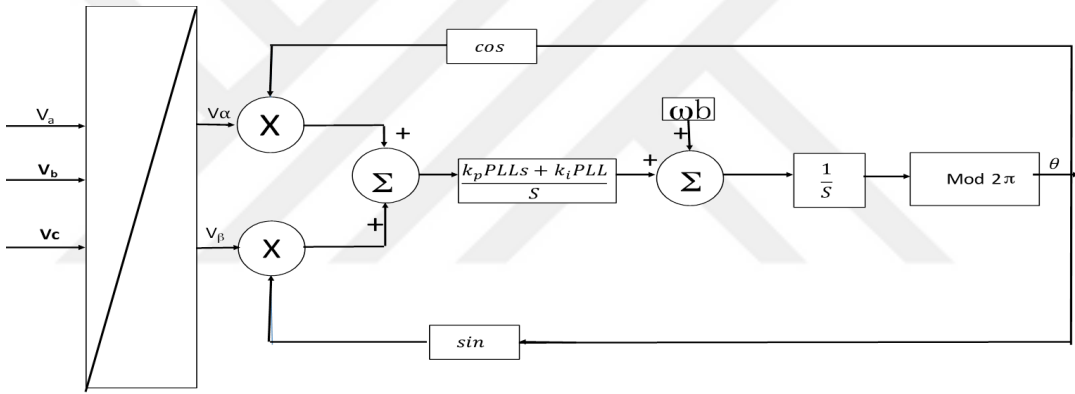
Figure 4.4 DQZ type PLL circuit [22]

4.3.2 Synchronous *d-q* Reference Frame

The decouple control of active power and reactive power flows is derived by synchronous rotating $d - q$ reference frame [25][26][27]. A three-phase balanced system is considered.

Mathematically,

$$X_a + X_b + X_c = 0 \tag{4.3}$$

Using Clark transformation equation:

$$X_{\alpha\beta} = X_\alpha + jX_\beta = kX_a + X_b e^{j\frac{2\pi}{3}} + X_c e^{j\frac{4\pi}{3}} \tag{4.4}$$

51

where k is a constant and X represent phase voltage
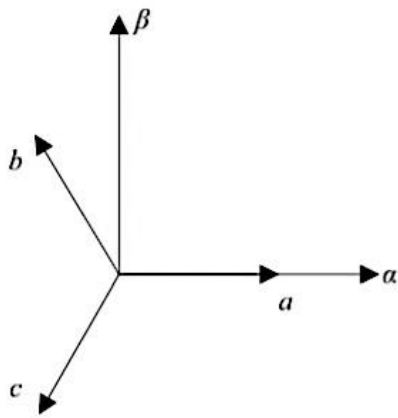
Figure 4.5 abc to α-β reference frame [25]

In matrix form

$$\begin{bmatrix} X_\alpha \\ X_\beta \end{bmatrix} = k \begin{bmatrix} 1 & \frac{-1}{2} & \frac{-1}{2} \\ 0 & \frac{\sqrt{3}}{2} & \frac{-\sqrt{3}}{2} \end{bmatrix} \begin{bmatrix} X_a \\ X_b \\ X_c \end{bmatrix} \tag{4.5}$$

by Park transformation

$$X_{dq} = X_{\alpha\beta} e^{-j\theta} \tag{4.6}$$

in extended matrix form

$$\begin{bmatrix} X_d \\ X_q \end{bmatrix} = \begin{bmatrix} \cos\theta & \sin\theta \\ -\sin\theta & \cos\theta \end{bmatrix} \begin{bmatrix} X_\alpha \\ X_\beta \end{bmatrix} \tag{4.7}$$
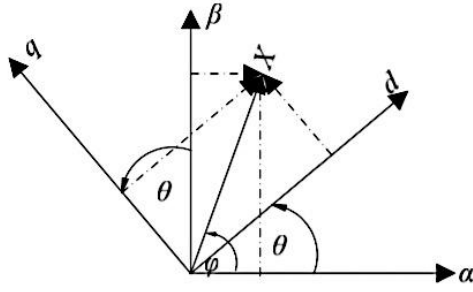
Figure 4.6 Rotating (*d-q*) and Stationary (*α-β*) reference frame [27]

when converting directly gives

$$\begin{bmatrix} X_\alpha \\ X_\beta \end{bmatrix} = k \begin{bmatrix} \cos\theta & \cos\left(\theta - \frac{2\pi}{3}\right) & \cos\left(\theta + \frac{2\pi}{3}\right) \\ -\sin\theta & -\sin\left(\theta - \frac{2\pi}{3}\right) & -\sin\left(\theta + \frac{2\pi}{3}\right) \end{bmatrix} \begin{bmatrix} X_a \\ X_b \\ X_c \end{bmatrix} \tag{4.8}$$

where θ is the angle of transformation

Substituting for current and voltage phasors;

$$\begin{bmatrix} V_\alpha \\ V_\beta \end{bmatrix} = k \begin{bmatrix} \cos\theta & \cos\left(\theta - \frac{2\pi}{3}\right) & \cos\left(\theta + \frac{2\pi}{3}\right) \\ -\sin\theta & -\sin\left(\theta - \frac{2\pi}{3}\right) & -\sin\left(\theta + \frac{2\pi}{3}\right) \end{bmatrix} \begin{bmatrix} V_a \\ V_b \\ V_c \end{bmatrix} \tag{4.9}$$

$$\begin{bmatrix} i_\alpha \\ i_\beta \end{bmatrix} = k \begin{bmatrix} \cos\theta & \cos\left(\theta - \frac{2\pi}{3}\right) & \cos\left(\theta + \frac{2\pi}{3}\right) \\ -\sin\theta & -\sin\left(\theta - \frac{2\pi}{3}\right) & -\sin\left(\theta + \frac{2\pi}{3}\right) \end{bmatrix} \begin{bmatrix} i_a \\ i_b \\ i_c \end{bmatrix} \tag{4.10}$$

when $k = \sqrt{2/3}$,

Power invariant transformation matrix

$$\begin{bmatrix} X_\alpha \\ X_\beta \end{bmatrix} = \sqrt{\frac{2}{3}} \begin{bmatrix} \cos\theta & \cos\left(\theta - \frac{2\pi}{3}\right) & \cos\left(\theta + \frac{2\pi}{3}\right) \\ \sin\theta & \sin\left(\theta - \frac{2\pi}{3}\right) & \sin\left(\theta + \frac{2\pi}{3}\right) \end{bmatrix} \begin{bmatrix} X_a \\ X_b \\ X_c \end{bmatrix} \tag{4.11}$$

inverse matrix thus:

$$\begin{bmatrix} X_a \\ X_b \\ X_c \end{bmatrix} = \sqrt{\frac{2}{3}} \begin{bmatrix} \cos\theta & -\sin\theta \\ \cos\left(\theta - \frac{2\pi}{3}\right) & -\sin\left(\theta - \frac{2\pi}{3}\right) \\ \cos\left(\theta + \frac{2\pi}{3}\right) & -\sin\left(\theta + \frac{2\pi}{3}\right) \end{bmatrix} \begin{bmatrix} X_\alpha \\ X_\beta \end{bmatrix} \tag{4.12}$$

when $k=2/3$

Matrix transformation is obtained thus

$$\begin{bmatrix} X_\alpha \\ X_\beta \end{bmatrix} = \frac{2}{3} \begin{bmatrix} \cos\theta & \cos\left(\theta - \frac{2\pi}{3}\right) & \cos\left(\theta + \frac{2\pi}{3}\right) \\ -\sin\theta & -\sin\left(\theta - \frac{2\pi}{3}\right) & \sin\left(\theta + \frac{2\pi}{3}\right) \end{bmatrix} \begin{bmatrix} X_a \\ X_b \\ X_c \end{bmatrix} \tag{4.13}$$

and inverse matrix

$$\begin{bmatrix} X_a \\ X_b \\ X_c \end{bmatrix} = \begin{bmatrix} \cos\theta & -\sin\theta \\ \cos\left(\theta - \frac{2\pi}{3}\right) & -\sin\left(\theta - \frac{2\pi}{3}\right) \\ \cos\left(\theta + \frac{2\pi}{3}\right) & -\sin\left(\theta + \frac{2\pi}{3}\right) \end{bmatrix} \begin{bmatrix} X_\alpha \\ X_\beta \end{bmatrix} \tag{4.14}$$

4.4 Control strategy

The VSC based HVDC control is established by two controllers:

- Inner current controller and
- Outer controller.

Inner current controller is used to control AC current while outer controllers supply its reference values. The outer controllers are:

- Active power controller
- Reactive power controller and
- DC voltage controller

The active power and DC voltage controllers provide reference values of active current while AC voltage and reactive power controllers provide reference values of reactive

current. Steady state errors for these controllers are removed using integrators. In this strategy, one converter controls the DC voltage to attain power stability. The other converter can set a value of any active power within the limit for the system [23].
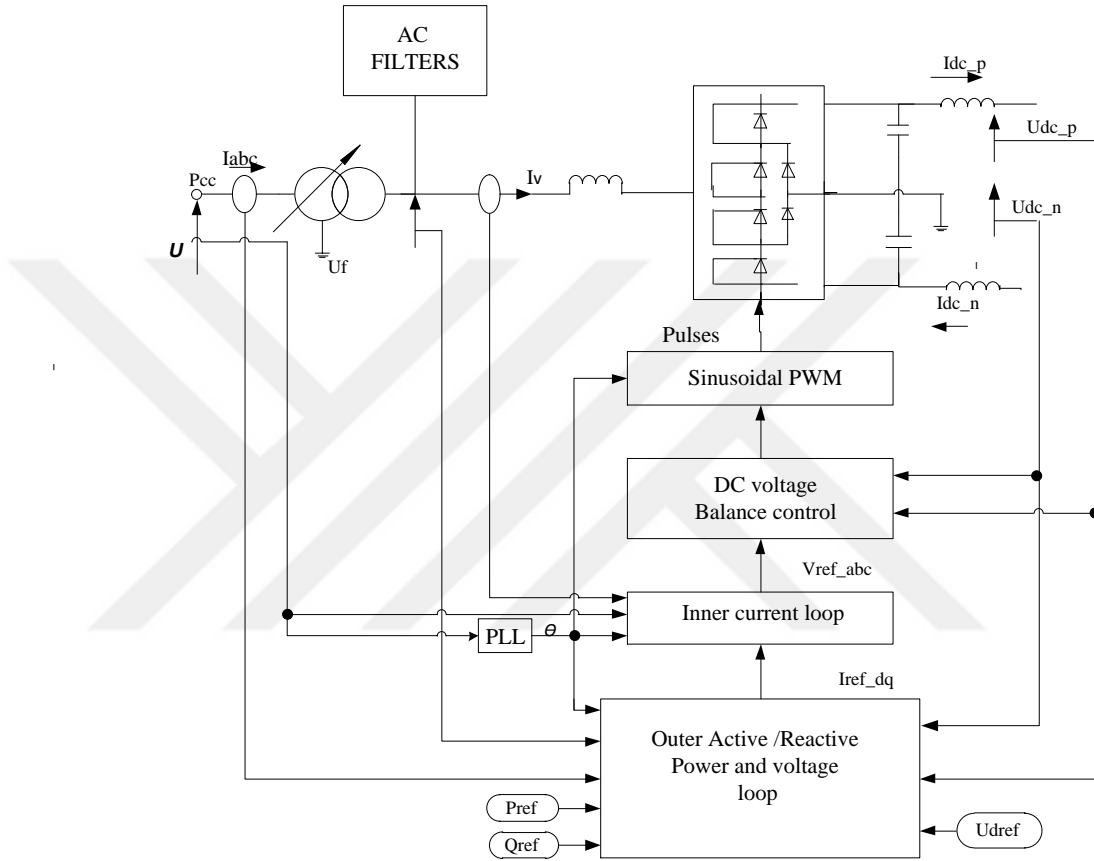
Figure 4.7 Control system of VSC [24]

4.4.1 The inner current controller

The objective of this controller is to follow the reference values of AC current assigned by the outer controllers, then generates voltage references U_d and U_q and fed to voltage controller as shown in Figure 4.8. It is implemented in the $d - q$ reference frame [23]. From Figure 4.8,

$$V = L\frac{d}{dt}i + U \tag{4.15}$$

transformed into Laplace yields

$$V = sLi + U \tag{4.16}$$

in *dq*-component

$$V_d = sLi_d - wLi_d + U_d \tag{4.17}$$

$$V_q = sLi_q + wLi_d + U_q \tag{4.18}$$

where

i is the current flowing at the AC side of the converter,

V is the common bus voltage,

U is the converter-generated voltage,

L is phase reactor leakage inductance,

S is the Laplace operator,

i_d *and* i_q are the *d*-axis and *q*-axis component of current flowing at the AC side of the converter,

U_d and U_q are the *d*-axis and *q*-axis component of the voltage generated by the converter,

V_d *and* V_q are the *d*-axis and *q*-axis component of the common base voltage [23].
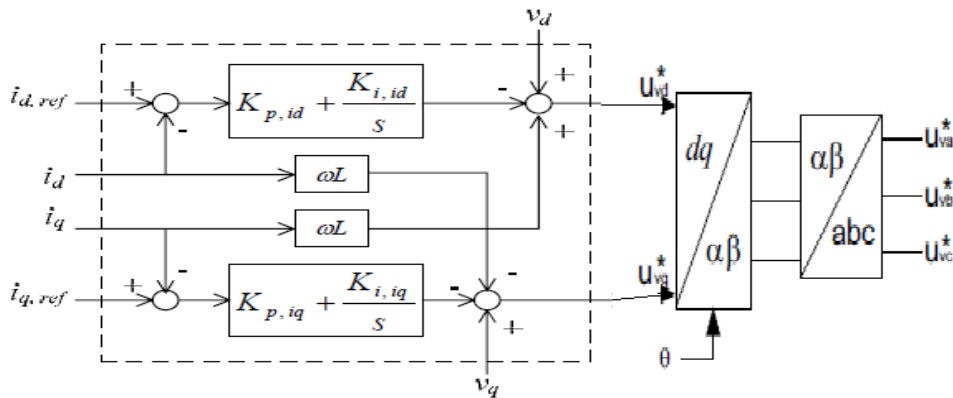
Figure 4.8 Inner current controller [23]

4.4.2 The outer controllers

4.4.2.1 DC voltage controller

The instantaneous active and reactive power transmitted in three-phase system and the power transmitted on the side of the VSC are expressed in *d-q* frame as

$$P(t) = V_d(t) * i_d(t) \tag{4.19}$$

$$Q(t) = -V_d(t) * i_q(t) \tag{4.20}$$

$$P_{dc} = U_{dc} * i_{dc} \tag{4.21}$$

Neglecting the losses in the phase reactor and converter, the power on the DC and AC sides of the converter using the above equations [23]

$$i_{dc} = \frac{V_d(t)*i_d(t)}{U_{dc}} \tag{4.22}$$

Any unbalance between AC and DC power leads to change in voltage over the DC link capacitor.

$$C_{dc}\frac{d}{dt}(Udc) = i_{dc} - i_i \tag{4.23}$$

where i_i is the current through the DC cable

The control structure for DC voltage is shown in Figure 4.9.

$$\frac{C_{dc}}{T_s}\{U_{dc}^*(k) - U_{dc}^*(k)\} = i_{dc}(k) - i_i(k) \tag{4.24}$$

Substituting the equation (4.22) in (4.24)

$$\frac{C_{dc}}{T_s}\{U_{dc}^*(k) - U_{dc}^*(k)\} = \left(\frac{V_d(k)*i_d^*(k)}{U_{dc}(k)}\right) - i_i(k) \tag{4.25}$$

Finally from the control equation for the current reference $i_d^*(k)$ is

$$i_d^*(k) = K_{dcp}\{U_{dc}^*(k) - U_{dc}^*(k)\} + k_i i_i(k) \tag{4.26}$$

where

$$K_{dcp} = K_{dcpf} * \frac{U_{dc}(k)}{V_d(k)} * \frac{C_{dc}}{T_s} \tag{4.27}$$

$$k_1 = \frac{U_{dc}(k)}{V_d(k)} \tag{4.28}$$

By integrating between KT_s and $(K + 1)T_s$ and dividing by T_s, assuming that the average value of i_{dc} and i_i are constant during the interval and that the DC voltage tracks the reference equation is [23].
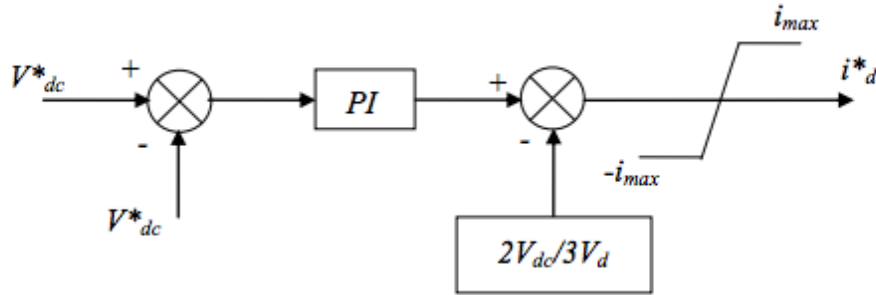
Figure 4.9 Structure of DC voltage control [25]

4.4.2.2 Active power controller

An open loop control is the easiest way to control active power. Active current references is found thus:

58

$$i_{dref} = \frac{P}{V_d} \qquad\qquad (4.29)$$

where *P* is the desired active power.

To develop more accurate control, an open loop and a feedback loop control are used together and their configuration is shown in Figure 4.10 [23].

4.4.2.3 Reactive power controller

An open loop control is a simple method for reactive power control. Its reference current is found thus:

$$i_{qref} = \frac{Q}{V_d} \qquad\qquad (4.30)$$

where *q* is the desired reactive power.

If more accurate control is needed then a feedback loop and an open loop control is used. The control structure of active and reactive power is shown in Figure 4.10 [23].
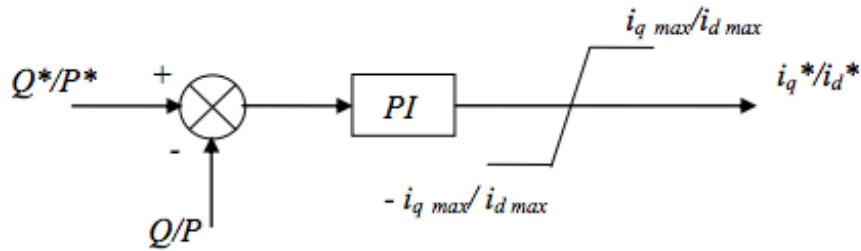
Figure 4.10 Active and reactive power controllers

CHAPTER 5

OFFSHORE WIND FARM WITH UNDERSEA HVDC TRANSMISSION

5.1 Introduction

In this chapter, the design is implemented to test the feasibility of the model that consists of offshore wind farm, HVDC transmission converters for offshore and onshore stations and the AC main grid.

5.2 Parameters under consideration

The offshore wind farm includes a collection of several wind turbines coupled together to generate electrical power and it is connected to converters in order to reach MPPT. The adopted system is used to study the impact of DFIG based offshore wind farm connected by VSC-HVDC link on power system stability. The test system consists of 60 wind turbines 1.5 MW each that are connected to offshore converter (rectifier) through an individual step-up transformer. The component and variable specification for the wind turbine and the DFIG is given in Table 5.1 and the value in per unit is given in Table 5.2.

Table 5.1 Wind turbine generator parameters

Parameters	Value
Base power	1.5 MW
Base voltage	575 V
Stator voltage	380 V
Base frequency	50 Hz
Wind speed	15m/s
Cut-in speed	11m/s

Table 5.2 Per unit system of parameters for the DFIG

Parameters	Ratings
Stator resistance R_s	0.023 p.u
Stator leakage reactance L_{Is}	0.18 p.u
Rotor resistance R_r	0.016 p.u
Rotor leakage reactance L_{Ir}	0.16 p.u
Magnetizing inductance L_m	2.9 p.u
Lumped inertia constant H	0.685
Friction coefficient F	0.01
Pair of poles P	3

Table 5.3 Drive train data for 1 wind turbine and its control parameter

Grid-side coupling inductor	$L = 0.3\,p.u\ \ R = 0.003\,p.u$
Grid-side converter maximum current	0.8 p.u
Nominal DC bus voltage	1150 V
Line bus capacitor	$10000\mu F$
Line filter capacitor $Q = 50$	$120\,KVar$
Frequency of the grid side PWM carrier	2700Hz
Frequency of the rotor side PWM carrier	1620Hz
Maximum pitch angle	27°
Maximum rate of change of pitch angle	10°/sec
Wind turbine inertia constant	4.32
Turbine initial speed	1.2 p.u
Initial output torque	0.83 p.u

There are 60 unit of individual DFIGs, connected to stator side converter through a transformer, there is a DC capacitor between the converters for smoothing the DC link

voltage and prevention against AC harmonics, these power is then transmitted to the rotor side converter which is connected to the grid through a crowbar protection circuit. A 90 MW offshore wind farm is modeled in a simulation program. The wind farm contains ten aggregated DFIGs with 9 MW each, respectively. It is assumed that each aggregated model represent six 1.5 MW wind turbines. The drive train model of one wind turbine and the DFIG control parameters are given in Table 5.3 and Table 5.4 respectively.

Table 5.4 DFIG control Parameters

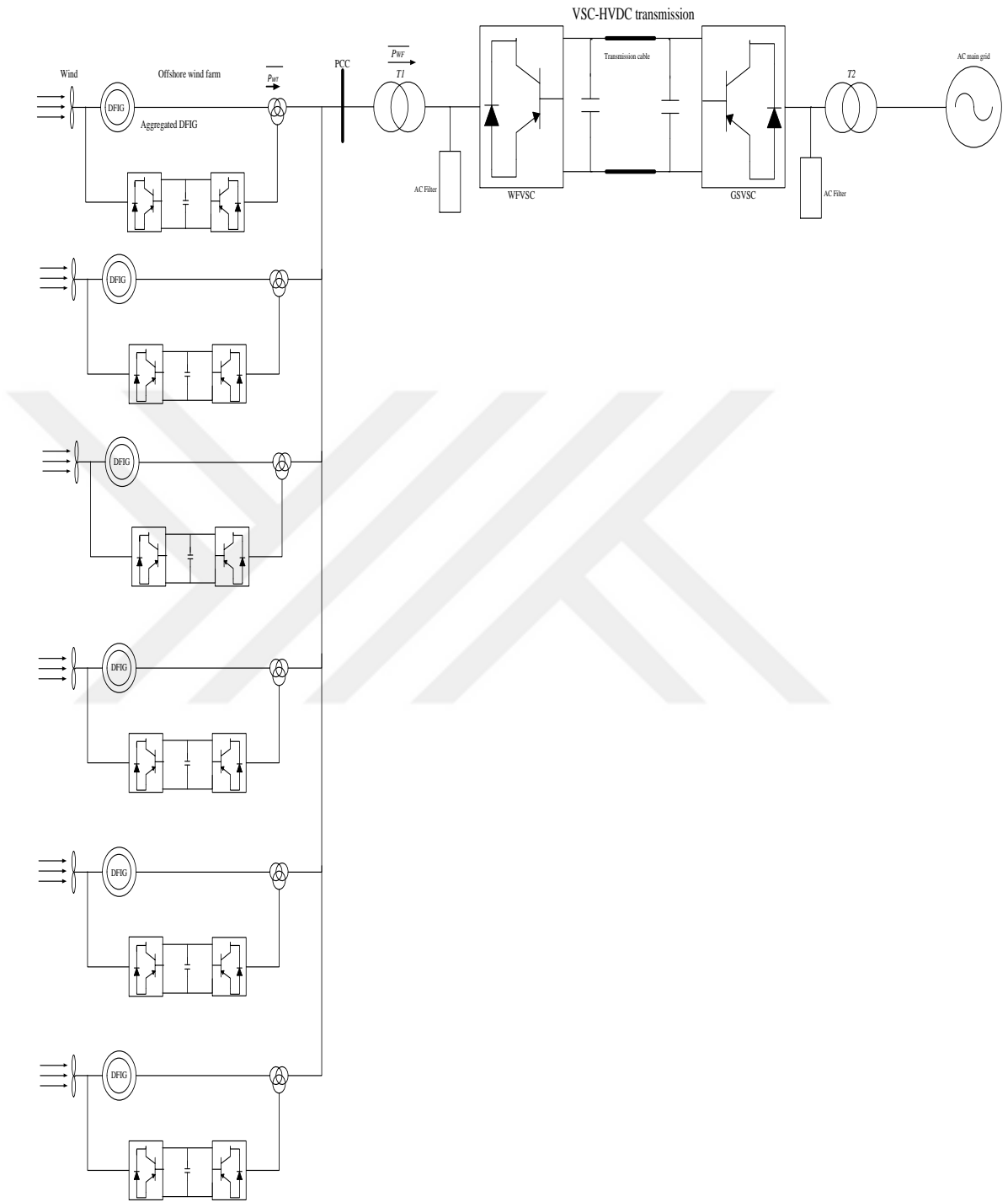| Parameter gain	K_P	K_i
Grid side converter current regulator gains	0.83	5
DC voltage regulator gains	8	400
Speed regulator gains	3	0.6
Rotor side converter current regulators gains	0.6	8
Q and V regulator gains	0.05Var	20 volt
Pitch controller gain	150	-
Pitch compensation gains	3	30

Figure 5.1 The designed offshore wind farm model connected to main grid with HVDC transmission.

5.3 HVDC submarine cable selection

In this study, a ±100 KV submarine cable polymer cables are used. This cable differs from the conventional thyristor-based HVDC cable which uses self-contain oil filled or mass impregnated paper insulated cable. Power reversal is achieved by changing the direction of current flow. Generally HVDC transmission link uses a submarine cable with the properties shown in Table 5.5 [29]

Table 5.5 Properties of Submarine cables used for HVDC transmission

Layer	Material	Thickness	Resistivity	Relative permittivity	Relative permeability
Core	Copper	22	1.68e-8	-	1
Insulator	XLPE	5	-	2.3	1
Armor	Steel	5	1.8e-7	-	10
Insulator	PP	4	-	2.1	1
Sheath	Lead	3	2.2e-7	-	1
Insulator	XLPE	17	-	2.3	1

When locating a submarine environment, there are some requirement that have to be comply to run power cables:

1. It has to be of continuous length
2. High reliability
3. Corrosion and abrasion resistance should be good
4. Overcome resistance to mechanical stress during installation
5. Environmental impact
6. Reduce water penetration in case of cable damage [30].

In this study, the HVDC link parameters are given in Table 5.6. Control parameters for HVDC converters (offshore and onshore) were given Table 5.7 and Table 5.8.

Table 5.6 HVDC link Parameters

Parameters	Value
DC capacitance	$70\mu F$
Smoothing reactor resistance	0.0251Ω
Smoothing reactor inductance	$8mH$
DC filter capacitance	$12\mu F$
DC filter resistance	0.14737Ω
DC filter inductance	$46.908mH$

Table 5.7 Control parameters for offshore converter

Controllers	Ki	Kp	Kf
P regulator	20	-	-
P control	3.0	3.0	-
Q regulator	20	-	
Inner current regulator	0.6	6.0	0.3

Table 5.8 Control parameters for onshore converter

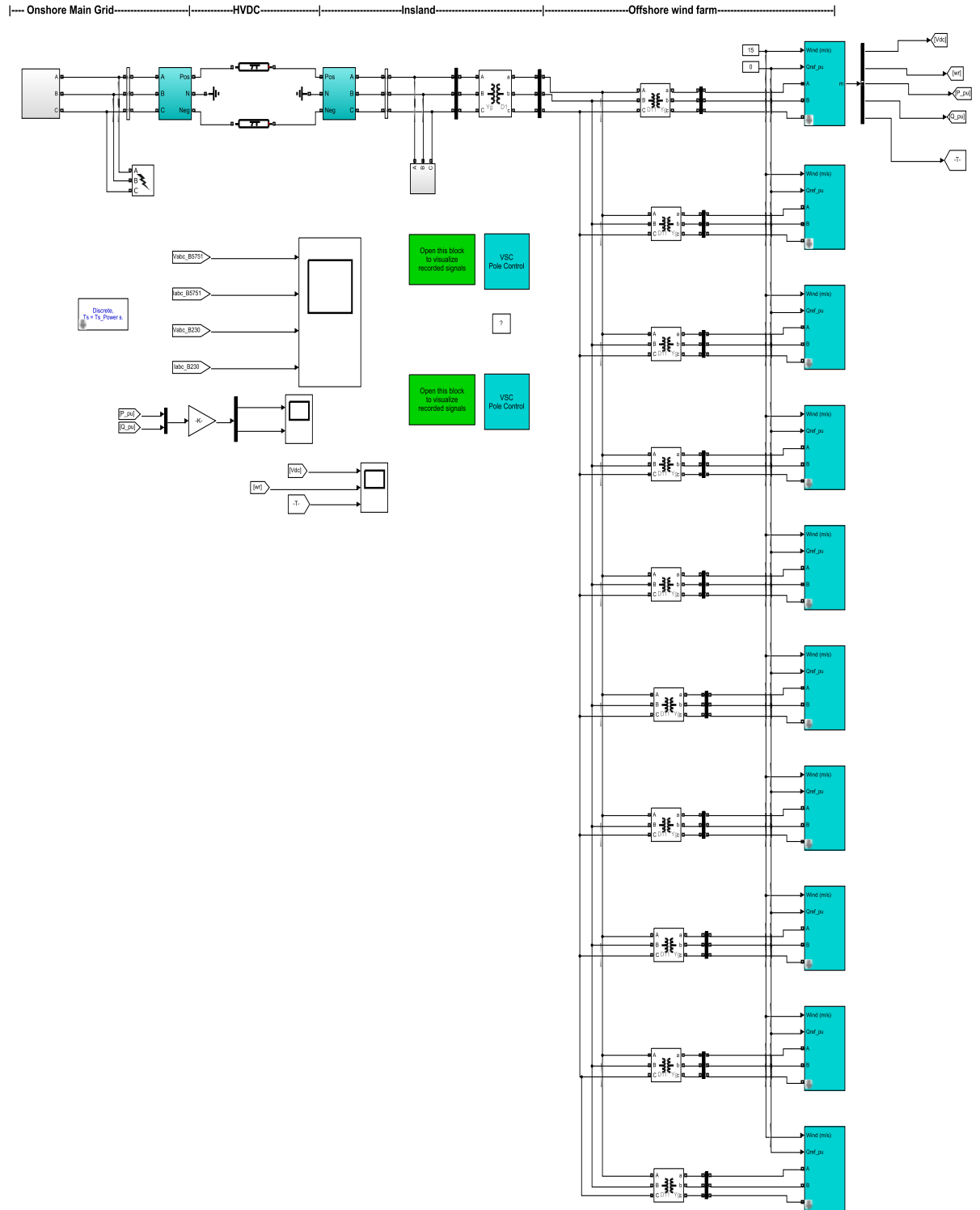| Controllers	Ki	Kp	Kf
DC voltage regulator	40	20	-
Q regulator	20	-	-
Q control	3.0	3.0	
Inner current regulator	6.0	0.6	0.3
DC voltage balance control	0.03	0.2	-

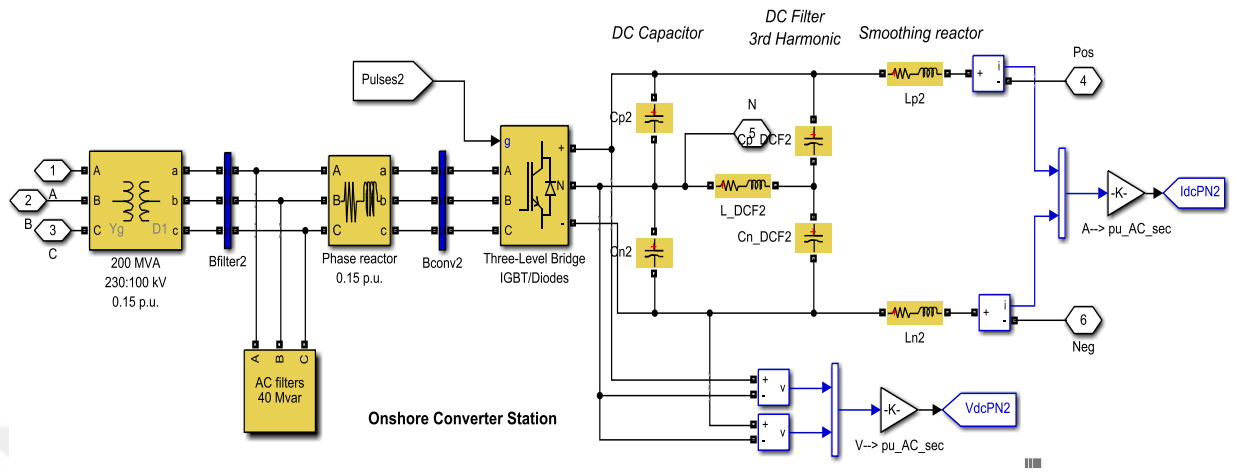**Figure 5.2** The designed model in a simulation environment

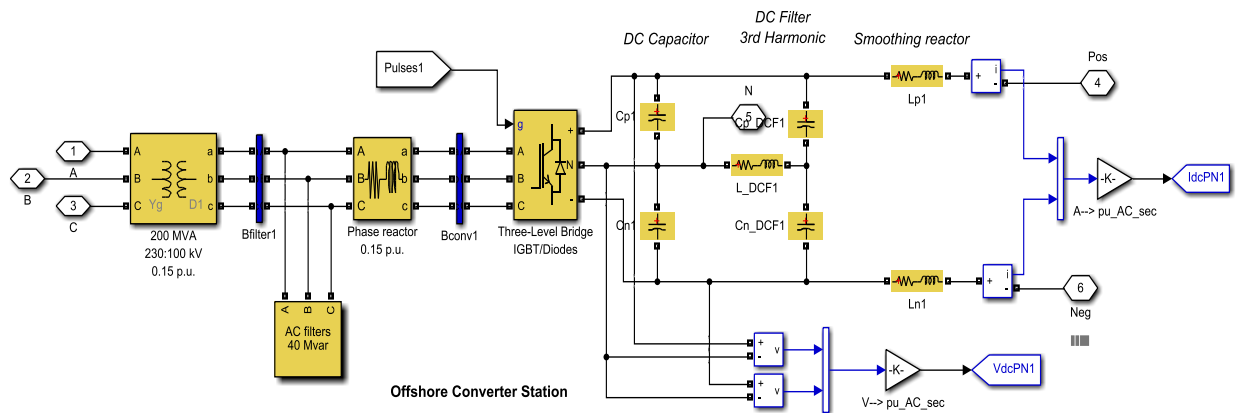**Figure 5.3** Onshore converter station in a simulation environment

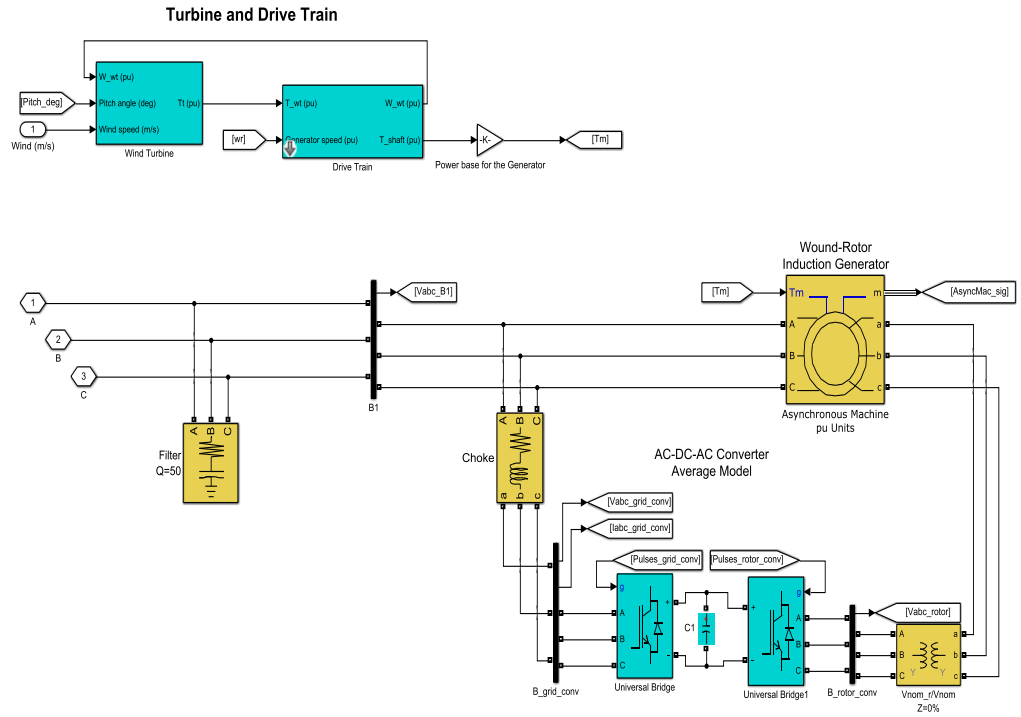**Figure 5.4** Offshore converter station in a simulation environment

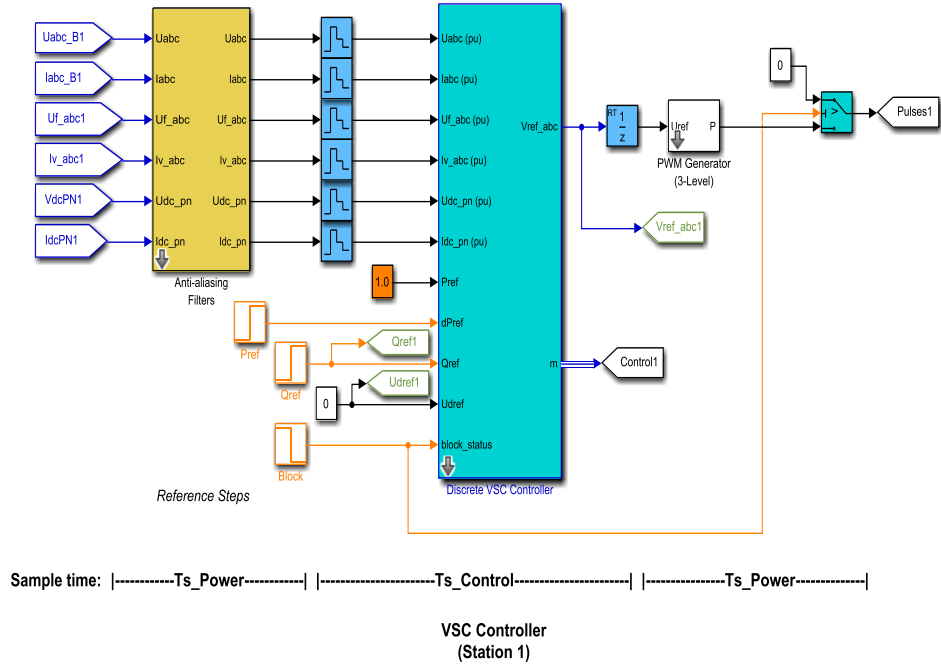**Figure 5.5** DFIG wind turbine in a simulation environment

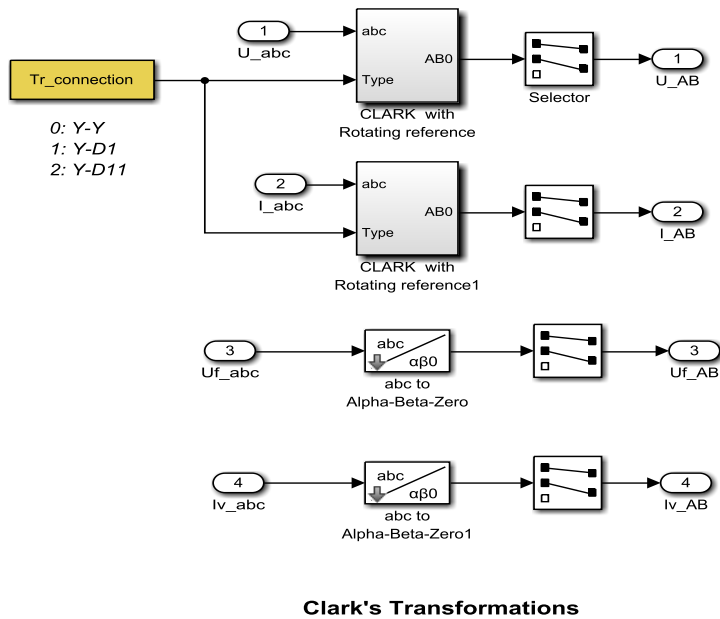**Figure 5.6** VSC-HVDC controller in a simulation environment

Figure 5.7 Clark transformation in a simulation environment

CHAPTER 6

SIMULATION STUDIES

6.1 Introduction

This section is based on simulation studies of the performance of an offshore wind farm connected to VSC based HVDC for the control of wind turbine generator, offshore converter, onshore converter and to ensure quality output of power to the grid from offshore wind farm. The simulation software was used for designing and simulation of the model.

Initially, the wind turbine generator controller was designed to control the generator speed at a certain wind speed (in this thesis 15m/s wind speed was selected to test the performance of controllers) and ensure high quality of power was delivered to the grid. This power is then transmitted to the grid side VSC that controls the DC voltage. The converter is a three-phase consisting of double pole VSI employing 6-IGBT switches. It allows bi-directional power flow. A DC link voltage should be constant when the converter draws current from the grid and as reference to keep DC link voltage. Capacitors values are chosen appropriately to maintain constant DC-link voltage.

6.2 Test system under study

As described in Chapter 5, the offshore wind farm contains a number of wind turbines coupled together to generate electrical power and it is connected to converters in order to reach MPPT. The adopted system is used to study the impact of DFIG based offshore wind farm connected through VSC-HVDC link on power system stability. The test system consists of 60 wind turbines 1.5 MW each that are connected to offshore converter (rectifier) through an individual step-up transformer.

The generator rated capacity is chosen to be 1.5 MW, and its parameters are shown in Table 6.1. Per unit system parameters of DFIG is given in Table 6.2. The simulation period is 3 sec.

Table 6.1 DFIG Parameter

Parameter	Rating
Power rated	1.5 MW
Base voltage	575 V
Base frequency	50 Hz
Base impedence on stator side	0.2381Ω
Base stator current	2.37 kA
Base speed	1400r/min
Torque	11.9 kNm
Rotor voltage	690 V
Rotor current	1.5 kA

Table 6.2 Per unit (p.u) parameters for DFIG

Parameter	Value
Rated rotor speed	1.23 p.u
Friction coefficient	0.01 p.u
Stator resistance	0.023 p.u
Stator leakage inductance	0.18 p.u
Rotor resistance	0.016 p.u
Rotor leakage inductance	0.16 p.u

The VSC-HVDC system connecting offshore wind farm to the grid was designed initially to control active and reactive power generated from wind farm via rectifier at the offshore side, and also the AC main grid supplies its power from inverter that attend to control line reactive power and DC voltage at onshore location.

The control strategy used for controlling DFIG voltage is similar to the method used in VSC transmission. Connecting AC filter at stator side of DFIG can eliminate harmonics caused by the interaction between two converters. To achieve better result, since it is three systems interconnected together, it is good to simulate each system separately and

observed its behavior, then interconnected gradually. The HVDC transmission parameters were given in Table 6.3 [31]

Table 6.3 HVDC transmission parameters

Parameter	Rating	Per unit (p.u) value
Base generated power	90 MW	1.0
Base dc voltage	100 KV	1.0
Converter transformer rating	200 MVA	-
Simple AC system at offshore station	230 KV / 50Hz	1.0
Offshore side transformer ratio	25KV/230 KV/100 KV	-
DC transmission line	2*75km Pi section	-
DC line Inductance per kilometer	0.156H/km	-
DC line resistance per kilometer	0.517Ω/km	-
DC line capacitance per kilometer	2.85mF/km	-
Phase reactor inductance	0.024 H	0.15
Phase reactor resistance	0.075Ω	0.015
Onshore side transformer rating	100KV/230KV 200MVA	-
AC filter	40 MVar at 27th and 54th harmonics	-
AC Grid system	230kV/ 50Hz	1.0

6.3 Simulation Results

6.3.1 Dynamic performance of the system

Case 1: Steady state performance

The active and reactive power generated by the wind farm at a nominal speed of 11m/s is shown in Figure 6.1. As the wind increased from 11 to 15m/s, the generator speed and air gap torque both increases. Also generator active power and reactive power tend to increase because of the constrained due to changes in the system voltage and frequency. These voltage and frequency stability is as a result of the control effect of the HVDC rectifier since it limits and also stabilizes changes in measured value of system frequency at the rectifier end.
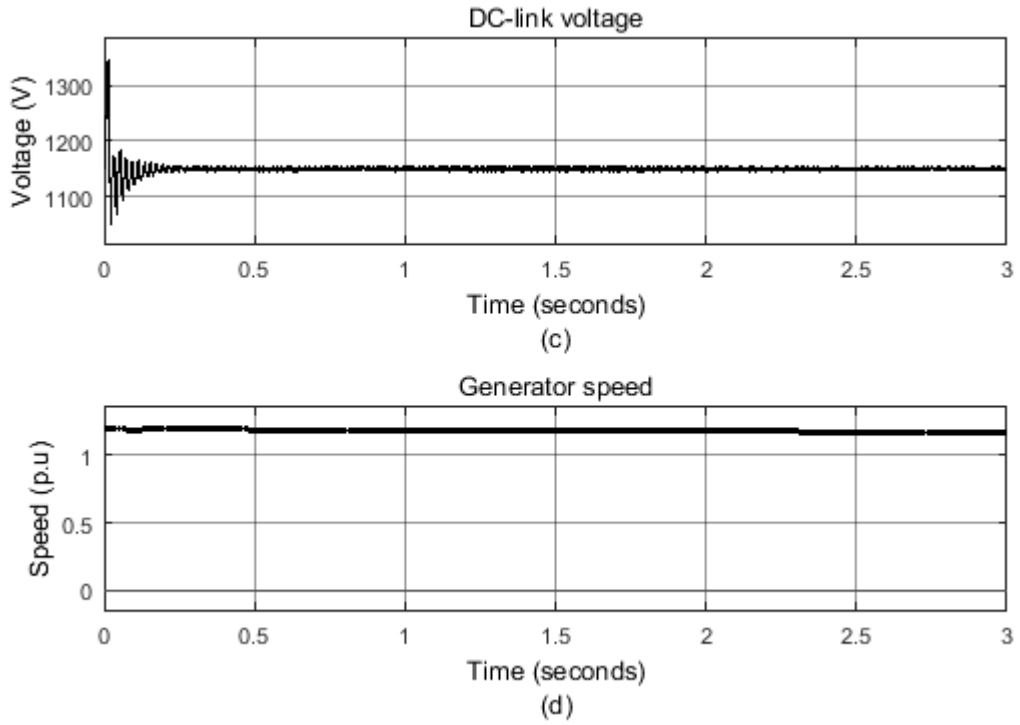

Active Power generated by wind farm

(a)

Reactive Power generated by wind farm

(b)
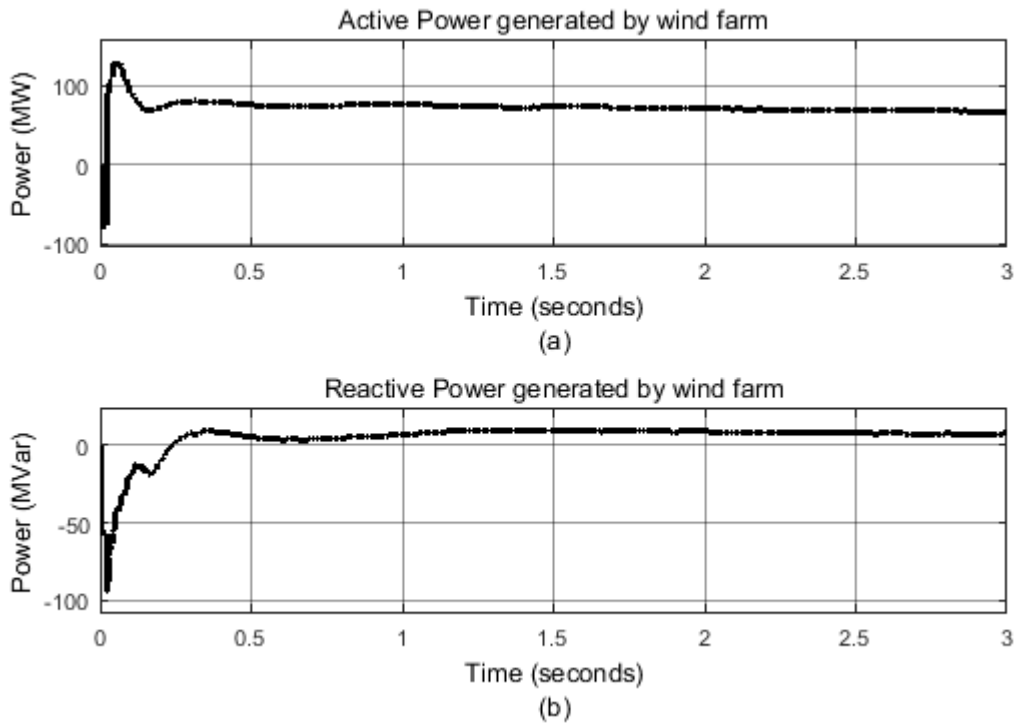
Figure 6.1 Waveforms for generator at nominal wind speed to (a) active power (b) reactive power (c) DC link voltage (d) generator speed.
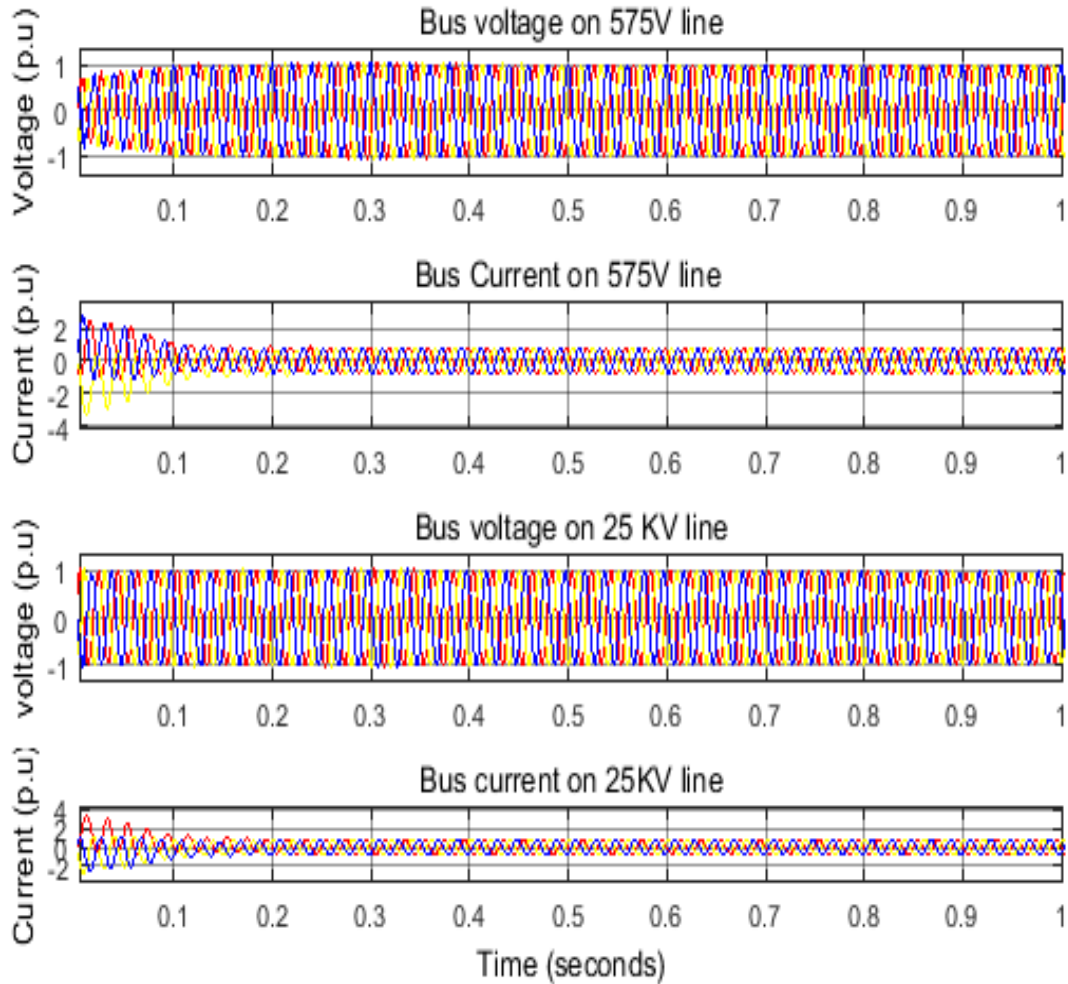
Figure 6.2 Offshore wind farm voltage and current on 575V and 25KV line

When wind speed is increased, which occurred due to increase in the *d*-axis current component of the generator stator, reactive power compensation is needed by the HVDC converter to compensate for the increase in active and reactive power. Therefore, more power can be delivered to the grid as result of increase in rectifier DC voltage and DC current due to reduction in firing angle delay. The nominal DC voltage of the DFIG is set as 1150V and is shown with some ripples at the start up which is caused by charging and discharging of capacitors. It was observed that the voltage has reached its stable value at approximately 0.3 second as shown in Figure 6.1. The DC link voltage at HVDC side is shown in Figure 6.3. The nominal voltage was set at 1p.u (100KV)
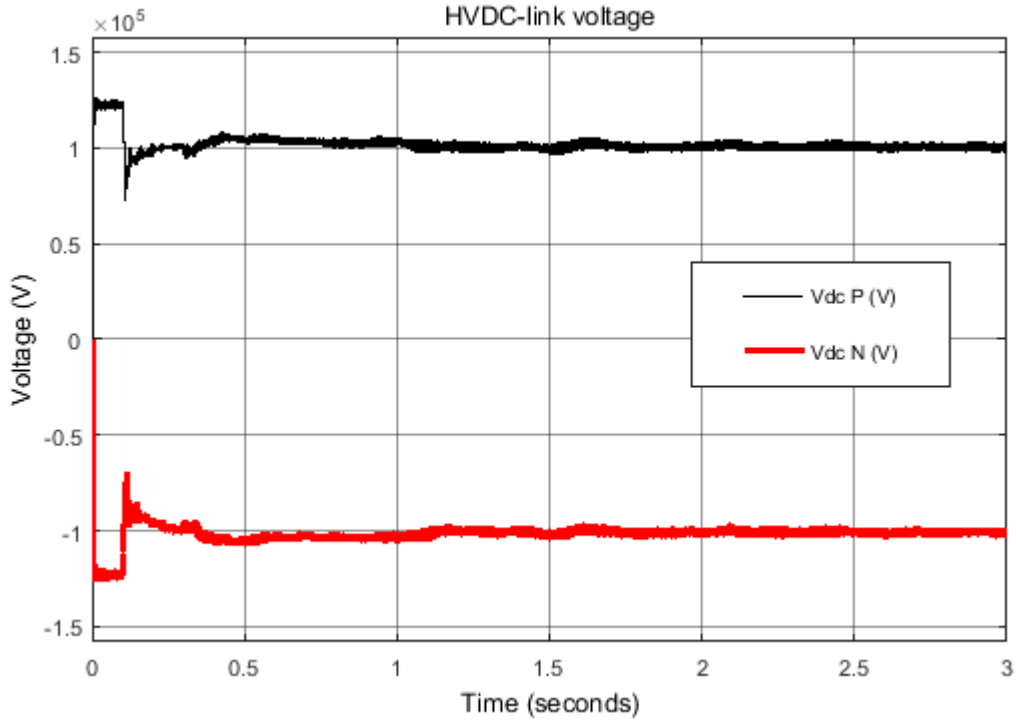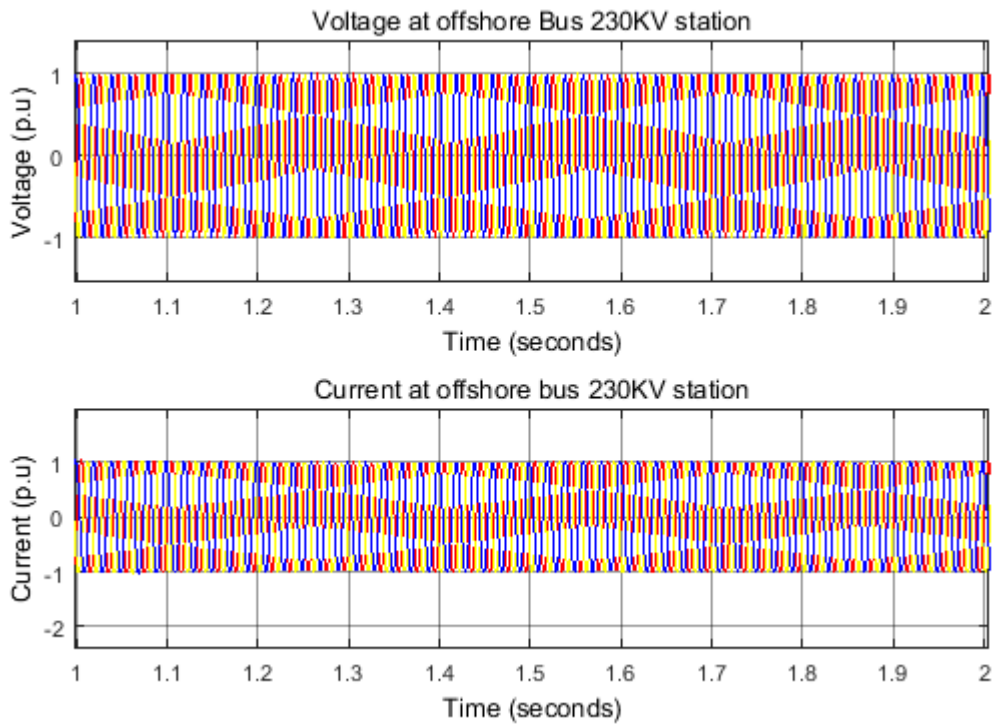
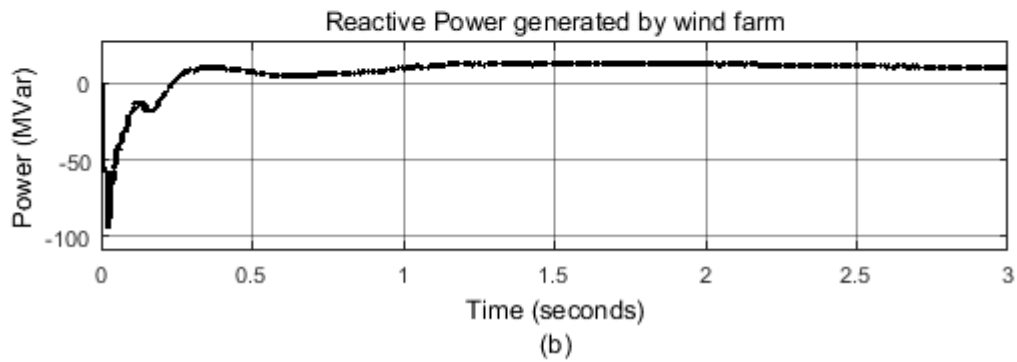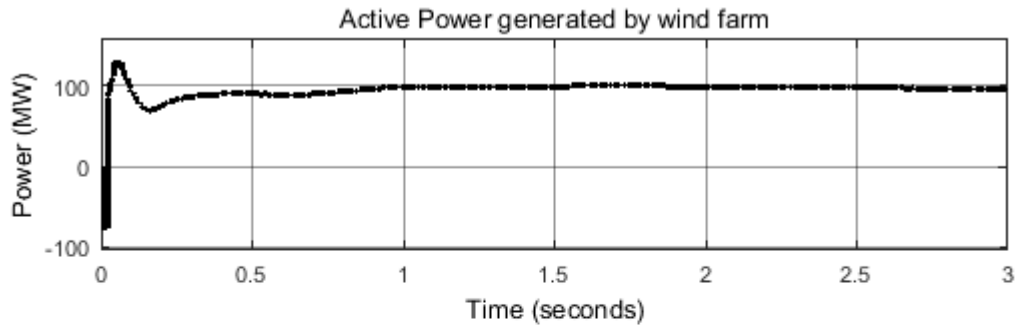**Figure 6.3** HVDC link voltage.

Figure 6.4 Voltage and current at offshore bus B1 (230KV) converter station

Case 2: Response to change in wind speed

Initially, wind speed is predetermined at 11m/s, and it rapidly increases to 15m/s. Also at this time interval, the active power tends to rise smoothly until when at 1 sec reached its rated value as shown in Figure 6.5.
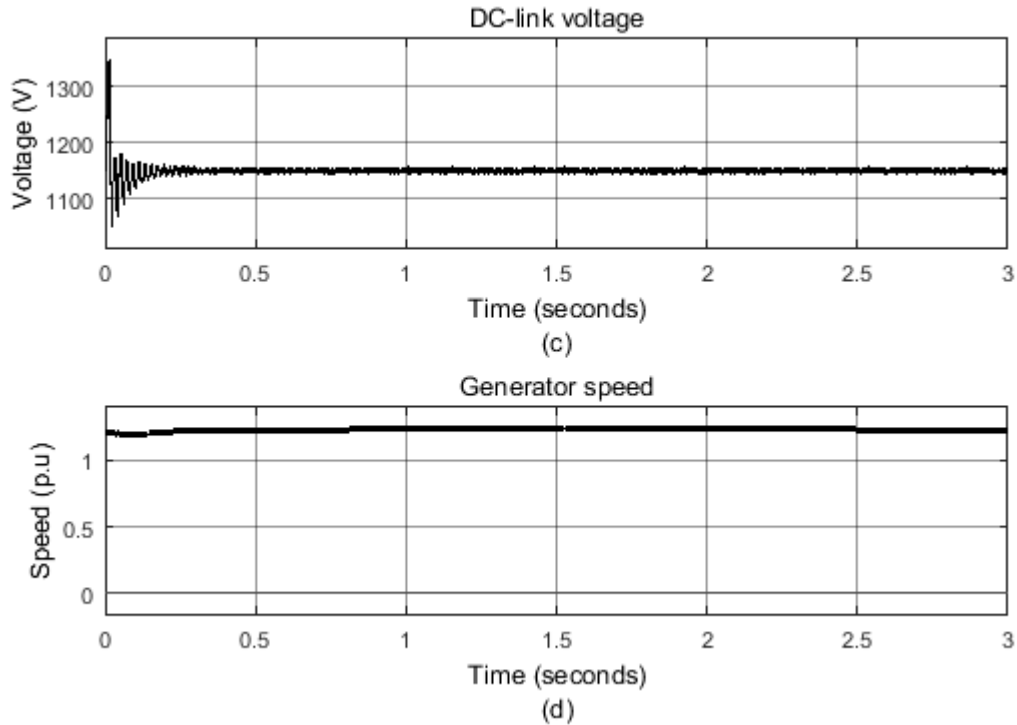

(a)

(b)

Figure 6.5 Responses to change in wind speed to (a) active power (b) reactive power (c) DC-link voltage (d) generator speed

6.3.2 Step changes to HVDC controllers

In the following case studies, reference values are applied to the VSC-HVDC controllers to monitor their performance to the system under four different modes of controls. Initially, the offshore VSC is design for active and reactive control of power generated from offshore wind farm. The HVDC side is controlled using VSC with six-pulse switches used to control frequency and voltage output from the wind farm. The design of controllers involves two strategies:

1. Offshore converter controller design to control active power (P) and reactive power (Q)
2. Onshore converter controller design to control reactive power (Q) and DC voltage (V_{dc})

78

Case 3: Step change to active power controller

The wind farm VSC controller reference is set to 1p.u. At 0.3s the power ramped up slowly to reach its set value of active power reference (90 MW at 0.9 power factor) at 1.0 sec. Also at 1.5 sec, a -0.1p.u step is applied to the active controller reference and response is observed, it shows from Figure 6.6 that the controller can respond to any change in the system subsequently the measured active power follows its reference active power at any instant in the simulation process. Similarly, an active power reference (Pref) is set to 0.5p.u and at 1.5sec, a step change of 0.1p.u is applied to the controller reference and the response is observed.
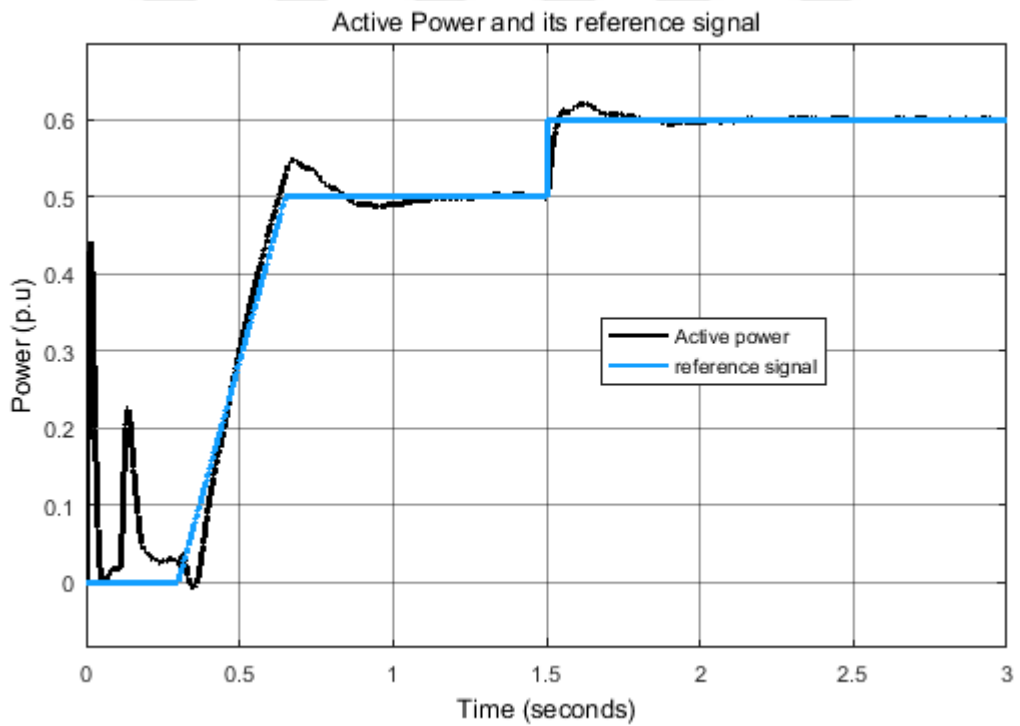
Figure 6.6 Response to different step changes in active power at HVDC rectifier station
(increase and decrease)

Case 4: Step change to reactive power controller

A step change of 0.1p.u is applied at 1.5sec for reactive reference power and the response from Figure 6.7 shows that the measured reactive power follows its reference power at any instant. Also step change to the decrease in reactive power at 1.5sec is also observed. The reactive power can be controlled to a null value in offshore converter station since it is a common control at both converter stations.
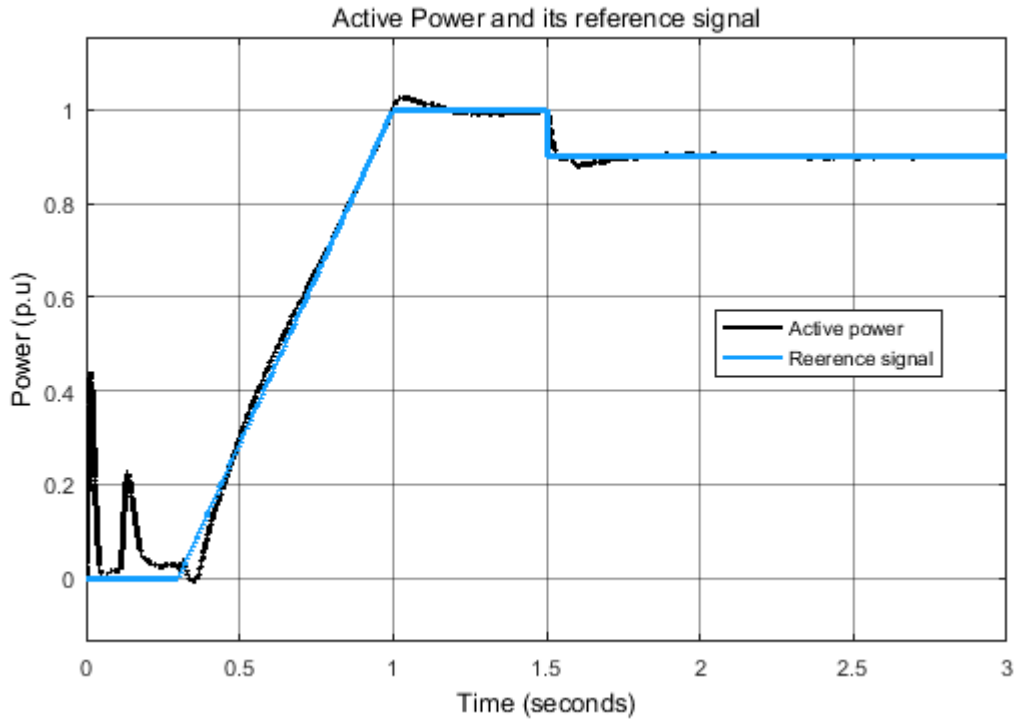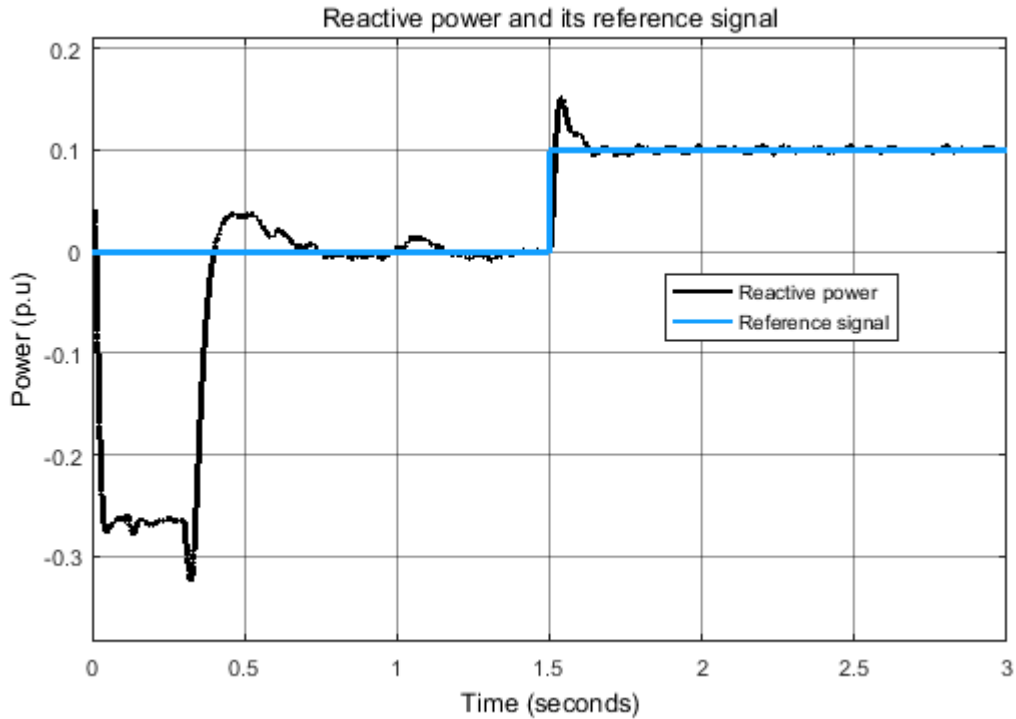

Reactive power and its reference signal
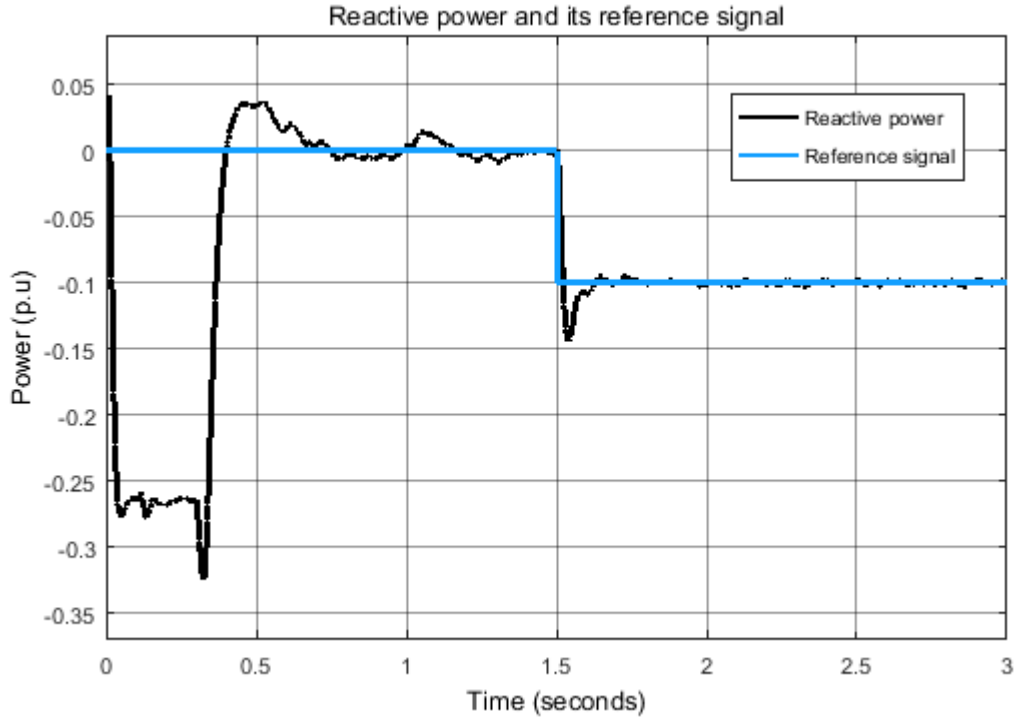
Figure 6.7 Response to different step changes in reactive power at HVDC rectifier station (increase and decrease)

Case 5: Step change to DC voltage controller

The grid side converter controller is established to control reactive power and ensures constant DC voltage at the HVDC side. The DC voltage reference is set to 1p.u. Steady state is reached at about 0.15sec. Observe the controller performance to the change in DC voltage. It was observed that there is decrease in voltage to about 0.05p.u (5 KV) at 1.5 sec because of the step change in the DC reference voltage from 1 p.u to 0.95 p.u as shown in Figure 6.8.

Figure 6.8 Response to step change of DC voltage at onshore converter station

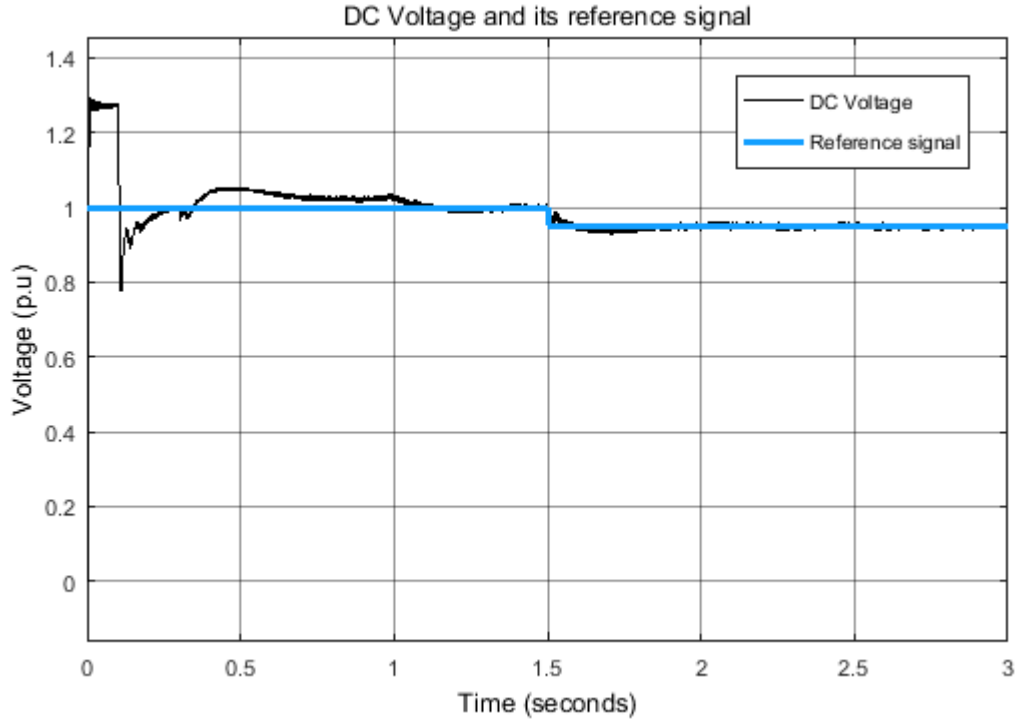The power generated from offshore wind farm delivered the amount of energy to the grid through HVDC transmission, which later converted to three-phase alternating current and ready consumption. In this thesis, a simple AC system of 230 KV is modeled that operate at 50Hz frequency. It was observed from Figure 6.2 and Figure 6.4 that the voltage and current at offshore converter bus is 1.0 p.u (230 KV), which is sufficient to supply energy to consumer terminal voltage.

6.3.3 Fault Analysis

Case 6: Voltage sag at offshore side of the wind farm

A three-phase programmable voltage source is employed at the offshore side of the wind farm and voltage sag is applied at 1.5 s. As a result, the active power delivered from the wind farm tends to deviate from the pre-disturbance state by 0.2 p.u and reactive power by 0.2 p.u. The system returns back to its normal operation after 0.14s from the perturbation as shown in Figure 6.9. The simulation time is 3sec. Response to HVDC controllers at HVDC link under this fault is shown in Figure 6.10. Also response to fault

at the wind farm side for active and reactive power is shown in Figure 6.11.
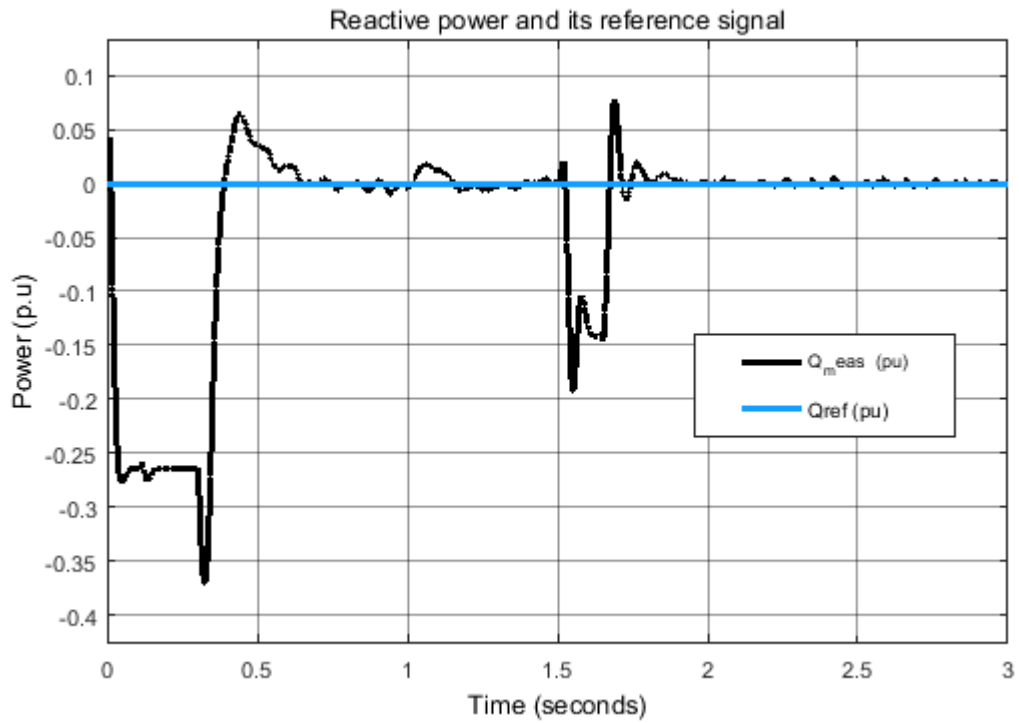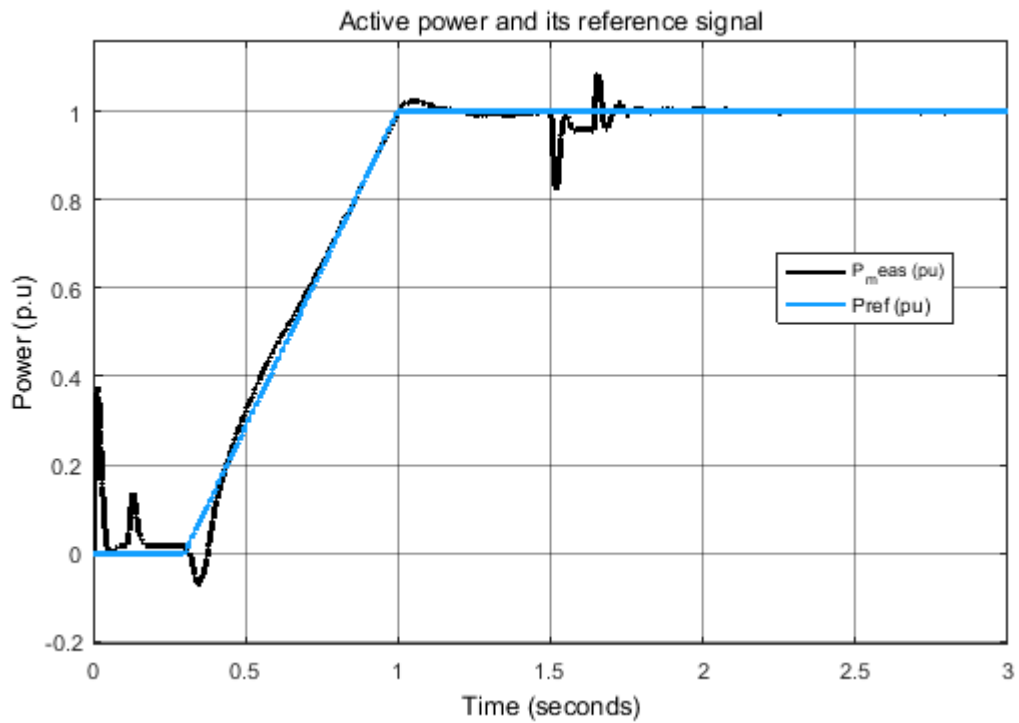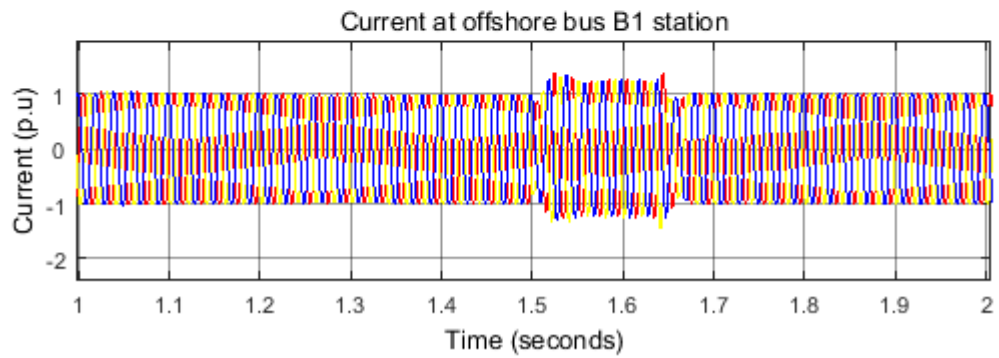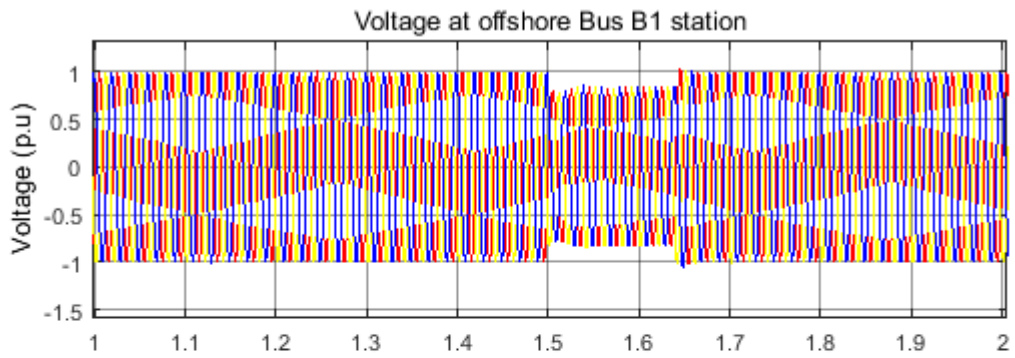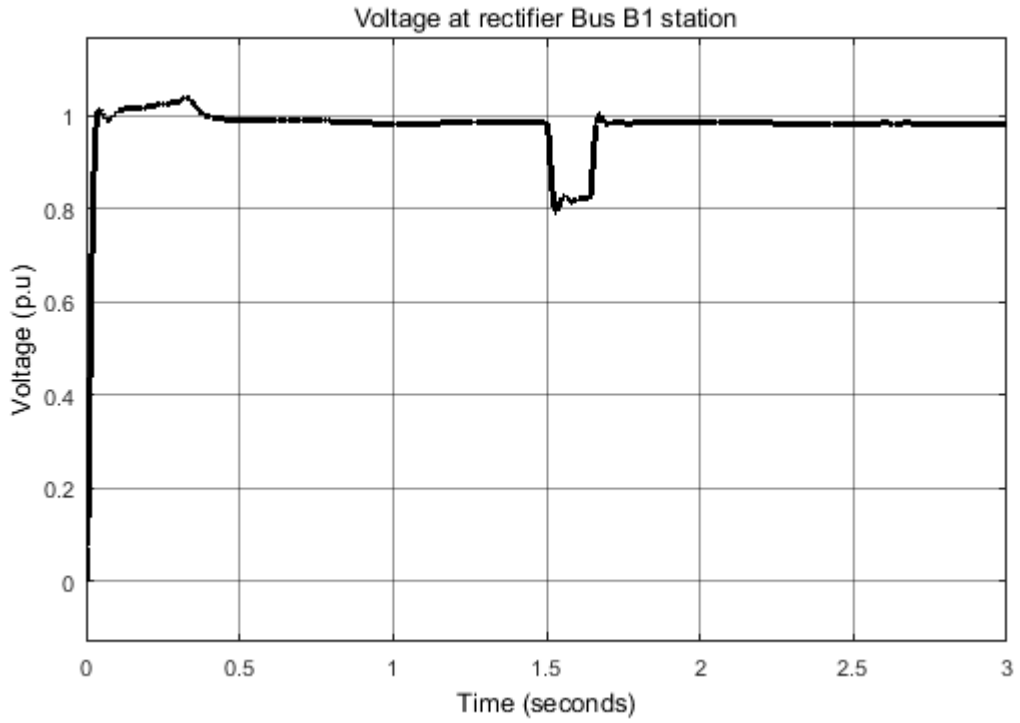
Figure 6.9 Voltage sag at wind farm rectifier bus station
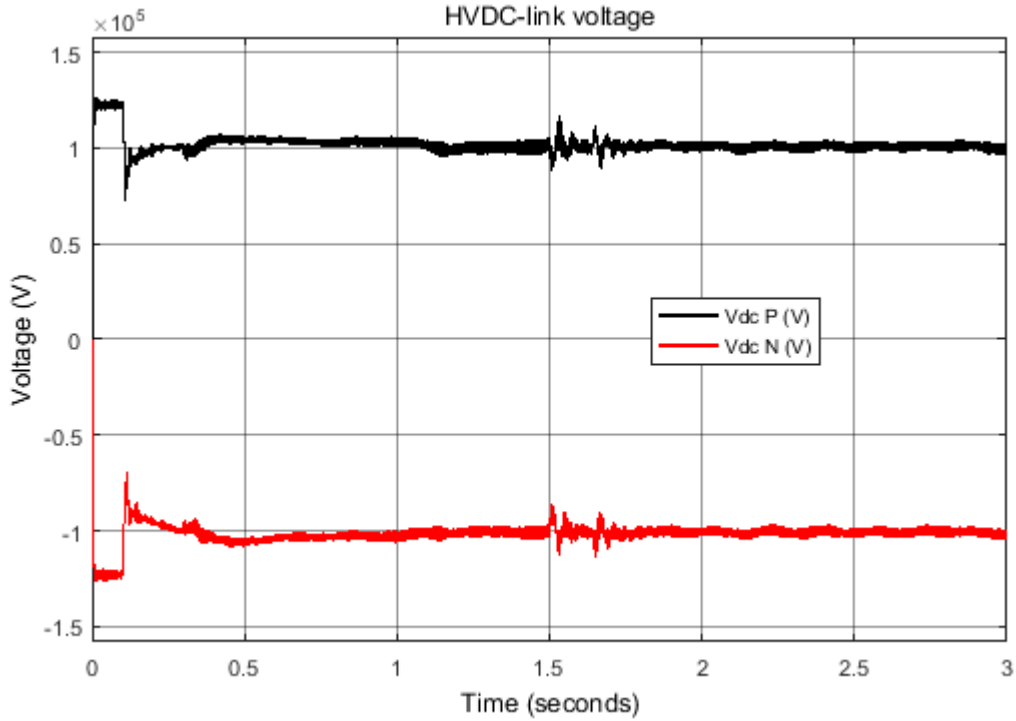
Figure 6.10 Response to the fault at the HVDC side
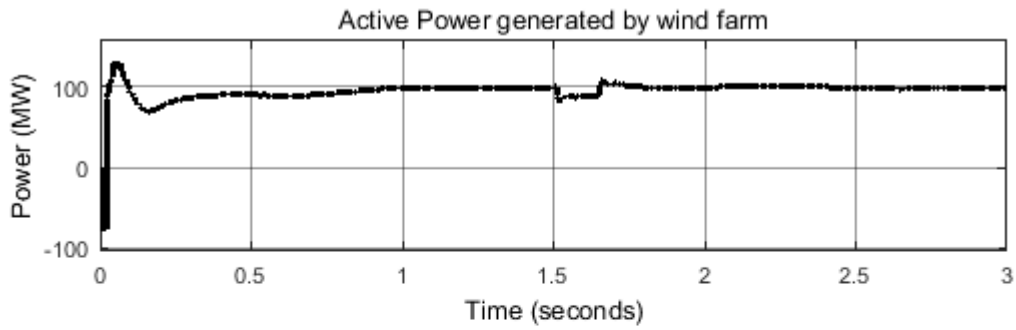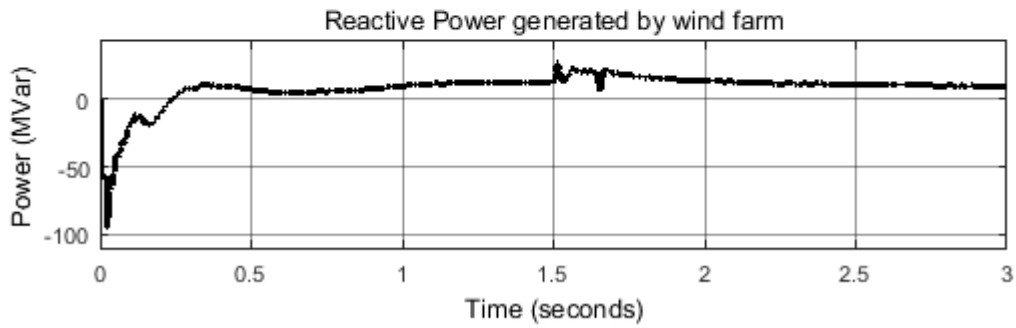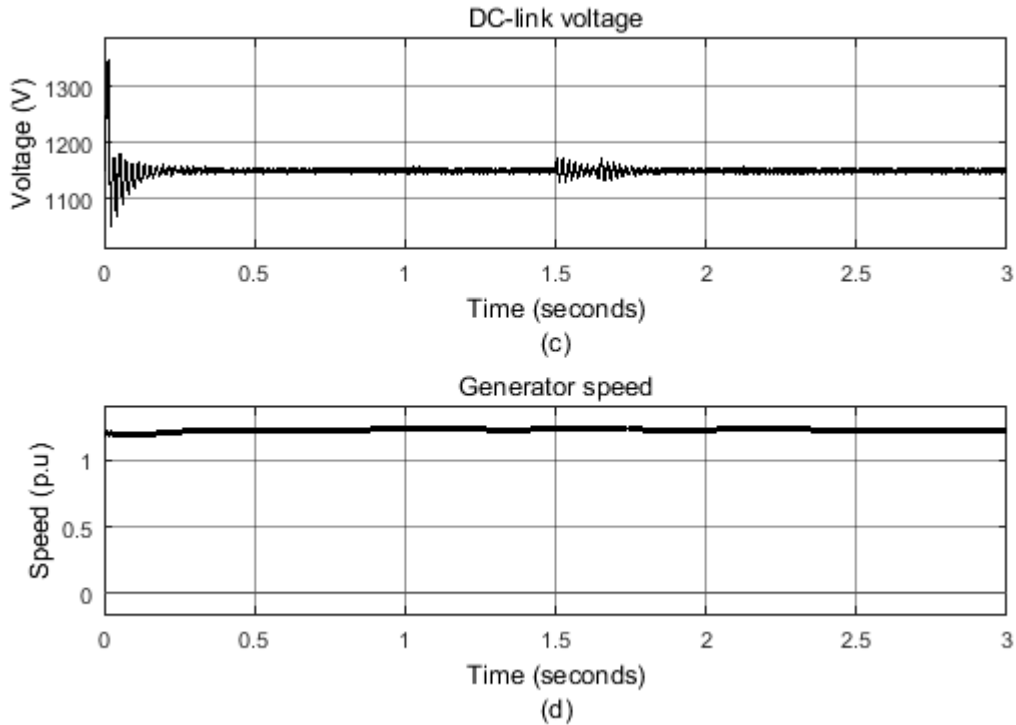
Figure 6.11 Response to fault at offshore wind farm to (a) active power (b) reactive power (c) DC voltage and (d) generator speed

Case 7: Three-phase to ground fault at the onshore main grid

A three phase to ground fault is applied at the grid side of the wind farm and at 1.5s, the DC power delivered by the wind farm almost ceased then DC voltage rise to 1.2p.u as shown in Figure 6.13 due to excessive charging of the DC capacitors. The recovery time from perturbation is 0.12s as shown from the simulation diagrams in Figure 6.12. DC voltage control override, which is a function in the active power controller, limits the DC voltage to a specified range. Wind farm active and reactive power under this fault is shown in Figure 6.14.
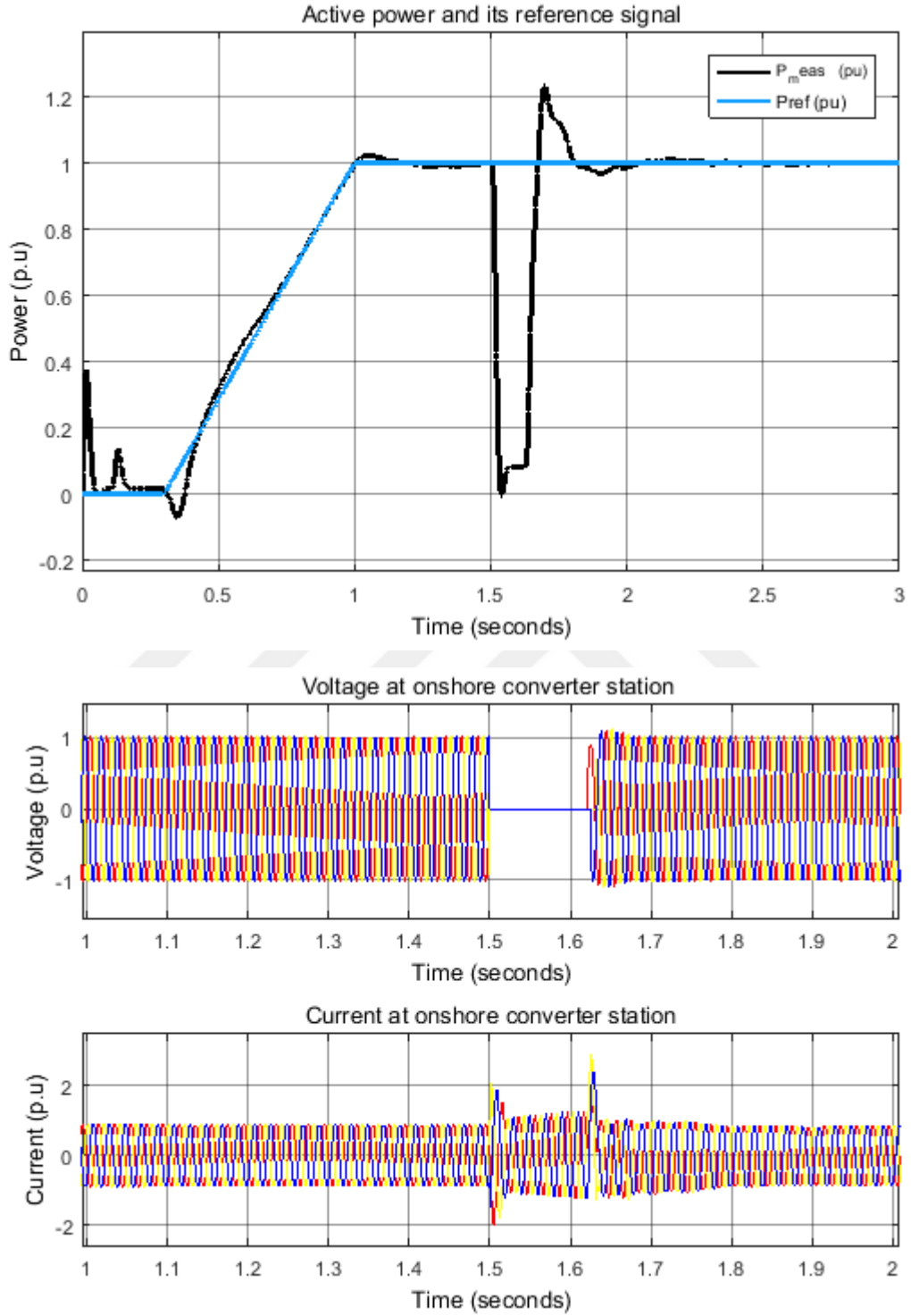
Figure 6.12 Three-phase to ground fault at onshore converter station
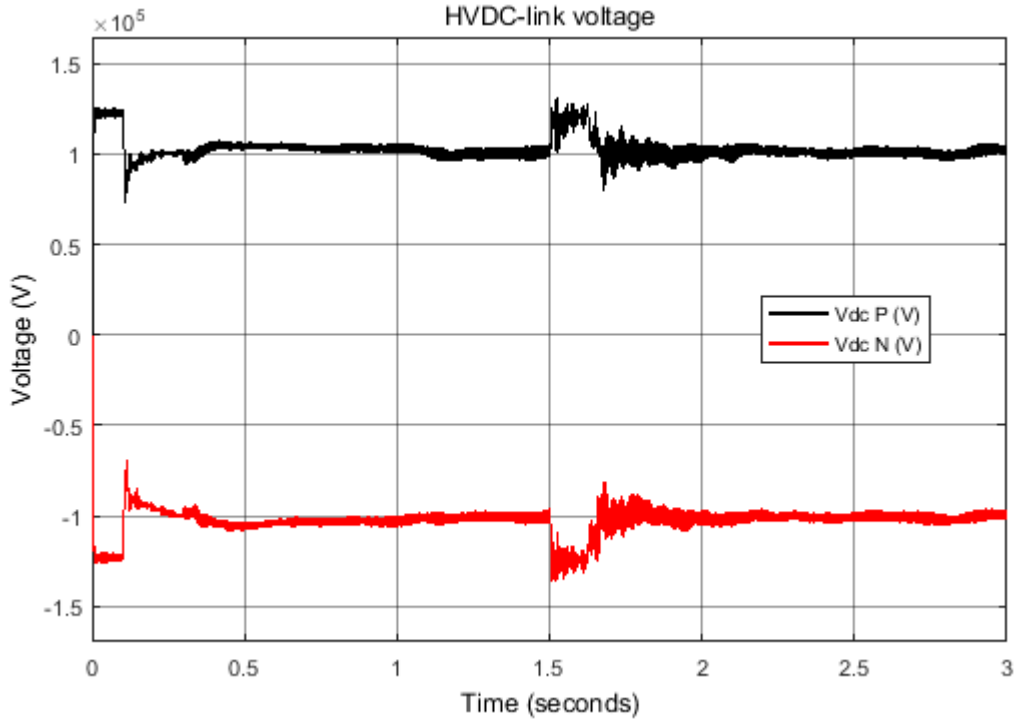
Figure 6.13 DC voltage at onshore converter under fault condition
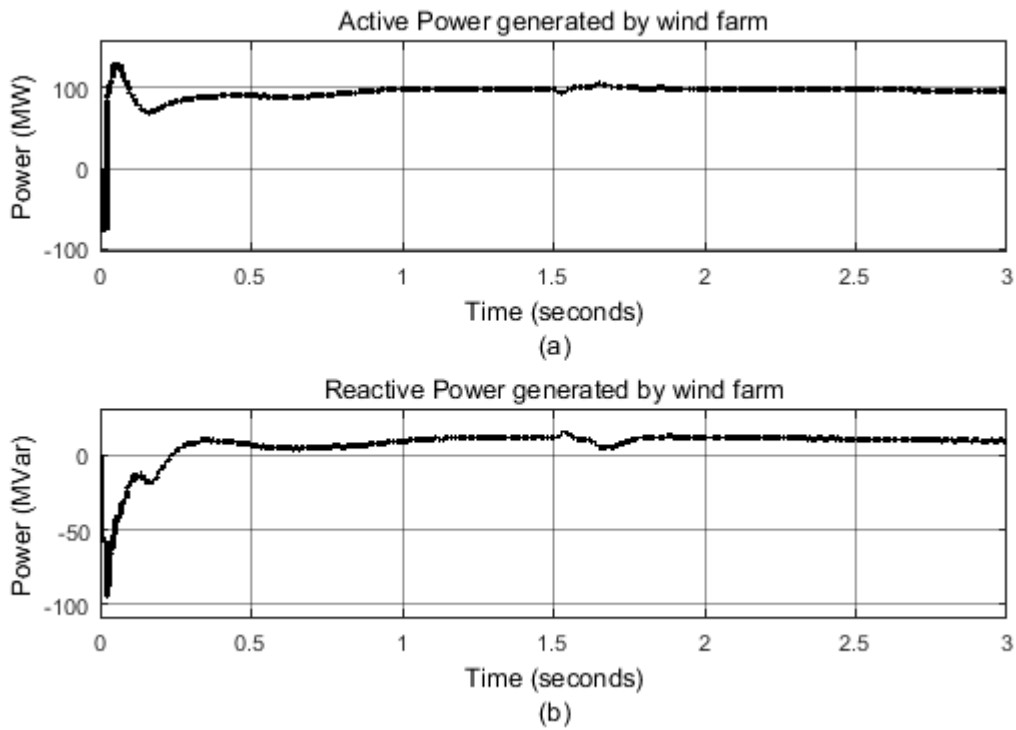
Figure 6.14 Wind farm active and reactive power under fault condition.

CHAPTER 7

CONCLUSION

7.1 Summary

In this thesis, design and control of an offshore wind farm connected through HVDC transmission is implemented. Initially, an offshore wind farm is designed to deliver power to an AC main grid using HVDC by an undersea cable transmission. Unlike the conventional thyristor based converters that uses thyristor valve, a VSC employing IGBT switches with SVPWM techniques were used. A DFIG is used for driving the wind turbines due to its variable speed operation. The transmission of power to the grid over long distance requires conversion of power from AC to DC, and is achieved by the used of converter (rectifier station) at offshore side for converting the AC voltage supplied by wind turbine generators into DC and then transmitted through undersea cables. This transmitted power is then converted back (inverter station) to AC to feed the grid. The control of this system is achieved through control of wind turbine generator and wind speed by ensuring that high quality power is delivered to the grid.

The developed control strategy verified the dynamic and transient operation of the system to VSC-based-HVDC transmission. It involves control of active and reactive power at the offshore side and maintaining DC voltage and reactive power at the onshore side. It has been verified that active and reactive power can be controlled independently to one another and by increasing and decreasing step changes to their reference value. Also variation in wind speed can have effect on the dynamic performance of the system.

The performance of the controllers is analyzed during fault and it is verified that three-phase fault could be very critical as regards the system when compared to an unbalance fault. The generated power from offshore wind farms delivered the amount of energy to the grid through HVDC transmission, which later converted to three-phase alternating current and ready for consumption.

7.2 Recommendation for future work

For better analysis of this composite system, different renewable energy sources like solar power plant can be connected to the system. We can also connect two different plants such as solar and wind power plant together to the HVDC system. FACTS device can also be connected to the system for efficiency improvement.

HVDC based VSC transmission is used in this work, the use of HVDC based MMC should be studied and investigated. Also, the HVDC transmission system fault is considered, the fault located at the wind farm and the wind turbine may be focused in future.

In this thesis, an ideal three-phase AC source were used for the design of AC main grid, in further work, synchronous machine may be used to study the converter interaction to the HVDC system.

REFERENCES

[1]   A. B. Attya *et al.*, "Power-Flow Control and Stability Enhancement of Four Parallel-Operated Offshore Wind Farms Using," **vol. 28**, November 2007, pp. 1356–1363, 2010.

[2]   F. Careri, S. Member, C. Genesi, and P. Marannino, "Centralized coordinated control of VSC-HVDC link and DFIGs in very large offshore wind power plants," pp. 1–8, 2011.

[3]   M. Y. Keche and J. Lin, "Integrating the First HVDC-Based Offshore Wind Power into PJM System - A Real Project Case Study," pp. 1–8, 2015.

[4]   W. Musial and B. Ram, "Large-Scale Offshore Wind Power in the United," *Risk Anal.*, September, 2010.

[5]   "http://gwec.net/global-figures/graphs/." 10th September 2017.

[6]   H. Ergun, S. Member, D. Van Hertem, S. Member, and R. Belmans, "Transmission System Topology Optimization for Large-Scale Offshore Wind Integration HE European Union has set ambitious goals regarding," **vol. 3(4)**, pp. 908–917, 2012.

[7]   N. G. Khani, M. Abedi, G. B. Gharehpetian, S. Member, and G. H. Riahy, "Offshore Wind Farm Power Control Using HVdc Link Control de puissance d ' un parc éolien en mer utilisant la liaison CCHT," **vol. 39(2)**, pp. 168–173, 2016.

[8]   W. Rik, "HE AIM OF WIND TURBINE SYS-," pp. 26–33, 2002.

[9]   D. Version, "Design and Control of A DC Grid for Offshore Wind Farms By," 2012.

[10]   R. Safaeian, S. Ebrahimi, and M. Parniani, "Performance Improvement of Steady-State and Transient Operation of Offshore Wind Farm HVDC Power Transmission," 2015.

[11]   F. Deng, S. Member, Z. Chen, and S. Member, "An Offshore Wind Farm with DC Grid Connection and Its Performance under Power System Transients," pp. 1–8, 2011.

[12]   F. Blaabjerg, Z. Chen, S. Member, and S. B. Kjaer, "Power Electronics as Efficient Interface in Dispersed Power Generation Systems," **vol. 19(5)**, pp. 1184–1194, 2004.

[13]   Z. Chen, Y. Hu, and F. Blaabjerg, "Stability improvement of induction generator-based wind turbine systems," pp. 81–93.

[14]   S. M. Muyeen *et al.*, "Comparative study on transient stability analysis of wind turbine generator system using different drive train models," pp. 131–141.

[15]   J. B. Ekanayake, L. Holdsworth, and N. Jenkins, "Comparison of 5th order and 3rd order machine models for doubly fed induction generator (DFIG) wind turbines," **vol. 67**, pp. 207–215, 2003.

[16]   M. Mohseni, "An Improved Modeling and Control Approach for DFIG-Based Wind Generation Systems."

[17]   A. Dekhane, S. Lekhchine, T. Bahi, S. Ghoudelbourg, and H. Merabet, "DFIG Modeling and Control in a Wind Energy Conversion System," pp. 287–292, 2012.

[18]   R. Meenakshi, M. S. Kumaran, R. Muthu, and E. Engineering, "MODELING AND DIRECT POWER CONTROL OF DFIG FOR WIND ENERGY CONVERSION SYSTEM WITH A BACK TO BACK CONVERTER," no. 1.

[19]   M. M. Z. Moustafa, O. Nzimako, and A. Dekhordi, "Modelling of Wind Energy Sources in Real Time Platform," pp. 189–192, 2016.

[20]   F. Obeidat, X. Lie, and L. Yongdong, "Simulation of Grid Connected HVDC

Offshore Wind Farm Topolgies," pp. 897–902, 2013.

[21]   L. Xu, S. Member, L. Yao, and C. Sasse, "Grid Integration of Large DFIG-Based Wind Farms Using VSC Transmission," **vol. 22(3),** pp. 976–984, 2007.

[22]   T. M. Haileselassie, "Control of Multi-terminal VSC-HVDC Systems," June, 2008.

[23]   E. Engineering and E. Engineering, "VSC BASED HVDC SYTEM DESIGN AND PROTECTION AGAINST OVER VOLTAGES," **vol. 10(12)** , pp. 46–57, 2014.

[24]   "https://www.mathworks.com/help/physmod/sps/powersys/ug/vsc-based-hvdc-link.html."

[25]   T. M. Haileselassie, M. Molinas, and T. Undeland, "Multi-Terminal VSC-HVDC System for Integration of Offshore Wind Farms and Green Electrification of Platforms in the North Sea," pp. 1–8, 2008.

[26]   N. Mohan, *Advanced Electric Drives*. 2001.

[27]   C. Bajracharya, M. Molinas, M. Ieee, J. A. Suul, T. M. Undeland, and F. Ieee, "Understanding of tuning techniques of converter controllers for VSC-HVDC," 2008.

[28]   H. M-vsc-hvdc, W. Lu, and B. Ooi, "DC Overvoltage Control During Loss of Converter in Multiterminal Voltage-Source Converter-Based," **vol. 18(3)**, pp. 915–920, 2003.

[29]   F. Deng, Z. Chen, and S. Member, "Operation and Control of a DC-Grid Offshore Wind Farm Under DC Transmission System Faults," **vol. 28(3)** , pp. 1356–1363, 2013.

[30]   S. Knowledge, *HVDC Submarine Power Cables in the World*. 2015.

[31]   M. Y. Keche, "Integrated operation of Grid and HVDC connected Offshore Wind Farm," pp. 666–674, 2016.

APPENDICES

Simulation code for DFIG wind turbine

```
%Generator data
Pnom=nom(1)*Nb_wt;
Vnom=nom(2);
Vnom_r=nom(3);
Fnom=nom(4);
Rs=sta(1);
Lls=sta(2);
Rr=rot(1);
Llr=rot(2);
H=mec(1);
F=mec(2);
p=mec(3);

% Converters data
L_RL=RL_grid(1);
R_RL=RL_grid(2);
Q_filter=50;
C_DClink=C_DClink1*Nb_wt;
C_var_filter=C_var_filter1*Nb_wt;

% Controller data
Freq_filter=1000*10;    %Hz
Zeta_filter=0.707;
Mod_index_max_grid=1.1;   %Maximum value of modulation
index for grid-side converter
Mod_index_max_rotor=2;    %Maximum value of modulation index
for rotor-side converter
Lim_grid_side_cur_reg=1.1; %Limit for grid-side PI current
regulator (pu)
Lim_rotor_side_cur_reg=0.1; %Limit for rotor-side PI
current regulator (pu)
Min_var_reg=0.9; %Minimum output value for integral var
regulator (pu)
Max_var_reg=1.1; %Maximum output value for integral var
regulator (pu)
Max_speed_reg=1; %Maximum output value for PI speed
regulator (pu)
```

```matlab
Kp_dc=Kdc(1);
Ki_dc=Kdc(2);
Kp_grid_side_cur_reg=Kgrid_side_cur_reg(1);
Ki_grid_side_cur_reg=Kgrid_side_cur_reg(2);
Kp_speed=Kspeed(1);
Ki_speed=Kspeed(2);
Kp_compensation=Kcompensation(1);
Ki_compensation=Kcompensation(2);
Kp_rotor_side_cur_reg=Krotor_side_cur_reg(1);
Ki_rotor_side_cur_reg=Krotor_side_cur_reg(2);
Ki_var=Ki_QV(1);
Ki_volt=Ki_QV(2);
Iq_ref_limit_time_constant=0.3;  %(s)
T_speed=5;         %s
Min_mag_flux=0.5;      %(pu)
Max_Idr_ref=0.9;       %(pu)
Speed_max=1.2;    %(pu)
Speed_min=0.7;    %(pu)
Pitch_time_constant=0.01;      %(s)


% Turbine data
Pmec=Pmec1*Nb_wt;
c1 = 0.6450;
c2 = 116;
c3 = .4;
c4 = 5;
c5 = 21;
c6 = .00912;   % Set Pmin in stall condition (does not vary
with wind_speed_Pmax)
c7 = .08;
c8 = .035;
theta=0;
CpMax=.5;
lambda_CpMax=9.9495;

c1_c8=[c1 c2 c3 c4 c5 c6 c7 c8];


%    Cp = c1*(c6*lambda + (-c4 - c3*(2.5 + theta) +
c2*(1/(lambda + ...
%    c7*(2.5 + theta)) - c8/(1 + (2.5 +
theta)^3)))/exp(c5*(1/(lambda + ...
%    c7*(2.5 + theta)) - c8/(1 + (2.5 + theta)^3))))
```

```matlab
%%%%%%%%%%%%%%%%%%%%%%%%%%%%%%%%%%%%%%%%%%%%%%%%%%%%%%%%%%%%%%
%%%%%%%%%%%%%%%%
         % Operation at Cp max

%%%%%%%%%%%%%%%%%%%%%%%%%%%%%%%%%%%%%%%%%%%%%%%%%%%%%%%%%%%%%%
%%%%%%%%%%%%%%%%


        rated_omegar=1.2;
        omegar = rated_omegar;

        % Enforce boundaries on wind speed
        % A warning could be displayed
        if wind_speed_CpMax < 6
            wind_speed_CpMax=6;
            disp('Warning: Wind speed at nominal speed and
at Cp max has been set to 6 m/s')
        end
        if wind_speed_CpMax > 30
            wind_speed_CpMax=30;
            disp('Warning: Wind speed at nominal speed and
at Cp max has been set to 30 m/s')
        end

        K1=lambda_CpMax/omegar*wind_speed_CpMax;

        % Calculation of K2 needed to get P equal to the
requested value at
        % Cp max for the requested wind speed

        Prated=Pmec1*Nb_wt;
        P_rated_omegar_theta_zero=0.75;

        K2 =
P_rated_omegar_theta_zero*Prated/(wind_speed_CpMax^3*CpMax)
;

        K1_K2=[K1 K2];


%%%%%%%%%%%%%%%%%%%%%%%%%%%%%%%%%%%%%%%%%%%%%%%%%%%%%%%%%%%%%%
%%%%%%%%%%%%%%%%
         % End of calculation for operation at Cp max

%%%%%%%%%%%%%%%%%%%%%%%%%%%%%%%%%%%%%%%%%%%%%%%%%%%%%%%%%%%%%%
%%%%%%%%%%%%%%%%
```

```matlab
%%%%%%%%%%%%%%%%%%%%%%%%%%%%%%%%%%%%%%%%%%%%%%%%%%%%%%%%%%%%%%%%%%%%%%%%
%%%%%%%%%%%%%%%%
% Plot turbine characteristics
%%%%%%%%%%%%%%%%%%%%%%%%%%%%%%%%%%%%%%%%%%%%%%%%%%%%%%%%%%%%%%%%%%%%%%%%
%%%%%%%%%%%%%%%%

DisplayTurbChar=get_param(gcb,'DisplayTurbChar');
if strcmp(DisplayTurbChar,'on')
    vect_theta = 0:2:30;

    vect_lambda = 1:0.2:30;

    clear Cp;

    for i=1:length(vect_theta)
     for j=1:length(vect_lambda)
                Cp(i,j) = c1*(c6*vect_lambda(j) + (-c4 -
c3*(2.5 + vect_theta(i)) + c2*(1/(vect_lambda(j) + ...
                c7*(2.5 + vect_theta(i))) - c8/(1 + (2.5 +
vect_theta(i))^3)))/exp(c5*(1/(vect_lambda(j) + ...
                c7*(2.5 + vect_theta(i))) - c8/(1 + (2.5 +
vect_theta(i))^3))));
      end
     end

    figure(1);
    clf;
    hold on;

    plot(vect_lambda, Cp);
    axis([0, 25, 0, .6]);
    title('Wind Turbine Cp Characteristic (pitch angle
increases by step of 2 deg.)');
    ylabel('Cp');
    set(gca,'ytick',[0 .1 .2 .3 .4 .5 .6]);
    xlabel('Lambda');
    grid on;
    text(10.1,0.51,'Pitch angle 0 degree');

    hold off

    % Plot of the wind turbine mechanical power output (pu)
lambda and Cp
    % characteristics against wind speed (m/s) for a range
of theta.
```

```matlab
    wind_speed_range = [1,.2,30];
    vect_wind_speed = 1:0.2:30;

    clear lambda;
    clear Cp;
    clear P;

    for i=1:length(vect_theta)
        for j=1:length(vect_wind_speed)
            lambda(i,j) = K1*omegar/vect_wind_speed(j);
            Cp(i,j) = c1*(c6*lambda(i,j) + (-c4 - c3*(2.5 +
vect_theta(i)) + c2*(1/(lambda(i,j) + ...
            c7*(2.5 + vect_theta(i))) - c8/(1 + (2.5 +
vect_theta(i))^3)))/exp(c5*(1/(lambda(i,j) + ...
            c7*(2.5 + vect_theta(i))) - c8/(1 + (2.5 +
vect_theta(i))^3))));
            P(i,j) =
K2/Prated*vect_wind_speed(j)^3*Cp(i,j);
        end
    end


    figure(2);
    clf;
    hold on

    subplot(3,1,1);
    plot(vect_wind_speed, P);
    axis([0, 35, 0, 1.5]);
    title('Wind Turbine Characteristics (w = 1.2 pu, pitch
angle increases by step of 2 deg.)');
    ylabel('P (pu)');
    set(gca,'ytick',0:.5:4);
    grid on;

    subplot(3,1,2);
    plot(vect_wind_speed, lambda);
    axis([0, 35, 0, 20]);
    ylabel('Lambda');
    grid on;

    subplot(3,1,3)
    plot(vect_wind_speed, Cp);
    axis([0, 35, 0, .6]);
    xlabel('Wind Speed (m/s)');
    ylabel('Cp');
    set(gca,'ytick',[0 .1 .2 .3 .4 .5 .6]);
```

```matlab
    grid on;

    hold off
    set_param(gcb,'DisplayTurbChar','off')

end
```

Simulation code of VSC-HVDC controller

```matlab
if (Mode == 1)
    P_control = 1;
else
    P_control = 0;
end

% Nominal AC & DC values:
VacNom1 = Xnom(1); VacNom2 = Xnom(2); Fnom = Xnom(3);
VdcNom = Xnom(4); Pnom = Xnom(5);
% Normalisation Calculation
Uac_sec_to_pu   = 1/(VacNom2*sqrt(2)/sqrt(3));       %
Vrms(L-L) ==> pu Vac
k_nom2pu_Vdc = (VdcNom/2) * Uac_sec_to_pu;           % pu
Vdc ==> pu Vac
k_pu2nom_Vdc = 1/k_nom2pu_Vdc;                       % pu
Vac ==> pu Vdc
k_nom2pu_Idc = ((VacNom2)*sqrt(3))/(sqrt(2)*VdcNom);% pu
Idc ==> pu Iac
k_pu2nom_Idc = 1/k_nom2pu_Idc;                       % pu
Iac ==> pu Idc
% Transformer connexion:
Tr_connection = 1;
% P regulator:
Ki_apc = XP(1); P_max = XP(2); P_min = XP(3); Ramp_apc =
XP(4);
max_i_apc = 10; min_i_apc = -max_i_apc; V_level_apc = 0.9;
% (pu)
% DC Voltage Control Override:
Ki_apc_vco = Xdvco(2); Kp_apc_vco = Xdvco(1);
Udc_max = Xdvco(3)*k_nom2pu_Vdc; Udc_min =
Xdvco(4)*k_nom2pu_Vdc;
max_apc_vco = 1.0; min_apc_vco = -max_apc_vco;
% Q regulator:
Ki_rpc = XQ(1);Q_max = XQ(2); Q_min = XQ(3);
```

```matlab
max_i_rpc = 10; min_i_rpc = -max_i_rpc; V_level_rpc = 0.9;
% (pu)
% AC Voltage Control Override:
Ki_rpc_vco = Xvco(2); Kp_rpc_vco = Xvco(1);
U_max = Xvco(3); U_min = Xvco(4);
max_rpc_vco = 1.0; min_rpc_vco = -max_rpc_vco;
% Current Reference Calculation:
lim_d_crc = Xcrc(1); lim_q_crc = Xcrc(2); %(pu)
U_level_crc = 0.7; %(pu)
f0_crc = 100; % (Hz)
% Current Reference Limitation:
Iref_max = sqrt(lim_d_crc^2 + lim_q_crc^2);
% DC Voltage regulator:
Ki_dcvc = XUdc(2); Kp_dcvc = XUdc(1);
max_i_dcvc = lim_d_crc; min_i_dcvc = -max_i_dcvc;
max_out_dcvc = max_i_dcvc; min_out_dcvc = -max_out_dcvc; %
(pu)
f0_Udc = 10.0; % (Hz)
% Inner Current Loop:
Ki_accc = Xaccc(2); Kp_accc = Xaccc(1); Kf_accc = Xaccc(3);
max_out_accc = 2.0; min_out_accc = -max_out_accc;
%PLL
f_min_pll = 0.75*Fnom; % (Hz)
Kp_pll = 60.0;
Ki_pll = 1400;
% Inner Current Loop:
K_pwm = 1.0;
% DC Voltage Balance Control:
Ki_dcvbc = Xdcvbc(2); Kp_dcvbc = Xdcvbc(1);
f0_dcvbc =  1.0;    % (Hz)
max_out_dcvbc = 0.2; min_out_dcvbc = -max_out_dcvbc;
% Signal Calculations:
f0_sc = 17; %(Hz)
zeta_sc = 1/sqrt(2);
```